

1 **Field Intercomparison of Ice Nucleation Measurements: The**  
2 **Fifth International Workshop on Ice Nucleation Phase 3**  
3 **(FIN-03)**  
4

5 Paul J. DeMott<sup>1</sup>, Jessica A. Mirrielees<sup>2,a</sup>, Sarah Suda Petters<sup>3,b</sup>, Daniel J. Cziczo<sup>4,c</sup>, Markus D.  
6 Petters<sup>3,b</sup>, Heinz G. Bingemer<sup>5</sup>, Thomas C. J. Hill<sup>1</sup>, Karl Froyd<sup>6,7,d</sup>, Sarvesh Garimella<sup>4,e</sup>, A.  
7 Gannet Hallar<sup>8,9</sup>, Ezra J.T. Levin<sup>1,f</sup>, Ian B. McCubbin<sup>8,9</sup>, Anne E. Perring<sup>6,7,g</sup>, Christopher N.  
8 Rapp<sup>c</sup>, Thea Schiebel<sup>10,h</sup>, Jann Schrod<sup>5</sup>, Kaitlyn J. Suski<sup>1,i</sup>, Daniel Weber<sup>3,j</sup>, Martin J. Wolf<sup>4,k</sup>,  
9 Maria Zawadowicz<sup>4,l</sup>, Jake Zenker<sup>2,m</sup>, Ottmar Möhler<sup>10</sup> and Sarah D. Brooks<sup>2</sup>

10  
11 <sup>1</sup>Department of Atmospheric Science, Colorado State University, Fort Collins, CO, USA

12 <sup>2</sup>Department of Atmospheric Sciences, Texas A&M University, College Station, TX, USA

13 <sup>3</sup>Department of Marine, Earth and Atmospheric Sciences, North Carolina State University,  
14 Raleigh, NC, USA

15 <sup>4</sup>Department of Earth, Atmospheric and Planetary Sciences, Massachusetts Institute of  
16 Technology, Cambridge, MA, USA

17 <sup>5</sup>Institute for Atmospheric and Environmental Sciences, Goethe University Frankfurt, 60438  
18 Frankfurt am Main, Germany

19 <sup>6</sup>NOAA Earth System Research Laboratory, Boulder, CO, USA

20 <sup>7</sup>CIRES, University of Colorado, Boulder, CO, USA

21 <sup>8</sup>Storm Peak Laboratory, Department of Atmospheric Sciences, University of Utah, Salt Lake  
22 City, Utah, USA

23 <sup>9</sup>Department of Atmospheric Sciences, University of Utah, Salt Lake City, Utah, USA

24 <sup>10</sup>Institute of Meteorology and Climate Research (IMK-AAF), Karlsruhe Institute of Technology  
25 (KIT), Eggenstein-Leopoldshafen, Germany

26 <sup>a</sup>now at: Chemistry Department, University of Michigan, Ann Arbor, MI

27 <sup>b</sup>now at: College of Engineering Center for Environmental Research and Technology (CE-  
28 CERT); Department of Chemical and Environmental Engineering, University of California  
29 Riverside, Riverside, CA

30 <sup>c</sup>now at: Department of Earth, Atmospheric, and Planetary Sciences, Purdue University, West  
31 Lafayette, IN, USA

32 <sup>d</sup>now at: Air Innova, Boulder, CO, USA

33 <sup>e</sup>now at: ACME AtronOmatic, LLC, Portland, OR, USA

34 <sup>f</sup>now at: Colorado Department of Public Health and Environment, Denver CO, USA

35 <sup>g</sup>now at: Department of Chemistry, Colgate University, Hamilton, NY, USA

36 <sup>h</sup>now at: Faculty 8- Mathematics and Physics, University of Stuttgart, Stuttgart, Germany

37 <sup>i</sup>now at: Rainmaker Technology Corporation, El Segundo, CA, USA

38 <sup>j</sup>now at: Federal Waterways Engineering and Research Institute, Karlsruhe, Germany

39 <sup>k</sup>now at: Yale Center for Law and Policy, New Haven, CT, USA

40 <sup>l</sup>now at: Brookhaven National Laboratory, Richland, WA, USA

41 <sup>m</sup>now at: Sandia National Laboratories, Albuquerque, NM, USA

42 Correspondence: Paul J. DeMott ([Paul.Demott@colostate.edu](mailto:Paul.Demott@colostate.edu))

43

Deleted :

Deleted: Field Intercomparison of Ice Nucleation  
Measurements ...

47 **Abstract**

48 The third phase of the Fifth International Ice Nucleation Workshop (FIN-03) was  
49 conducted at Storm Peak Laboratory in Steamboat Springs, Colorado in September 2015 to  
50 facilitate the intercomparison of instruments measuring ice nucleating particles (INPs) in the field.  
51 Instruments included ~~a subset of~~ two online and four offline measurement systems for INPs, a  
52 subset of those utilized in the laboratory study that comprised the second phase of FIN (FIN-02).  
53 Composition of ~~the total aerosols was~~ characterized ~~using~~ the Particle Ablation by Laser Mass  
54 Spectrometry (PALMS) and Wideband Integrated Bioaerosol Sensor (WIBS) instruments, and  
55 aerosol size distributions were measured by a Laser Aerosol Spectrometer (LAS). The dominant  
56 total particle compositions present during FIN-03 were composed of sulfates, organic compounds,  
57 and nitrates, as well as particles derived from biomass burning. Mineral dust containing particles  
58 ~~types~~ were ubiquitous throughout and represented 67% of supermicron particles. Total WIBS  
59 fluorescing particle concentrations for particles with diameters  $> 0.5 \mu\text{m}$  were  $0.04 \pm 0.02 \text{ cm}^{-3}$  ( $0.1$   
60  $\text{cm}^{-3}$  highest,  $0.02 \text{ cm}^{-3}$  lowest), typical for the warm season in this region and representing  $\approx 9\%$   
61 of all particles in this size range as a campaign average.

62 The primary focus of FIN-03 was the measurement of INP concentration via immersion  
63 freezing at temperatures  $> -33 \text{ }^\circ\text{C}$ . Additionally, some measurements were made in the deposition  
64 nucleation regime at these same temperatures, representing one of the first efforts to include both  
65 mechanisms within a field campaign. INP concentrations via immersion freezing ~~agreed within~~  
66 ~~factors ranging from nearly 1 to 5 times on average between matched (time and temperature)~~  
67 ~~measurements and disagreements only rarely exceeded one order of magnitude for~~ sampling times  
68 coordinated to within three hours. ~~Comparisons were restricted to temperatures lower than  $-15 \text{ }^\circ\text{C}$~~   
69 ~~due to limits of detection related to sample volumes and very low INP concentrations~~. Outliers of

Formatted: Justified

Formatted: Font color: Red, Strikethrough

Deleted: total aerosols were

Deleted: by

Formatted: Font color: Red, Strikethrough

Deleted: ~

Deleted: reported by all ice nucleation instruments

Deleted: generally agreed to within one order of magnitude for measurement and

Deleted: Sometimes, much better agreement was obtained.

77 up to two orders of magnitude occurred between  $-25\text{ }^{\circ}\text{C}$  and  $-18\text{ }^{\circ}\text{C}$ ; better agreement was seen at  
78 higher and lower temperatures. Although the 5-10 factor agreement of INP measurements found  
79 in FIN-03 aligned with the results of the FIN-02 laboratory comparison phase, giving confidence  
80 in progress of this measurement field, this level of agreement still equates to temperature  
81 uncertainties of 3.5 to 5  $^{\circ}\text{C}$  that may not be sufficient for numerical cloud modeling applications  
82 that utilize INP information.

83 INP activity in the immersion freezing mode was generally found to be an order of  
84 magnitude or more, more efficient than in the deposition regime at 95-99% water relative  
85 humidity, although this limited data set should be augmented in future efforts.

86 To contextualize the study results an assessment was made of the composition of INPs  
87 during the late Summer to early Fall period of this study, inferred through comparison to existing  
88 ice nucleation parameterizations and through measurement of the influence of thermal and organic  
89 carbon digestion treatments on immersion freezing ice nucleation activity. Consistent with other  
90 studies in continental regions, biological INPs dominated at temperatures  $> -20\text{ }^{\circ}\text{C}$  and sometimes  
91 colder, while arable dust-like or other organic-influenced INPs were inferred to dominate at most  
92 times below  $-20\text{ }^{\circ}\text{C}$ .

Formatted: Justified

Formatted: Font color: Red, Strikethrough

Formatted: Font color: Red

93 **1 Introduction**

94 Atmospheric ice nucleation is one of the least certain aerosol-cloud interactions influencing  
95 climate (Kanji et al., 2017). ~~Particles that physically catalyze freezing, known as ice-nucleating~~  
96 particles (INPs) (Vali et al., 2015), are found in the atmosphere in concentrations that span many  
97 orders of magnitude, ranging from  $10^{-3}$  L<sup>-1</sup> or fewer at  $-5$  °C to 1000 L<sup>-1</sup> or greater at  $-35$  °C  
98 (Petters and Wright, 2015). INP number concentrations typically increase exponentially with  
99 degree of supercooling below 0 °C. However, chemical composition plays an important role in  
100 determining if, and at what temperature, individual particles may serve as INPs (Murray et al.,  
101 2012). INPs initiate the formation of ice in cold and mixed-phase clouds and in turn influence  
102 their physical and optical properties. An increase in INP concentration over a geographic area  
103 may increase the frequency of glaciated clouds at constant temperature, which in turn increases  
104 precipitation and decreases cloud lifetime (Lohmann and Feichter, 2005). Nevertheless, INP  
105 impacts on clouds simulated in global climate models are highly sensitive to how aerosol's ability  
106 to nucleate ice is parameterized (Boucher et al., 2013). Parameterizations can only be as accurate  
107 as the measurements on which they are based (e.g., Knopf et al., 2021).

108 Measurements of atmospheric INPs remain challenging due to the difficulty representing  
109 the physical processes involved in ice nucleation instruments. At temperatures below  ~~$\approx -38$  °C,~~  
110 micrometer-sized, dilute water droplets spontaneously freeze due to homogeneous freezing  
111 nucleation. Homogeneous freezing nucleation is well understood and included in most cloud  
112 formation models. However, at temperatures between 0 and  $-38$  °C, freezing requires INPs to  
113 facilitate nucleation through a heterogeneous nucleation mechanism (Kanji et al., 2017; Murray et  
114 al., 2012; Vali, 1985). Nucleation is hypothesized to proceed through (1) immersion freezing,  
115 which occurs when an INP embedded within a water droplet enters a cooler environment, and  
116 nucleates an ice crystal, (2) condensation freezing, which occurs when freezing ensues as an

Formatted: Justified

Deleted: Aerosols

Deleted: ~

119 aqueous droplet condenses on the surface of an aerosol particle, (3) contact freezing, which occurs  
120 when an aerosol in contact with a water droplet surface initiates freezing (Durant and Shaw, 2005;  
121 Fornea et al., 2009), and (4) deposition nucleation, which is thought to occur through the direct  
122 deposition of water vapor on an INP surface. Of these mechanisms, immersion freezing nucleation  
123 is thought to be the most active heterogeneous nucleation process in the atmosphere, though there  
124 is considerable disagreement in the literature about the relative importance of other mechanisms  
125 (Kanji et al., 2017; Ullrich et al., 2017). When the ambient humidity is below water saturation,  
126 nucleation can occur via deposition of water from the vapor phase. In some cases, this behavior  
127 may be ascribable instead to water condensation in pores and cavities in aerosols facilitating  
128 freezing through a non-deposition mechanism (Marcolli, 2014; Wagner et al., 2016). However,  
129 this process is unlikely to be of importance at temperatures  $> -38$  °C (David et al., 2020), which  
130 are the focus of this study. We will thus refer to ice nucleation at  $> -38$  °C and below water  
131 saturation as happening within the “deposition regime”. Study of the efficiency of the deposition  
132 nucleation process in comparison to immersion freezing has been limited for natural INPs.

133 Ice nucleation measurements have been made with instruments designed and built by  
134 individual scientists, and more recently with commercial instruments. The ice nucleation  
135 community has a history of collaborating to address instrument performance and inconsistencies  
136 through participating in instrument intercomparisons, in which the custom-built instruments were  
137 operated side-by-side, to evaluate instrument response to the same aerosol populations. Ice  
138 nucleation workshops have a history to 1967, with repetitions occurring in 1970, 1976, and 2007  
139 (DeMott et al., 2011). These exercises were repeated not due to a difference in goals but due to the  
140 development and improvement of new ice nucleation instrumentation and a focus on better  
141 characterization of heterogeneous ice nucleation processes. An additional factor that has motivated

Deleted: ,

143 formal and informal instrument intercomparisons is growing recognition of the importance of  
144 having coordinated detailed aerosol characterizations and better instruments to provide that  
145 information (e.g., Coluzza et al., 2017; DeMott et al., 2011, DeMott et. al, 2018; Knopf et al, 2021;  
146 Brasseur et al., 2022; Lacher et al., 2024). To compare concentrations and compositions of INPs,  
147 a three-part workshop series, the Fifth International Ice Nucleation Workshop, or “FIN” was held  
148 in 2014-2015. The first two phases were held at the Karlsruhe Institute of Technology’s Aerosol  
149 Interactions and Dynamics in the Atmosphere (AIDA) facility. FIN-01 focused on determination  
150 of composition of INPs by mass spectroscopy (Shen et al., 2024), while FIN-02 entailed a  
151 laboratory ice nucleation instrument comparison (DeMott et al., 2018). FIN-03, the mountaintop  
152 field intercomparison of ice nucleation instruments is the focus of this manuscript. While  
153 laboratory experiments can easily provide broad concentration ranges of particles of specific types  
154 for testing, measurements in the ambient atmosphere are the ultimate application of INP measuring  
155 systems, and the ambient atmosphere presents the most challenging measurement scenario due to  
156 sometimes very low INP concentrations and a host of potential INP source compositions.

Deleted: , in preparation

157 Ice nucleation measurements have experienced a renaissance in the past decade, resulting  
158 in a proliferation in both the number of custom-built instruments and a diversification of  
159 measurement techniques employed (Zenker, 2017; DeMott, 2018; Möhler, 2021). Participation in  
160 FIN-02 was twice that of the previous formal international workshop intercomparison in 2007 (the  
161 International Workshop on Comparing Ice Nucleation Measuring Systems, or ICS-2007 held at  
162 the (AIDA) facility (Jones et al., 2011; Kanji et al., 2011). During FIN-02, online and offline  
163 instruments sampling the same population of aerosolized particles reported INP concentrations  
164 that generally agreed within one order of magnitude across a broad temperature range. Agreement  
165 was best in tests of immersion freezing on soils, dusts and bacteria but spanned up to 2 orders of

167 magnitude (or 3 °C in temperature for the same active site density) for illite NX and K-feldspar  
168 (DeMott et al., 2018). While relatively good agreement in the laboratory between different  
169 measurement methods during FIN-02 represented ~~ed~~ significant progress for the atmospheric ice  
170 nucleation community, intercomparisons in ambient atmospheric settings are more difficult due to  
171 lower typical INP concentrations (Lacher et al., 2018) and variations in the chemistry and size of  
172 source aerosol and INPs (DeMott et al., 2017; Knopf, 2021; Lacher et al., 2024; [Brasseur et al.,](#)  
173 [2022](#)).

Deleted: s

174 To evaluate how a suite of instruments operating collectively perform under the greater  
175 measurement challenges of the field setting, FIN-03 was conducted from September 12 to 28, 2015  
176 at Storm Peak Laboratory (SPL) in Steamboat Springs, CO, USA (Elevation: 3220 m MSL).  
177 Unlike the ~~closure~~ studies of Knopf et al. (2021) and the similar comparative sampling studies of  
178 Lacher et al. (2024), both of which occurred in regions surrounded by agricultural activities and  
179 possible nearby urban influences, ~~or the study of Brasseur et al. (2022) that was focused within a~~  
180 ~~boreal forest~~, this remote continental mountaintop site at an elevation of 3220 m provided the  
181 opportunity to sample both regional and long-range INP sources within both the boundary layer  
182 and free troposphere. The site is typically in the free troposphere during the nighttime and early  
183 morning, and in the boundary layer from the late morning to early evening, although topography  
184 and wind direction influence this timing (Collaud Coen et al., 2018). When in the free troposphere,  
185 the site is more likely to reflect influences by regional or long-range transport of aerosols. For  
186 example, during FIN-03, the variety of air masses that were sampled and sensed by aerosol  
187 instruments included ones passing over phosphate mines in Idaho (on September 18 and 20) and  
188 mined deposits of rare earth metals at Mountain Pass, CA (on September 27) (Zawadowicz et al.,  
189 2017). When the convective boundary layer height reaches the elevation of the laboratory, the site

Deleted: subsequent

192 is likely more impacted by local/regional aerosol sources. Additionally, meteorological transitions  
193 can occur (e.g., frontal boundary passage, wind direction shifts), driving changes in aerosol sources  
194 that may indirectly occur in response to those changes (e.g., biological aerosols, carbonaceous  
195 particles from biomass burning, and mineral/soil dust). While the constantly fluctuating  
196 environmental conditions during FIN-03 added an additional challenge to the intercomparison,  
197 they also provided a realistic setting for atmospheric INP measurements. In addition to adding  
198 challenges, conducting the intercomparison in the presence of complex aerosols in the field  
199 provided the opportunity to survey instrument response to varied ~~particle~~ sources.

Deleted: aerosol

200 Participation in FIN-03 included online continuous flow diffusion chambers (CFDCs) and  
201 aerosol collections for offline INP measurements, representing a subset of the instruments that  
202 operated in FIN-02 (DeMott et al., 2018). Online instruments have the advantage that the aerosol  
203 being evaluated as INPs remain free-floating and unaltered, never touching a substrate nor  
204 requiring shipment of samples to a laboratory. Online techniques can also monitor INP  
205 concentration changes occurring over short time scales. Nevertheless, they are limited in the  
206 thermodynamic conditions that can be represented over a given time frame, and they are limited  
207 by volume sampling rates in assessing the low concentrations of INPs at modest supercooling.  
208 Offline techniques, i.e., those in which samples are collected in the field and subsequently  
209 processed in laboratory, provide the opportunity to capture large sample volumes (albeit over  
210 longer time scales) and consequently assess a wider temperature range of INP activation  
211 properties.

Moved (insertion) [3]

Deleted: in

212 Since aerosol physical and chemical properties strongly influence their ability to activate  
213 as INPs (Hoose and Möhler, 2012; Kanji et al., 2017; Murray et al., 2012), measurements of  
214 ~~particle~~ sizes and composition (see Section 2) were included to lend context to the variable

Deleted: aerosol



218 composition of aerosols and evaluate their potential role in ice nucleation activity. Rather than use  
219 these data for attempting closure, FIN-03 focused on using data to constrain existing  
220 parameterizations to diagnose INP compositions during the study period. Also, in contrast to other  
221 recent studies, special effort was made to characterize deposition nucleation activity in addition to  
222 immersion freezing.

## 223 2 Methods

### 224 2.1 Aerosol property measurements

225 Measurements of aerosol physical, chemical, and biological particle properties were made  
226 during FIN-03 to provide context to INP measurements. Sampling manifolds, which draw air into  
227 SPL from outdoors at high flow, are as follows: Inlets were located in each of the two wings of  
228 SPL that frame the living area, referred to as the “instrument” laboratory (facing north) and the  
229 “chemistry” laboratory (facing south). The “original” inlet system in the instrument laboratory  
230 (Hallar et al. 2011; Petersen et al. 2019) feeds a nephelometer (see below) and a standard suite of  
231 aerosol instruments (not operational for FIN-03). This 15 cm diameter aluminum inlet rises 4 m  
232 above the roofline. At  $\approx 1$  m inside the laboratory, it transitions to a 15 cm horizontal manifold.  
233 With a flow of  $\approx 500$  L  $\text{min}^{-1}$ , aerosol transmission calculations have characterized the system to  
234 have a 50% upper particle size cut-off at an aerodynamic diameter of 5  $\mu\text{m}$  (Hallar et al., 2011).  
235 The “new” inlet system consists of two identical stainless steel, turbulent-flow, ground-based inlets  
236 described by Petersen et al. (2019), which are straight and enter the laboratory vertically. One is  
237 in the SPL instrument laboratory, and one is in the chemistry laboratory. These inlets that extend  
238 10 m above the laboratory roof have been demonstrated to have 50% upper particle size cut-offs  
239 at an aerodynamic diameter of approximately 13  $\mu\text{m}$  for a wind speed of 0.5  $\text{m s}^{-1}$ . Additional

Formatted: Justified

Deleted: ~

Deleted: ~

242 computational fluid dynamics simulations suggest that this size cut-off remains above 5  $\mu\text{m}$  even  
243 for exterior wind speeds up to 15  $\text{m s}^{-1}$  (Petersen et al., 2019), higher than achieved at any time  
244 during FIN-03 sampling. Little bias was seen in ambient aerosol sampling between the original  
245 inlet system and the new, turbulent flow-based inlets based on the metric of total aerosol scattering  
246 (Petersen et al., 2019). Flow rates and transfer lines to individual instruments are described after  
247 the aerosol property measurements are introduced, at the conclusion of this section.

248 A Laser Aerosol Spectrometer (LAS, model 3340, TSI Inc., St. Paul, Minnesota, USA)  
249 was used to measure the aerosol size distribution over the diameter range 0.089-10  $\mu\text{m}$ . Aerosols  
250 were assumed dry based on relative humidity always remaining below 30% when measured from  
251 its sample line. Sample was drawn at 0.1  $\text{L min}^{-1}$  and sampling was done from the turbulent flow  
252 inlet system located in the SPL chemistry laboratory, as described further below. Size calibrations  
253 were performed using polystyrene latex spheres (PSL, Duke Scientific). PSL diameters were  
254 converted to ammonium sulfate equivalent diameters using Mie theory (Froyd et al., 2019).  
255 Particle concentrations are reported as a function of equivalent ammonium sulfate diameter.  
256 Volume and surface area distributions are derived assuming spherical particles. Number  
257 concentrations and surface areas, further informed by aerosol composition measurements, allows  
258 for connection to INP concentration predictions, and this information is used herein to  
259 diagnostically infer mineral and soil dust influences on INPs during the study. We will particularly  
260 reference the parameterizations of Niemand et al. (2012) that links mineral surface area to INP  
261 concentrations and DeMott et al. (2015) that links dust number concentrations at sizes larger than  
262 0.5  $\mu\text{m}$  to INP concentrations.

263 Measurements using a three-wavelength integrating nephelometer (TSI Model-3563,  
264 Shoreview, MN) also provided information on aerosol distributions via their optical properties.

Deleted:

266 This nephelometer is part of the National Oceanic and Atmospheric Administration Federated  
267 Aerosol Network (Andrews et al., 2019). The nephelometer splits scattered light into red (700 nm),  
268 green (550 nm), and blue (450 nm) wavelengths. Impactors to cut aerosols at aerodynamic sizes  
269 below 1 and 10  $\mu\text{m}$  are alternately used upstream of air flowing into the instrument. The  
270 nephelometer sampled within the original inlet in the SPL instrument laboratory. A blunt tap from  
271 this original SPL inlet manifold provided air samples to the nephelometer system via 1" i.d.  
272 conductive tubing.

273 The Particle Analysis by Laser Mass Spectrometry (PALMS) instrument performed  
274 measurements of the composition of 0.2 to 3.0  $\mu\text{m}$  aerosol particles. The PALMS was designed  
275 and operated by the National Oceanic and Atmospheric Administration (NOAA) as described in  
276 Thomson et al. (2000). Particles are sampled, focused, and accelerated via an aerodynamic lens  
277 inlet (Schreiner et al., 2002) before passing into a vacuum chamber where they successively pass  
278 through two continuous-wave detection laser beams (532 nm Nd:YAG) and scatter light. Vacuum  
279 aerodynamic diameter is determined based on the transit time. The detection signal triggers an ArF  
280 excimer laser that emits a 193 nm pulse to simultaneously ablate and ionize single particles. The  
281 resulting ions are analyzed with a unipolar time-of-flight mass spectrometer, which allows polarity  
282 switching during the particle flight, thereby producing positive or negative ion mass spectra

283 for individual particles. PALMS spectra are classified into compositional categories, and  
284 fractions are averaged over 5 min sample periods. Number, surface area, and mass concentration  
285 products for the different particle types are generated by combining PALMS size-dependent  
286 fractional composition data with absolute particle concentrations measured by the LAS instrument  
287 (Froyd, et al. 2019; Froyd et al., 2022). When PALMS compositional concentrations are referenced

Deleted: and

Formatted: Justified

289 in the results of FIN-03 aerosol compositions in Section 3.2, they have been determined by these  
290 methods.

291 The NOAA Wideband Integrated Bioaerosol Sensor, Model 4A (WIBS-4A; Droplet  
292 Measurement Technologies, Longmont, CO) was used to detect fluorescent properties of  
293 individual particles and assess the presence of biological particles. Measurements are presumed  
294 to characterize dry particles. The WIBS-4A is described in detail elsewhere (Gabey et al., 2010;  
295 Kaye et al., 2005; Perring et al., 2015) and is only briefly summarized here. As described in  
296 Zawadowicz et al. (2019), the gain for the WIBS-4A used at SPL was set to detect and classify  
297 particles between 0.4 and 10  $\mu\text{m}$ . First, the optical diameter of particles entering the detection  
298 cavity is determined by light scattered during transit through a 635 nm laser beam. This signal  
299 triggers the sequential firing of two xenon flash lamps filtered to produce narrow excitation  
300 wavebands centered at 280 and 370 nm. The resulting fluorescence is detected by two wideband  
301 photomultiplier detectors observing 310-400 nm and 420-650 nm. Fluorescing particles were  
302 categorized according to the intensity of the signal in each of three channels (channel A excitation  
303 280 nm/emission 310-400 nm, channel B excitation 280 nm/emission 420-650 nm, channel C  
304 excitation 370 nm/emission 420-650 nm). Particles for which the measured emission intensity in  
305 only one channel met the threshold (such that the signal intensity exceeded the value equal to three  
306 standard deviations above the mean) were assigned Type A, B, or C, and particles for which the  
307 measured emission intensity in two or more channels met the threshold were assigned Type AB,  
308 BC, BC, or ABC (Perring et al., 2015). The interpretation of particle composition according to  
309 the seven WIBS-4A channels is not straightforward, as many fluorophores are active in each  
310 channel, including non-biological components (Perring et al., 2015; Pöhlker et al., 2012). Channel  
311 A fluorophores include biological components such as tryptophan, phenylalanine as well as

312 nonbiological components which interfere with the determination of biological content, including  
313 polycyclic aromatic hydrocarbons (PAHs) (pyrene, naphthalene, phenanthrene). Biological  
314 fluorophores, which produce a signal in channel C, include the reduced form of nicotinamide  
315 adenine dinucleotide (NADH), nicotinamide adenine dinucleotide phosphate (NADPH), and  
316 riboflavin, and potential non-biological interference in channel C may result from the presence of  
317 humic acid in aerosol particles. Channel B fluorophores are not generally considered to be  
318 biological in nature, though riboflavin and dry cellulose both produce signals in this channel.

319 We report WIBS-4A channel data herein under these noted caveats and further utilize these  
320 data to explore links to immersion freezing biological INP concentrations, as has been done in  
321 some previous efforts. Tobo (2013) previously reported relations of biological INPs acting in the  
322 immersion freezing mode (measured by the [Colorado State University \(CSU\), CFDC](#)) to  
323 fluorescent biological aerosol particles (FBAP) at sizes > 0.5 μm measured in the understory of a  
324 Ponderosa pine forest in Colorado. In that work, an ultraviolet aerodynamic particle sizer (UV-  
325 APS) with excitation wavelength at 355 nm and emission wavelengths 420-575 nm was used as a  
326 reference for FBAP concentrations. Due to differences between the excitation and emission  
327 wavelengths, UV-APS measurements correspond most closely with Type C particles detected by  
328 the WIBS-4A (Healy et al., 2014). Consequently, a conservative or “low” estimate of FBAP for  
329 use in the parameterization of Tobo et al. (2013) we employ herein uses the sum of C, AC, BC and  
330 ABC particles. A “high” FBAP for this parameterization has also been used by Twohy et al.  
331 (2016), considering all non-B-only particles (A, AB, ABC, AC, BC, C). We will use both  
332 definitions in our presented results and partly justify the higher estimate because the CSU-CFDC  
333 assuredly does not capture all biological INPs due to the use of the upstream impactor ([see below](#)).  
334 A final class of particles defined by WIBS-4A data for relation to immersion freezing INPs are

Deleted: CSU

Deleted:

337 denoted as FP3 particles (Wright et al., 2014). FP3 particles are particles that show strong emission  
338 in the 310 to 400 nm spectral band when excited by 280 nm light (A type) but are only weakly  
339 represented as B and C types. A threshold of 1900 arbitrary fluorescence units in the 310 to 400  
340 nm band is used to denote FP3 particles (Wright et al., 2014). FP3 particles have been connected  
341 to immersion freezing INP concentrations in multiple environments (Wright et al., 2014; Suski et  
342 al., 2018; Cornwell et al., 2023).

343 Flow rates and transfer lines to each instrument are summarized as follows. The PALMS,  
344 LAS, and WIBS-4A sampled from the SPL turbulent flow inlet stack at 0.75, 0.1, and 0.3 vlp~~m~~,  
345 respectively, via a common 0.19" i.d. aluminum tube. The total flow was held at 1.2 vlp~~m~~ using a  
346 variable dump flow, and the line was split into multiple 0.115" o.d. stainless steel tubing sections  
347 connecting to each instrument. All tubing junctions employed Y-splitters, and all reducing fittings  
348 were internally beveled to prevent impaction losses. Sample lines were not actively dried, but  
349 relative humidity was < 30% in LAS and WIBS-4A. For the LAS instrument, the theoretical  
350 transmission of the inlet system was 98%, 84%, and 57% for 1, 3, and 5 μm aerodynamic diameter  
351 particles, respectively, with gravitational settling being the dominant loss process. Transmission  
352 to WIBS-4A for the same sizes was 99%, 90%, and 76%. Size distributions were not corrected for  
353 transmission losses. The nephelometer sampled from the original inlet in the SPL instrument  
354 laboratory via a blunt tap manifold and 1" i.d. conductive tubing.

## 355 2.2 INP measurement methods

356 All specific instruments used in FIN-03 were also used in the FIN-02 laboratory campaign.  
357 A summary listing of all ice nucleation instruments utilized in FIN-03 is provided in Table 1.  
358 Detailed operating principles, siting of samplers (rooftop versus within SPL), and experimental  
359 methods for each instrument follow below. In this work, we will refer to the FIN-03

Deleted:

Deleted:

Deleted: a common

Deleted: 1/4

Deleted: o

Deleted: 1/8

Formatted: Justified

366 “intercomparison period” to define the times that all INP instruments co-sampled air with  
 367 substantial temporal overlap for direct comparison. This means that on a given day a sample was  
 368 fully collected within the comparison time unit of 3 hours (informed by aerosol data, as discussed  
 369 later) or overlapped the comparison period if the collection time was somewhat longer. Other times  
 370 of sampling by the different instrument groups were devoted to special science investigations only  
 371 partly covered herein.

372  
 373 **Table 1** Descriptions of INP instruments.

	Instrument	Type	Institute	References
Online/direct	Continuous flow diffusion chamber (CSU-CFDC)	Continuous flow diffusion chamber (cylindrical)	Colorado State University	(Eidhammer et al., 2010; Rogers, 1988; Rogers et al., 2001)
	Spectrometer for ice nuclei (MIT-SPIN)	Continuous flow diffusion chamber (parallel)	Massachusetts Institute of Technology	(Garimella et al., 2016; Garimella et al., 2017; Kulkarni & Kok, 2012)
Offline/post-processing	Frankfurt Ice Nuclei Deposition Freezing Experiment deposition mode (FRIDGE-DC)	Low pressure diffusion chamber (on wafers)	Goethe University Frankfurt	(Schrod et al., 2016)
	Frankfurt Ice Nuclei Deposition Freezing Experiment immersion freezing mode (FRIDGE-CS)	Cold stage droplet freezing array (on wafers)	Goethe University Frankfurt	(Schrod et al. 2020; DeMott et al. 2018)
	Ice spectrometer (CSU-IS)	Aliquot freezing array	Colorado State University	(Hill et al., 2016; Hiranuma et al., 2015)
	Cold stage (NCSU-CS)	Cold stage droplet freezing array (on hydrophobic glass slides)	North Carolina State University	(Wright & Petters, 2013; Yadav et al., 2019)

Deleted: FRIDGE-DEP

Deleted: IMM

Deleted: State

377

378

379 **2.2.1 Online INP measurements**

380

381

382

383

384

385

386

387

388

389

390

391

392

393

394

395

396

397

398

399

Two online instruments participated in intercomparison experiments in FIN-03. We describe the basic design and operating principles and procedures, sampling inlets, measurement uncertainties and correction for false counting issues, and any special studies reported herein for the CFDC instruments from CSU and the Massachusetts Institute of Technology (MIT). A third CFDC from Texas A&M University was used primarily for special studies to develop depolarization detection of ice, already reported (Zenker et al., 2017).

The CSU-CFDC

This online INP instrument has the most established history as an online technique for activating and counting INPs. The CSU-CFDC operating principles are described in prior works (Rogers, 1988; Rogers et al., 2001; Eidhammer et al., 2010). Application and considerations for interpreting data have been described by DeMott et al. (2018). The CSU-CFDC is composed of nested cylindrical copper walls that are chemically ebonized to be hydrophilic so they can be evenly coated with ice. The chamber is divided into two sections vertically. For FIN-03, the CSU-CFDC was operated to establish a temperature gradient between the colder (inner) and warmer (outer) ice walls in the upper  $\approx 50$  cm “growth” section to produce either water subsaturated or water supersaturated conditions at various temperatures within a central lamina. Aerosol particles were directed into that central lamina. For the flow rates used (10 vlp total flow, 1.5 vlp sample flow) the residence time was  $\approx 5$  s in the growth region. Ice crystals forming on INPs in the growth section continued to grow for  $\approx 2$  s in the lower  $\approx 35$  cm “evaporation” section of the chamber where the outer wall temperature was adjusted to be at an equivalent temperature to the inner (cold) wall

**Moved up [3]:** Online instruments have the advantage in that the aerosol being evaluated as INPs remain free-floating and unaltered, never touching a substrate nor requiring shipment of samples to a laboratory. Online techniques can also monitor INP concentration changes occurring over short time scales. Nevertheless, they are limited in the thermodynamic conditions that can be represented over a given time frame, and they are limited by volume sampling rates in assessing the low concentrations of INPs at modest supercooling. Offline techniques, i.e., those in which samples are collected in the field and subsequently processed in laboratory, provide the opportunity to capture large sample volumes (albeit over longer time scales) and consequently assess a wider temperature range of INP activation properties.

**Deleted: 2.2 INP measurement methods**  
A combination of direct-processing (online) and post-processing (offline) ice nucleation instruments were employed during the FIN-03 field campaign. All these instruments were also used in the FIN-02 laboratory campaign. Online instruments have the advantage in that the aerosol being evaluated as INPs remain free-floating and unaltered, never touching a substrate nor requiring shipment of samples to a laboratory. Online techniques can also monitor INP concentration changes occurring over short time scales. Nevertheless, they are limited in the thermodynamic conditions that can be represented over a given time frame, and they are limited by volume sampling rates in assessing the low concentrations of INPs at modest supercooling. Offline techniques, i.e., those in which samples are collected in the field and subsequently processed in laboratory, provide the opportunity to capture large sample volumes (albeit over longer time scales) and consequently assess a wider temperature range of INP activation properties. A summary listing of all ice nucleation instruments is provided in Table 1. Detailed operating principles, siting of samplers (rooftop versus within SPL), and experimental method... [1]

**Deleted:** . One, the Colorado State University

**Deleted:** (CSU-CFDC)

**Formatted:** Underline

**Formatted:** Underline

**Deleted:** ,

**Formatted:** Justified

**Deleted:** several

**Deleted:** in detail in several publications, most recently by

**Deleted:** . (

**Deleted:** ~

**Moved (insertion) [1]**

**Moved up [1]:** Aerosol particles were directed into that central lamina. Ice crystals forming on INPs in the growth

**Deleted:** ~

**Deleted:** ~

**Deleted:** ~



477 to promote evaporation of liquid drops. When operating in the water supersaturated regime, water  
478 relative humidity was controlled to be nominally at 105% during FIN-03 to stimulate droplet  
479 growth and subsequent freezing, for best comparison to offline immersion freezing methods. For  
480 probing ice nucleation in the deposition nucleation regime, relative humidity (RH) was controlled  
481 to  $\approx 95\%$ . ~~Temperature uncertainty is  $\pm 0.5$  °C at the reported CSU-CFDC lamina processing~~  
482 ~~temperature and relative humidity uncertainty depends inversely on temperature, as discussed by~~  
483 ~~DeMott et al., (2018), estimated for example as 2.4 % for a lamina RH of 105% at  $-25$  °C.~~  
484 ~~Processing temperatures spanned  $-15$  to  $-32$  °C during FIN-03.~~

Deleted: ~

485 The CSU-CFDC sampled from one of the turbulent aerosol inlet ports, located in the SPL  
486 instrument laboratory. Connection was via  ~~$\frac{1}{4}$ " o.d (0.19" inner diameter)~~ conductive tubing. Prior  
487 to entering the CFDC, aerosol was further dried using two inline diffusion driers and then size-  
488 limited using dual single-jet impactors that achieve a 50% upper particle size cut-off at an  
489 aerodynamic diameter of  $2.5$   $\mu\text{m}$ . This limitation on aerosol sizes helps to remove ambiguity when  
490 distinguishing ice crystals at  $\approx 4$   $\mu\text{m}$  sizes from aerosol particles using an optical particle counter  
491 at the CSU-CFDC outlet. ~~Counts greater than this size divided by sample volume define INP~~  
492 ~~concentrations.~~

Deleted: .

Formatted: Font color: Red, Strikethrough

493 ~~Uncertainty in calculation of INP concentrations must account~~ for background counts that  
494 can occur due to ejection of frost emanating from interior surfaces of the CSU-CFDC over  
495 operational periods. ~~We follow Levin et al. (2019) in this regard.~~ Frost corrections are defined  
496 ~~through via use of time intervals of~~ sampling ambient air through a HEPA filter. ~~A typical daily~~  
497 ~~cycle at each temperature point was to bookend 10-min ambient air sampling with 5-min filter~~  
498 ~~periods.~~ Sample data were background corrected by subtracting the interpolated filter period  
499 concentration before and after each sampling period. Background corrected data were then

Deleted: ~

Deleted: Temperature uncertainty is  $\pm 0.5$  °C at the reported CSU-CFDC lamina processing temperature and relative humidity uncertainty depends inversely on temperature, as discussed by DeMott et al., (2018), estimated for example as 2.4 % at  $-25$  °C.

Deleted: To correct

Deleted: , and for defining measurement uncertainties, we

Formatted: Font color: Red, Strikethrough

Formatted: Font color: Red, Strikethrough

510 averaged to ~~≈~~5-min sampling times to increase statistical confidence. Poisson counting errors  
511 during filtered and ambient sampling periods were added in quadrature, and INP concentrations  
512 were judged statistically significant at the 95% confidence level if they were greater than 1.64  
513 times this combined INP error (one-tailed z test). Interior inlet tubing losses are not considered in  
514 the reported INP data because they have been estimated at 10% or less in the past. INP  
515 concentration correction underestimates inferred (by ~~a factor of 3~~ ~~2-time~~) to be due to aerosols  
516 spreading outside of the lamina during measurements specifically of mineral dust INPs (DeMott  
517 et al., 2015) are not generally applied to the data herein, though this is discussed ~~regarding the~~  
518 ~~intercomparison results and~~ INP parameterizations in this paper.

Deleted: ~

Formatted: Font color: Red, Strikethrough

Deleted: regarding

519 An aerosol concentrator (MSP Model 4240) was used at selected times during FIN-03 to  
520 improve sampling statistics, in the same manner as in previously published studies (Tobo et al.  
521 2013; Suski et al., 2018; Cornwell et al., 2019). The aerosol concentrator was positioned open to  
522 the air on the roof of the instrument laboratory room (covered and not used during rainfall), with  
523 a short ~~¼0.19" o.d.~~ inner diameter copper line containing the concentrated aerosol entering the  
524 laboratory vertically from about 3 m above the CFDC. Concentration factors for INPs can vary  
525 depending on the ambient INPs present in a given environment. These were evaluated in the same  
526 manner as Tobo et al. (2013), leading to an average increase of INPs by 90 times (~~±45~~) during  
527 operation of the aerosol concentrator compared to ambient inlet periods during ~~this~~ study (not  
528 shown here because analysis repeats ~~the efforts referenced above~~). A three-way manual stainless-  
529 steel valve was used to direct sample air to the CSU-CFDC from either the turbulent flow inlet or  
530 the aerosol concentrator.

Formatted: Font color: Red, Strikethrough

Formatted: Not Strikethrough

Formatted: Font color: Red, Strikethrough

Deleted: e

Moved (insertion) [2]

Deleted: numerous

Deleted: past efforts

Moved up [2]: A three-way manual stainless-steel valve was used to direct sample air to the CFDC from either the turbulent flow inlet or the aerosol concentrator.

Deleted: At times,

Deleted: or a single particle soot photometer (Schill et al., 2016) was

Deleted: or black carbon (not reported here)

531 Supplemental studies with the CSU-CFDC reported herein used a high temperature heating  
532 tube (Suski et al., 2018), placed in-line following the three-way valve for removing aerosol organics,

545 prior to INP measurements. The use of a tube heater upstream of the CSU CFDC to expose single  
546 particles to 300°C, is intended to isolate the action of total organic versus inorganic INPs via  
547 comparison of ambient versus heat-treated particle streams. Simultaneous measurements of heated  
548 and unheated aerosol streams are not possible with a single CFDC, so sampling was conducted by  
549 alternating the channel chosen following a flow splitter during subsequent 10-minute periods, and  
550 ignoring aerosol changes that rarely occurred over such short times.

551 The MIT Spectrometer for Ice Nuclei (SPIN)

552 The MIT-SPIN (Droplet Measurement Technologies, Boulder, CO), a commercially  
553 produced, parallel-plate CFDC, also sampled during FIN-03. Measurements were focused on ice  
554 nucleation below water saturation for FIN-03. Operating principles are described in Garimella et  
555 al. (2016) and Garimella et al. (2017). SPIN consists of two flat walls separated by 1.0 cm and  
556 coated in approximately 1.0 mm of ice. Aerosol particles are fed into the chamber in a lamina flow  
557 of about 1.0 liters per minute and are constrained to the centerline with a sheath flow of about 9.0  
558 liters per minute. The temperature and relative humidity that the aerosol lamina experiences were  
559 controlled by varying the temperature gradient between the two iced walls (Kulkarni & Kok,  
560 2012). After exiting the nucleation chamber, the particles enter SPIN's optical particle counter,  
561 which sizes aerosol on a particle-by-particle basis for diameters between 0.2 and 15 µm.

562 Temperature uncertainty was 0.5 °C. For the lamina RH conditions below 100% used in FIN-03,  
563 the RH uncertainties were 0.7, 1.3 and 1.7% at -20, -25, and -30 C, respectively.

564 The MIT-SPIN sampled from one of the turbulent flow inlet systems, located within the  
565 SPL aerosol chemistry laboratory. It was connected to the inlet system port with a short section of  
566 0.19" inner diameter conductive tubing.

**Deleted:** , following the methods of Suski et al. (2018),

**Deleted:** both

**Deleted:** is

**Deleted:** of course

**Deleted:** inlet

**Deleted:** any very short-term

**Deleted:** might

**Deleted:** This was a special contribution by the CSU CFDC group, for comparison to bulk aerosol treatments discussed in the next subsection.

**Formatted:** Underline

**Formatted:** Underline

**Formatted:** Underline

**Deleted:** A second online instrument, the SPectrometer for Ice Nuclei operated at the time by the Massachusetts Institute of Technology (

**Deleted:** ;

**Deleted:** continuous flow diffusion chamber style instrument...

**Deleted:** a

**Deleted:**

**Deleted:** For FIN-03, the SPIN

**Deleted:** ¼"

**Deleted:** o.d.

588 Data processing for SPIN, including definition of uncertainties, was performed following  
589 similar procedures as used for the CSU-CFDC instrument, with a few distinctions. A cut-size for  
590 potential ice particles was set to 5  $\mu\text{m}$  diameter. A low-pass filter was applied next to remove all  
591 1 Hz data that exceeded a total of three counts  $\text{s}^{-1}$ , as recommended by Richardson et al. (2007) to  
592 reduce frost background noise that equated to INP concentrations larger than about 200  $\text{L}^{-1}$  (>2  
593 standard deviations above mean values discussed later) for the SPIN sampling flow rate. A  
594 depolarization filter was next applied to isolate particle data specific to ice using 1 Hz averaged  
595 backscattering data from the SPIN's OPC, with instrument specific values of 3.5 and -0.25 for the  
596  $\log_{10}(\text{Size})$  and  $\log_{10}(\text{S1/P1})$  measurements respectively (Garimella et al., 2016). Ice particle data  
597 was then converted from counts per second to number density per volume of sample flow ( $\text{L}^{-1}$ ).  
598 Frost ejected from the plates of the SPIN chamber beyond that removed by the low-pass filter was  
599 characterized using particle-free sampling periods when the sample flow was diverted through a  
600 HEPA filter by an automated three-way valve. Linear interpolation of filter period INP  
601 concentrations was used to approximate background frost concentrations throughout the  
602 measurement period (a minimum of 4, 5-min filter periods for each set-point temperature within a  
603 2–3-hour period) and smoothed using a five-minute moving average. Sample data was background  
604 frost corrected by subtracting this smoothed background frost density from total number density  
605 in each 5-min sample period. Finally, a SPIN specific particle concentration correction factor of  
606 1.4 is applied to account for non-ideal instrument behavior (e.g., out of lamina particles) resulting  
607 in underestimation of INPs as described by Garimella et al. (2017). As the field measurements  
608 from this study predate the laboratory experiments performed to determine SPIN uncertainties, the  
609 minimum reported correction factor was selected to remain conservative in reported  
610 measurements.

**Deleted:** a

**Deleted:** Particle counts from the OPC were first filtered to only consider

**Deleted:** larger than

**Formatted:** Superscript

**Formatted:** Superscript

**Deleted:**

**Deleted:** Particle

**Deleted:** n

**Deleted:** using the combined sheath and sample flow exiting the OPC... A SPIN specific particle concentration A SPIN specific particle concentration correction factor of 1.4 is applied to account for non-ideal instrument behavior resulting in underestimation of INP as described by Garimella et al. (2017). As the field measurements from this study predate the laboratory experiments performed to determine SPIN uncertainties, we select the minimum reported correction factor to remain conservative in our measurements. A depolarization filter was then applied to isolate particle data specific to ice using 1 Hz averaged backscattering data from the SPIN's OPC, with instrument specific values of 3.5 and -0.25 for the  $\log_{10}(\text{Size})$  and  $\log_{10}(\text{S1/P1})$  measurements respectively.

**Deleted:** A SPIN specific particle concentration correction factor of 1.4 is applied to account for non-ideal instrument behavior resulting in underestimation of INP as described by Garimella et al. (2017). As the field measurements from this study predate the laboratory experiments performed to determine SPIN uncertainties, we select the minimum reported correction factor to remain conservative in our measurements. A depolarization filter was then applied to isolate particle data specific to ice using 1 Hz averaged backscattering data from the SPIN's OPC, with instrument specific values of 3.5 and -0.25 for the  $\log_{10}(\text{Size})$  and  $\log_{10}(\text{S1/P1})$  measurements respectively.

**Deleted:** by

**Deleted:** Lastly, data points that exceeded water saturation were excluded from analysis.

647 ~~As for the CSU-CFDC, estimation of INP concentration~~ measurement error for the MIT-  
648 SPIN ~~assumed~~ the background corrected INP concentration follows a Poisson distribution. Then,  
649 the Poisson error for both INP and background frost concentrations were defined as the square root  
650 of the sample mean. The significance test statistic was defined by the quadrature sum of counting  
651 errors multiplied by the z-score for a one-tailed z-test at the 95% confidence interval. INP  
652 measurements were deemed statistically significant if the mean INP concentration was greater than  
653 this test statistic.

**Deleted:** Estimation

**Deleted:** follows a similar procedure to the CSU-CFDC. Assuming...

### 654 655 2.2.2 Offline INP measurements

**Deleted:** A third online instrument, the Texas A&M CFDC that shares the same design aspects of the CSU CFDC, was used for special studies conducted outside of intercomparison exercises (Zenker et al., 2017).

656 Offline methods have undergone many improvements in recent years and have been  
657 successfully ~~used~~ in a complementary manner ~~for comparison~~ to online methods in other recent  
658 intercomparisons (DeMott et al., 2017; DeMott et al., 2018; Hiranuma et al., 2015; Wex et al.,  
659 2015; ~~Knopf et al., 2021; Brasseur et al., 2022; Lacher et al., 2024~~). In FIN-03 ~~particles~~ were  
660 collected ~~from the air using~~ liquid impingers and filter samplers. ~~Impinger liquid and water~~  
661 ~~suspensions created from immersed filters~~ were analyzed for immersion freezing of ~~distributed~~  
662 ~~droplet volumes~~, using the North Carolina State University Cold Stage (Wright et al., 2013), the  
663 CSU Ice Spectrometer (Hiranuma et al., 2015; DeMott et al., 2018), and the FRankfurt Ice Nuclei  
664 Deposition FreezinG Experiment (FRIDGE) instrument (Schrod et al., 2016). ~~All measurements~~  
665 ~~were made offsite after the return of impinger liquid and filters to the participant institutions, as~~  
666 ~~done in most intercomparisons of this type. The handling of samples is mentioned regarding each~~  
667 ~~instrument below.~~

**Formatted:** Justified

**Deleted:** demonstrated for being

**Deleted:** samples

**Deleted:** with

**Deleted:** and

**Deleted:** distributed

**Deleted:** liquid particle suspensions

668 The North Carolina State University Cold Stage (NCSU-CS)

**Deleted:** State

683 The North Carolina State University cold stage (NCSU-CS) has been previously described  
684 by Wright and Petters (2013) and Hader et al. (2014). Procedures used for collecting immersion  
685 freezing spectra are described below and by Yadav et al. (2019). During FIN-03, filter samples,  
686 impinger samples and precipitation samples were collected for analysis using the NCSU-CS. For  
687 the intercomparison, the filter and impinger results are considered. Filter samples were collected  
688 from the roof of Storm Peak Lab for 3–4 hours, twice daily using 47 mm Nuclepore polycarbonate  
689 filters (0.2 μm pore size) housed in an open-faced stainless-steel filter holder operated at 14 L  
690 min<sup>-1</sup> (at altitude) or ≈9 L min<sup>-1</sup> at standard temperature and pressure conditions (STP) of 1013 mb  
691 and 0 °C. Filter holders were directed downward and sheltered from precipitation by a large,  
692 inverted metal bowl. Images are shown in supplemental Section S1. Each filter was resuspended  
693 in 6 ml prefiltered HPLC grade ultrapure water. Impinger samples were collected directly into  
694 ultrapure water using a glass bioaerosol impinger (SKC, Inc.) as described by Hader et al. (2014)  
695 and DeMott et al. (2018). The impinger jets air at 10.6 L min<sup>-1</sup> (≈7 L min<sup>-1</sup> STP) into a 20 mL  
696 water reservoir, impacting 80% of particles ≥ 200 nm in diameter and ≈100% of particles ≥ 1 μm  
697 (Willeke et al., 1998). Impinger samples were collected in the same manner as was done for all  
698 shared liquid samples for the FIN-02 intercomparison (DeMott et al., 2018) except that Teflon tape  
699 replaced stopcock grease to seal the impinger glass lid to prevent jamming. Water evaporating  
700 from the reservoir was replaced hourly; the impinger was in a rooftop shelter with its inlet  
701 extending horizontally through a hole in the shelter wall, into the open air at a height of ≈6 feet  
702 below the position of filter sampling units that were mounted on an outside railing. Water used  
703 onsite was filtered (0.2 μm) Milli-Q water. All samples were stored at –20 °C onsite, shipped on  
704 dry ice, then stored at –80 °C until analysis at NCSU.

Deleted: NC State

Deleted: ,

Deleted: NC State

Deleted: rs

Deleted: ~

Deleted: ~

Deleted: ~

Deleted: ing

Deleted: ~

714 Freezing statistics for each liquid sample were acquired by pipetting an array of  
 715 approximately 256 droplets of  $1 \mu\text{L} \pm 0.88\%$  volume on four hydrophobic glass slides under dry  
 716  $\text{N}_2$  gas. Temperature was ramped at a rate of  $-2 \text{ }^\circ\text{C min}^{-1}$  and freezing was detected at a temperature  
 717 resolution of  $0.17 \text{ }^\circ\text{C}$  (every 5 s) using CCD camera images collected from an optical microscope.  
 718 Temperature uncertainty based on repeatability of homogeneous freezing tests is  $0.1 \text{ }^\circ\text{C}$  (Hiranuma  
 719 et al., 2015). Except for pure dust samples, the dependence of the population median freezing  
 720 temperature on cooling temperature is less than  $1 \text{ }^\circ\text{C}$  per decade in cooling rate, including  
 721 measurements of ambient INPs (Wright et al., 2013). A decade in cooling rate is much larger than  
 722 the variations in cooling rate used by instruments in FIN-03 ( $-0.33$  to  $2 \text{ }^\circ\text{C min}^{-1}$ ). The expected  
 723 shift in INP spectra due to variability in cooling rate is much less than the total uncertainty and  
 724 thus corrections for cooling rate are not further considered here. The concentration of ice nuclei at  
 725 temperature  $T$  per unit volume of liquid is given by Vali (1971):

$$c_{IN}(T) = \frac{-\ln(f_{\text{unfrozen}}(T))}{V_{\text{drop}}\Delta T} \quad (1)$$

727 where  $f_{\text{unfrozen}}$  is the fraction of unfrozen droplets at  $T$  and  $V_{\text{drop}}$  is the population-median droplet  
 728 volume. The concentration of ice nucleating particles (INP) in the atmosphere is given by:

$$c_{INP}(T) = \frac{c_{IN}(T) \cdot f \cdot V_{\text{liquid}}}{V_{\text{air}}} \quad (2)$$

730 where  $f$  accounts for any serial sample dilutions with pure water used to focus measurements within  
 731 different temperature ranges,  $V_{\text{liquid}}$  is the liquid suspension sample volume, and  $V_{\text{air}}$  is the volume  
 732 of air sampled (flow rate at STP  $\times$  duration). The high temperature resolution freezing data were  
 733 collected  $3\times$  per sample and  $f_{\text{unfrozen}}$  was binned into  $1 \text{ }^\circ\text{C}$  intervals for spectral calculations.  
 734 Confidence intervals reported in archived data were given as  $\pm 2$  standard deviations of the mean  
 735 temperature uncertainty of measurements (typically  $0.5$  to  $1 \text{ }^\circ\text{C}$ ). We will refer to the processed

Deleted: optically by a microscope

Formatted: Font: Not Italic

Formatted: Font: Not Italic

Formatted: Font: Not Italic

Formatted: Font: Not Italic

Formatted: Font: Not Italic

Formatted: Font: Not Italic

Formatted: Font: Not Italic

Deleted: Freezing temperature spectra are expected to be independent of cooling rate (Wright et al., 2013).

Formatted: Font: Not Italic

Formatted: Font: Not Italic

Deleted: Freezing

Deleted: spectra

Formatted: Font: Italic

Formatted: Font: Italic, Subscript

Deleted: are

742 filter samples as NCSU-CS (F) and processed impinger samples as NCSU-CS (I). Note that the  
743 filter samples were more concentrated by a factor  $\approx 5$  due to the greater  $V_{liquid}$  used in the impinger  
744 for the stated air collection volumes. Thus, the filter technique is more sensitive and has a lower  
745 limit of detection (LOD). The precise ratio for a specific experimental period depended on the  
746 exact sampling times of filter and impinger, and the exact number of droplets analyzed for the  
747 filter, impinger sampling, averaging across repeats, and binning into 1-degree intervals. For this  
748 reason, the ratio of LOD for the averaged samples may differ slightly from this estimate.

**Deleted:** NC State

**Deleted:** NC State

**Formatted:** Font: Italic

**Formatted:** Font: Italic, Subscript

749 As for all INP samples in FIN-03, “blanks” were collected for each of the NCSU-CS  
750 sample types. The normal procedure for most blank filter assessments in the field is to momentarily  
751 expose a clean filter to flow in a collection unit. In the spirit of procedural testing that typifies  
752 workshops like FIN-03, a different method was trialed by the NCSU group., Ten filter “blanks”  
753 were specially collected on days during FIN-03 by placing a 0.2  $\mu\text{m}$  pore size filter as a backing  
754 filter to an 0.05  $\mu\text{m}$  pore size filter in a secondary filter unit that was exposed to the same total  
755 ambient flow conditions as the primary INP filter unit. This 0.2  $\mu\text{m}$  filter was processed the same  
756 as the primary INP filter (rinsed in 6 ml ultrapure water) and freezing results were presumed to  
757 provide a quite conservative estimate of filter background INPs. It was indeed found that the  
758 number of INPs per blank filter in these collections were much higher than for standard blank filter  
759 method used by the other groups. The results from the 10 blank filters were averaged across the  
760 processed temperature range, and an upper confidence limit of 1  $^{\circ}\text{C}$  was defined. All INP  
761 concentration results for each ambient filter were rejected if in any given temperature bin they fell  
762 below this upper confidence bound. In sum, 20% of the original measurement points based on  
763 filter collections were removed from measurement intercomparisons by this blanking operation.  
764 Impinger blanks were collected via separation of some water from the pure water storage container

**Formatted:** Justified, Indent: First line: 0.5"



767 each time the impinger unit was filled with pure water to begin an air sampling period. Thus,  
768 blanks were specific to each ambient sample. The same 1 °C upper confidence bound that  
769 characterizes NCSU-CS measurements was applied in each case to identify sample temperature  
770 points where the liquid suspension INPs fell below the upper confidence limit of the impinger  
771 blanks. These were removed from intercomparisons.

772 CSU Ice Spectrometer (CSU-IS)

773 The CSU-IS also post-processed particles sampled onto filters during FIN-03. This  
774 instrument has been described in Hiranuma et al. (2015) and Suski et al. (2018). Samples were  
775 collected for approximate periods of 4 hours for intercomparison periods (longer for overnight  
776 samples – not part of the intercomparison) using pre-cleaned 0.2 µm pore diameter, 47 mm  
777 polycarbonate Nuclepore filters (Suski et al., 2018) mounted in disposable, sterile open-faced and  
778 face-up holders (Nalgene), with a typical sample flow rate of 14.9 L min<sup>-1</sup> (ambient) and 9.5 L  
779 min<sup>-1</sup> (STP). Filters were collected on the same exterior laboratory roof railing as the NCSU filters,  
780 approximately 2 m distant. All filter samples were frozen following collection and stored at -20 °C  
781 before transit on dry ice and storage again at -20 °C until processing at the CSU laboratory. Pre-  
782 sterilization procedures and overall clean protocols for preparation and handling of filters are  
783 detailed in Suski et al. (2018) and Barry et al. (2021b). Particle re-suspension was done through  
784 20 minutes of shaking filters in sterile 50 mL Falcon polypropylene tubes (Corning Life Sciences)  
785 with 6-10 mL of 0.02 µm pore diameter filtered deionized water. Further 20-fold dilutions using  
786 filtered water were made as needed to permit measurement of freezing spectra to the low  
787 temperature limit of operation of the CSU-IS.

788 Immersion freezing INP temperature spectra were obtained by distributing 24 - 32 aliquots  
789 of 50 µL particle suspensions into the sterile 96-well PCR trays that mount in the CSU-IS. Other

Deleted: NC State  
Deleted: distance away  
Deleted: ,

793 wells were filled with serial dilution samples and pure water. The cooling rate was  $-0.33\text{ }^{\circ}\text{C min}^{-1}$ . Frozen wells were counted at  $0.2 - 1\text{ }^{\circ}\text{C}$  degree intervals to a limit of about  $-28\text{ }^{\circ}\text{C}$ , and cumulative numbers of INP  $\text{mL}^{-1}$  of suspension estimated using Eq. 1. Conversion to ambient air concentrations  $\text{std L}^{-1}$  were made based on distributed suspension volume and the total air volumes collected (Eq. 2). Several filter blanks were collected during FIN-03, and one was tested and used to obtain background INP numbers per filter. Blank INPs were found to account for  $<5\%$  of INPs at  $-20$  and  $-25\text{ }^{\circ}\text{C}$ , and thus corrections were ignored. Binomial sampling confidence intervals (95%) were derived for INP concentrations following Agresti & Coull (1998). The temperature uncertainty of INP measurements is  $\pm 0.2\text{ }^{\circ}\text{C}$  (Hiranuma et al., 2015).

802 As a supplemental contribution to FIN-03, portions of IS aerosol suspensions were set aside (e.g., suspensions of 6 to 8 mL can serve up to three or more IS aliquot fills) for treatments to proximally isolate total biological, other organic and inorganic contributions to measured immersion freezing INP concentrations. To assess removal of heat labile INP entities, a 2 mL aliquot of suspension was re-tested in the IS after heating to  $95\text{ }^{\circ}\text{C}$  for 20 min (McCluskey et al. 2018). To attempt to remove all organic INPs, 1 mL of 30%  $\text{H}_2\text{O}_2$  was added to a 2 mL aliquot of suspension and the mixture heated to  $95\text{ }^{\circ}\text{C}$  for 20 min while illuminated with UVB fluorescent bulbs to generate hydroxyl radicals (residual  $\text{H}_2\text{O}_2$  is then removed using catalase) (Suski et al. 2018), and the INPs were again assessed for freezing spectra in the IS. Herein we describe a subset of samples collected on September 15, September 23, and September 25 that were subjected as IS suspensions to the two treatments. The interpretation of data from exposure of particle suspensions to  $95\text{ }^{\circ}\text{C}$  is that the reduction of INP concentrations under thermal treatment is a proxy for the concentration of biological (proteinaceous and microbial) INPs which have been eliminated or deactivated through treatment. A strong reduction in INP activity observed after peroxide

Deleted: -

Deleted: following Vali (1971) and

Deleted: Filter

Deleted: special

Deleted: 10

Deleted: These treatments are based on well-established methods which have been used to assess biological components in samples for more than 60 years (Alsante et al., 2023, and references therein).

825 treatment indicates dominant organic INP populations, whereas a lack of response to this treatment  
826 is assumed to indicate that inorganic INPs such as mineral dusts dominate non-heat labile INPs.  
827 This assessment for bulk suspensions of particles could be directly compared to measurements of  
828 300 °C heat treated single particles in the online CSU CFDC measurements on these same days,  
829 providing a more insightful investigation of INP compositions.

830 ~~Taken together, such treatment studies show general utility for estimating biological~~  
831 ~~contributions to INP, overall organic contributions and the importance of inorganic contributions,~~  
832 ~~as done~~ for a variety of locations (McCluskey et al., 2018; Suski et al., 2018; Barry et al., 2021a;  
833 Knopf et al., 2021; Testa et al., 2021). ~~However, we note that not all biological materials may be~~  
834 completely denatured or removed by heat (Testa et al., 2021; Daily et al., 2022; Alsante et al.,  
835 2023) and not all organics may be removed by peroxide. ~~For example, denaturation is the~~  
836 disruption of higher order (secondary, tertiary, and quaternary structure) in a protein which leads  
837 to a loss or lessening of function. ~~Simpler proteins or peptides, such as glutathione, have no higher~~  
838 order structure, and thus cannot be denatured (Alsante et al., 2023). Consequently, estimates of  
839 biological contributions to INP based on these treatments may be considered as lower limits ~~for~~  
840 ~~the FIN-03 samples analyzed.~~

#### 841 FRIDGE Cold Stage and Deposition Nucleation Measurements

842 The FRIDGE instrument ~~can operate as a low temperature cold chamber or low~~  
843 ~~temperature and pressure diffusion chamber device for measuring,~~ the concentration of INPs by  
844 two independent methods: a) a droplet freezing assay on a cold stage, ~~hereafter, FRIDGE-CS~~  
845 (Schrod et al., 2020; DeMott et al. 2018; Hiranuma et al. 2015) which addresses immersion  
846 freezing similarly to the ~~NCSU-CS and the CSU-IS and b) the diffusion chamber method, hereafter,~~  
847 FRIDGE-DC, ~~that addresses the deposition nucleation and condensation freezing modes~~

Moved (insertion) [6]

Deleted: .The use of such treatments and the insights they convey for atmospheric ice nucleation studies has been reported in published studies of INPs

Moved up [6]: Taken together, such treatment studies show general utility for estimating biological contributions to INP, overall organic contributions and the importance of inorganic contributions.

Deleted:

Deleted: It follows that s

Deleted: can be used to measure

Deleted: e (

Deleted: :

Deleted: NC State

Deleted: (

Deleted: :

Deleted: )

864 introduced in Schrod et al. (2016) and is the standard method for operating the FRIDGE device,  
865 (e.g., DeMott et al, 2018). The ice nucleation analysis is performed inside the FRIDGE instrument  
866 for both methods, yet the sampling process, addressed nucleation modes and the specific analytical  
867 procedures differ, as described below.

Deleted: referred to as the “

Deleted: ”

Deleted: in previous publications

Deleted: s

868 For the FRIDGE-CS method, aerosol particles were sampled via a short ¼” conductive  
869 tube from the shared turbulent flow aerosol inlet in the SPL instrument laboratory on Teflon  
870 membrane filters (Fluoropore PTFE, 47 mm, 0.2 µm, Merck Millipore Ltd.). The sampling  
871 duration ranged from 50 to 240 minutes, resulting in air volumes between 250 and 1000 std. L.  
872 The particles were extracted in 10 ml deionized water by shaking. Approximately 150, 0.5 µL  
873 droplets from that solution were pipetted onto a clean, silanized silicon wafer on the cold stage of  
874 the FRIDGE instrument and cooled by  $-1^{\circ}\text{C min}^{-1}$  at ambient pressure. A CCD camera detects  
875 freezing events and counts the number of frozen droplets as a function of temperature. This process  
876 is repeated with fresh droplets and fresh substrates until approx. 1000 droplets are attained. The  
877 INP number concentration is derived using Eqs. 1 and 2, as for the NCSU-CS and CSU-IS, An  
878 upper bound on temperature uncertainty is estimated as  $\pm 0.5^{\circ}\text{C}$ . Binomial sampling confidence  
879 intervals (95%) were derived for INP concentrations as done for the CSU-IS, following Agresti &  
880 Coull (1998). Pure water and suspensions of blank filters in pure water showed no freezing at  
881 temperatures  $> -20^{\circ}\text{C}$  and a contribution of no more than 15% toward total INPs at  $-29^{\circ}\text{C}$ , the  
882 lowest temperature for which data are reported herein. Consequently, corrections were ignored for  
883 this intercomparison.

Deleted: by

Formatted: Font: Bold

Formatted: Font: Not Bold

Formatted: Not Highlight

Formatted: Not Highlight

Formatted: Not Highlight

Formatted: Not Highlight

884 For the FRIDGE-DC measurements, particles were collected using an electrostatic aerosol  
885 collector (EAC) (Schrod et al., 2016) was connected to the same aerosol flow inlet via a short ¼”  
886 conductive tube. Within the EAC aerosol particles are electrostatically precipitated onto silicon

Deleted: an

Formatted: Justified

893 wafers, which are used as sample substrates. After sampling is completed, the analysis at select  
894 pairs of temperature and relative humidity set points follows in a separate step. For that, the wafer  
895 is placed on the cold stage inside a diffusion chamber. After the chamber is evacuated, the  
896 temperature is set to the first analysis temperature. In a second, much larger volume, pure water  
897 vapor is regulated by pressure control to the desired supersaturation. Once the water vapor diffuses  
898 into the chamber, ice forms on the activated INPs and a CCD camera is used to record and count  
899 the emerging ice crystals, which appear as bright objects. It is assumed that one ice crystal  
900 represents one INP. The water vapor atmosphere and thus the growth of ice crystals is maintained  
901 for up to 100 seconds until the valve to the water vapor source is closed and the chamber is  
902 evacuated again. The process is repeated at increasing humidity first, and then at progressively  
903 lower temperatures. At SPL samples were taken with the EAC for 50, 75 and 120 minutes,  
904 resulting in volumes of approximately 64-150 sL. The samples were analyzed by default at -20  
905 °C, -25 °C and -30°C and 95 %, 99% and 102% water saturation. In addition, a few samples were  
906 analyzed at -15 °C. This was a supplemental contribution by the FRIDGE group for  
907 comprehensive analysis of INP activation in the deposition regime, and for comparison to online  
908 data in this regime collected for some days. Temperature uncertainty is the same as for the  
909 FRIDGE-CS method. RH uncertainty is +/-2% on the basis of observing visible condensation on  
910 particles at 100% RH. INP concentration uncertainties are given as binomial confidence limits, the  
911 same as for the CSU-IS.

**Deleted:** The EAC consists of a cylindrical sampler, whose inlet is concentrically surrounded by 12 gold wires that are at 12 kV against a grounded silicon wafer, which is used as the sample substrate, at the bottom of the sampler. Once the airflow is pumped inside, aerosol particles are charged by electrons emitted from the gold wires and are precipitated onto the silicon wafer. The analysis at certain pairs of T and RH follows in a separate step.

**Deleted:** from the electrostatic sampler

**Deleted:** pecial

**Deleted:** ¶

### 913 **2.3 INP processing and sampling strategies**

914 As a campaign strategy, samples were collected over different time periods in the day to  
915 reflect both varied weather conditions and aerosol populations arriving at the mountain laboratory.  
916 For intercomparison, a select number of 3 to 4-hour sampling periods were allocated in which

**Formatted:** Font: Bold

**Formatted:** Normal, Space Before: 0 pt, Line spacing: single

**Formatted:** Justified

928 online instruments nominally operated at a few predesignated temperature and relative humidity  
929 ranges, while samples were collected continuously for off-line analysis. While aerosol conditions  
930 can change within a 4-hour time frame, this was agreed upon as a minimal reasonable period for  
931 comparability to obtain statistically reliable results. Similar sampling strategies have been  
932 employed in the past intercomparisons (DeMott et al., 2017; Knopf et al., 2021). Overall,  
933 measurements were conducted over a wide range of temperatures (-7 to -34 °C) in the  
934 heterogeneous ice nucleation regime.

**Deleted:** attempted to operate

**Deleted:** . Sampling such a broad data set allows for the consideration of instrument performance in response to the presence of highly active INPs (i.e., those facilitating freezing at temperatures  $\geq -10$  °C) as well as more modestly effective INP ( $-10$  °C  $\geq T \geq -30$  °C). In addition, the range of INP concentrations includes lower concentrations which challenge instrumental limits of detection.

### 935 3 Results and discussion

#### 936 3.1 Meteorological context

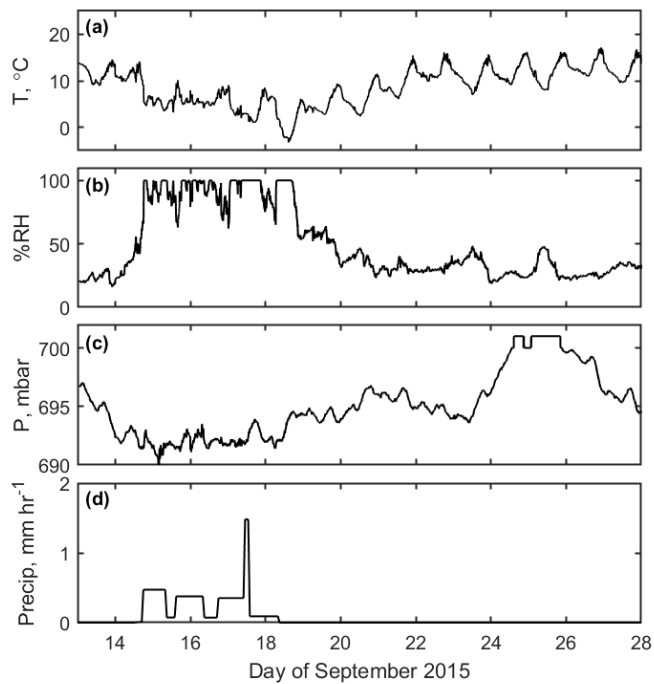
937 Weather conditions during FIN-03 were characterized using auxiliary measurements.  
938 Weather data (temperature, humidity, winds and pressure) were obtained for Storm Peak  
939 Laboratory through the MesoWest ([https://mesowest.utah.edu/cgi-](https://mesowest.utah.edu/cgi-bin/droman/meso_base_dyn.cgi?stn=STORM)  
940 [bin/droman/meso\\_base\\_dyn.cgi?stn=STORM](https://mesowest.utah.edu/cgi-bin/droman/meso_base_dyn.cgi?stn=STORM)) mesonet (STORM site), supplemented with  
941 measurements from instruments operated at SPL through the Western Regional Climate Center  
942 (WRCC) (<https://wrcc.dri.edu/weather/strm.html>) for the two days that were absent in the  
943 MesoWest record. Air temperature, relative humidity, and barometric pressure time series are  
944 shown in Figure 1(a), 1(b) and 1(c), respectively. Precipitation was measured via a rain gauge at  
945 Storm Peak Laboratory provided by NCSU. Precipitation rate was calculated from the quotient of  
946 precipitation (in mm) and time collected (in hours), as shown in Figure 1(d). Back trajectories for  
947 all the sampling days in FIN-03 are reported by Zawadowicz et al. (2017), showing 72-hr air mass  
948 transits from regions that included Southern California, Washington State and Eastern Nebraska.

**Deleted:** NC State

949 Relatively warm, dry conditions were observed initially at the Storm Peak Laboratory.  
950 Clear skies on September 11 and 12, 2015 gave way to clouds and haze on September 13. Cooler

**Formatted:** Justified

960 temperatures, lower barometric pressure, and higher relative humidity (generally above > 70%)  
961 accompanied rainfall on September 14. This was followed by continued rain on September 15,  
962 intermittent rain and short periods of hail on September 16, a mixture of rain, snow, and sleet on  
963 September 17, and snow on September 18. The next and longest period in the study, September  
964 19 to 28, was marked by an increase in temperature, an increase in barometric pressure, lower  
965 relative humidity, and a lack of precipitation. More detailed weather records including daily  
966 photographs and a summary of human-produced daily observations are summarized in  
967 supplemental Section S1. Daily wind rose plots are provided in Figure S1.



968  
969 **Figure 1.** Weather conditions over the course of FIN-03, including (a) air temperature, (b) relative  
970 humidity, (c) barometric pressure, and (d) precipitation rate.

Formatted: Centered

971

## 972 3.2 Aerosol context

### 973 3.2.1 Aerosol size distribution and surface area

974 The time series of aerosol size distribution measured by the LAS (in three hour means) is  
975 shown in Figure 2a. The maximum and minimum total LAS concentrations were  $706 \text{ cm}^{-3}$  and  $74$   
976  $\text{cm}^{-3}$  respectively, and the mean and standard deviation of the total LAS concentration throughout  
977 FIN-03 were  $410 \text{ cm}^{-3}$  and  $138 \text{ cm}^{-3}$ , respectively. The highest total LAS concentration recorded  
978 during FIN-03 ( $706 \text{ cm}^{-3}$ ) occurred in the early hours on September 25. Elevated aerosol  
979 concentration (at least one standard deviation above the mean) was also observed during midday  
980 on September 13, before and during midday on September 14, before midday on September 25, in  
981 the afternoon on September 26, and around midday on September 27.

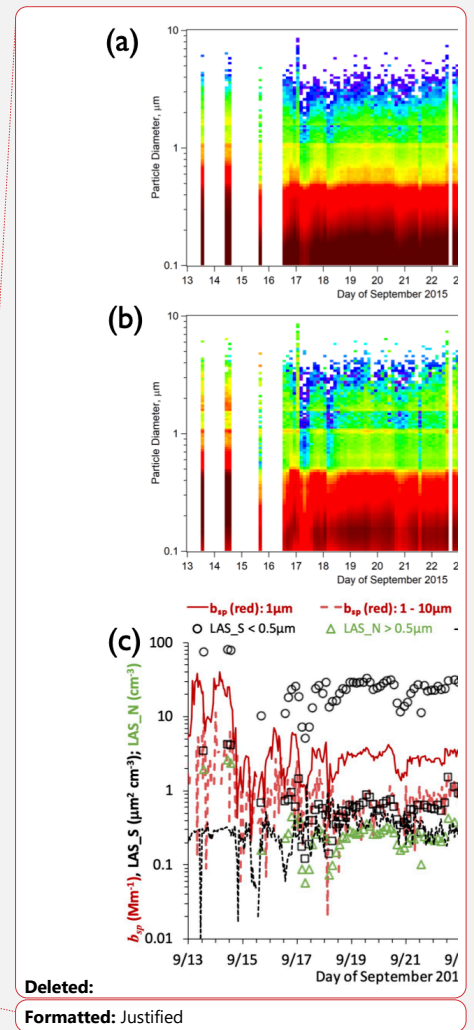
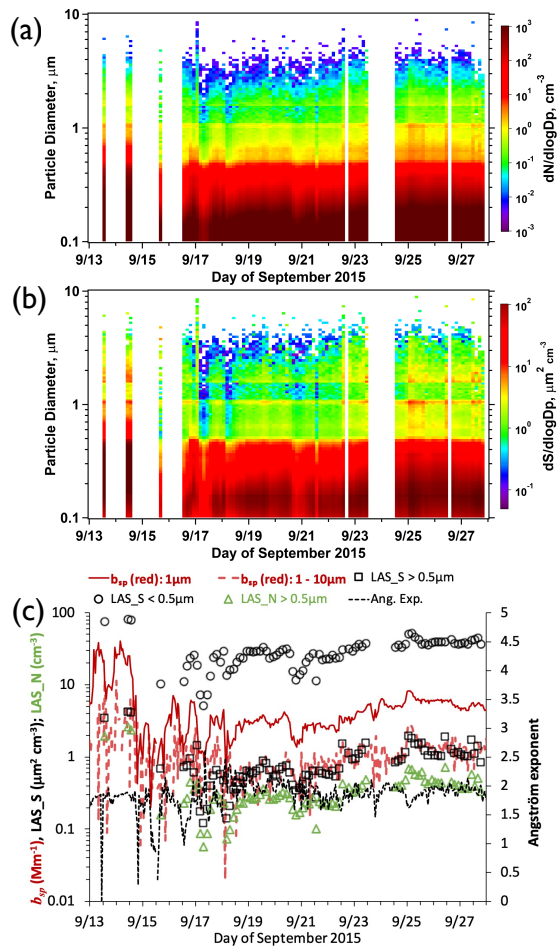
982 The timeline of LAS aerosol surface area in Figure 2b emphasizes that surface area was  
983 predominately submicron throughout the study, with a mode at about  $0.16 \mu\text{m}$ . This is important  
984 to note, in combination with chemical composition information discussed in the next section  
985 because it is relevant to understanding the likely sizes and surface areas of INPs. We will revisit  
986 the surface area of INPs for use in parameterizations in a later section. Quantitative timelines of

**Moved up [5]:** Relatively warm, dry conditions were observed initially at the Storm Peak Laboratory. Clear skies on September 11 and 12, 2015 gave way to clouds and haze on September 13. Cooler temperatures, lower barometric pressure, and higher relative humidity (generally above > 70%) accompanied rainfall on September 14. This was followed by continued rain on September 15, intermittent rain and short periods of hail on September 16, a mixture of rain, snow, and sleet on September 17, and snow on September 18. The next and longest period in the study, September 19 to 28, was marked by an increase in temperature, an increase in barometric pressure, lower relative humidity, and a lack of precipitation. More detailed weather records including daily photographs and a summary of human-produced daily observations are summarized in supplemental Section S1. Daily wind rose plots are provided in Figure S1.

**Deleted:** ¶

**Formatted:** Justified





1005

1006 **Figure 2.** Time series of dry particle number concentration distribution (ambient conditions, not STP) measured by the laser aerosol spectrometer (LAS) in a), shown as three-hour means at ambient pressure.

1007

1008 Time series of particle surface area distribution is in b). c) Timeline of nephelometer scattering (1-hr data)

1009 in the red channel for <math>1 \mu\text{m}</math> and 1 - 10  $\mu\text{m}</math> size ranges, 3-hr LAS number concentration > 0.5  $\mu\text{m}</math>, 3-hr$$

1010 LAS surface area at sizes below and above 0.5  $\mu\text{m}</math>, and Angström exponent (dashed, right axis).$

1011

1013 LAS surface area above and below 0.5  $\mu\text{m}$  are shown in Figure 2c. Surface area at above 0.5  $\mu\text{m}$   
1014 is about a factor of 30 lower than at below this size over most of the study period. Also shown in  
1015 Figure 2c is nephelometer scattering ( $b_{sp}$ ) in the red channel (700 nm) showing a dominant  
1016 contribution when the upstream impactor was set to 1  $\mu\text{m}$  (aerodynamic) and a much lower level  
1017 of 1 – 10  $\mu\text{m}$  scattering. This scattering from coarse mode particles is consistent with and trends  
1018 with the LAS surface area in the supermicron regime, while the Angström exponent (calculated  
1019 using red and blue channels) being close to 2 (small particle dominance) throughout the study is  
1020 consistent with the dominance of submicron contributions to total surface area. Figure 2 also  
1021 emphasizes that the lowest aerosol concentrations and surface areas occurred during varied time  
1022 in the wet period of the study from midday on the 14<sup>th</sup> through the 17<sup>th</sup> of September. Finally,  
1023 adjacent 3-hr periods rarely represented surface area changes of more than a factor of 2 in the size  
1024 range > 0.5  $\mu\text{m}$  and was usually within 10-20%. Large differences across 3-hour periods were less  
1025 frequent for surface area at smaller sizes. These factors confirm the validity of the selected  
1026 intercomparison time periods.

Formatted: Justified

Formatted: Font: Not Italic

Formatted: Font: Not Italic

Formatted: Font: Not Italic

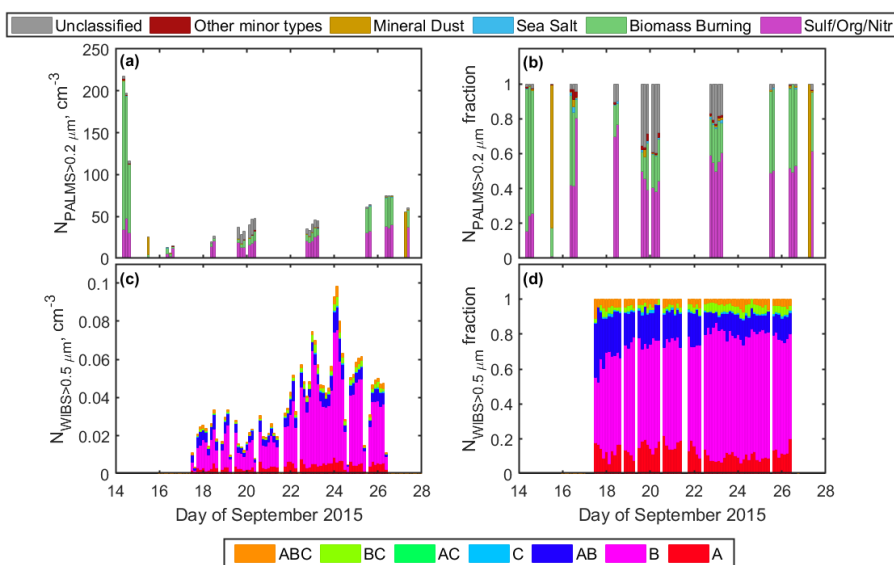
### 1027 3.2.2 Aerosol composition

1028 The number concentration of aerosol particles from 0.2 to 3  $\mu\text{m}$  with characteristic spectra  
1029 belonging to eight composition categories (sulfate/organic/nitrate, biomass burning, elemental  
1030 carbon, sea salt, mineral dust, meteoric, alkali salt, and fuel oil combustion), and the number  
1031 concentration of unclassified aerosol particles by the PALMS, were assessed for three-hour  
1032 averages through the FIN-03 period. For simplicity, four of these categories (elemental carbon,  
1033 meteoric, alkali salt, and fuel oil combustion) were combined into a category called “other” due to  
1034 the low concentration of particles in each of these categories resulting in 6 total classifications  
1035 (SulfOrgNit = sulfates/organics/nitrates, BioBurn = products of biomass burning, Sea salt, Mineral

Formatted: Justified

Deleted: (categories)

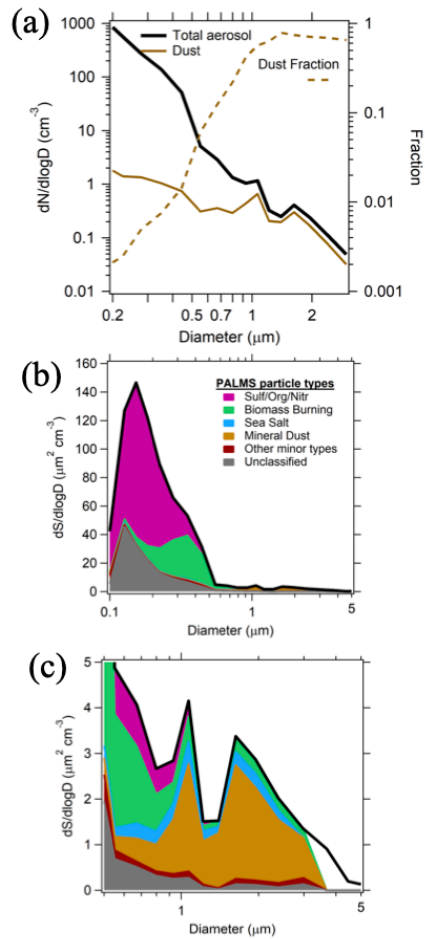
1037 dust, and Unclassified), as shown in Figure 3a. The three-hour averages of the number fractions of  
 1038 each particle type were also calculated as the fraction of the total aerosol number concentration  
 1039 measured by the PALMS in each of the six classifications, as shown in Figure 3b. The dominant  
 1040 categories throughout the FIN-03



1041  
 1042 **Figure 3.** Subplots (a) and (b) show the aerosol particle number (ambient conditions, not STP) and relative  
 1043 fractions (by cumulative count at all sizes) of each of the six PALMS compositional particle types for the  
 1044 three-hour periods during which the PALMS was used to sample ambient air. Subplots (c) and (d) show  
 1045 the aerosol particle number concentration and relative fractions (by count) of particles with diameter > 0.5  
 1046  $\mu\text{m}$  in each of the channels (A, B, AB, C, AC, BC, and ABC, which are described in Perring et al., 2015)  
 1047 over the course of the FIN-03 field campaign.

1048

Formatted: Justified



1049

1050 **Figure 4.** a) Total aerosol versus mineral/soil dust (ambient) number size distribution and dust fraction  
 1051 interpreted from PALMS and LAS data for all times that the PALMS was sampling during FIN-03. b)  
 1052 Surface area distribution differentiated for PALMS compositional types during the same sampling times.  
 1053 c) Expanded plot from b) for the coarse mode size range to emphasize progressive dominance of dust  
 1054 components at diameters > 0.5  $\mu\text{m}$ .

Formatted: Justified

1055 campaign were BioBurn (mean  $26 \pm 43 \text{ cm}^{-3}$ , maximum  $177 \text{ cm}^{-3}$ ), SulfOrgNit (mean  $22 \pm 13 \text{ cm}^{-3}$ , maximum  $48 \text{ cm}^{-3}$ ), and mineral dust (mean  $3 \pm 11 \text{ cm}^{-3}$ , maximum  $55 \text{ cm}^{-3}$ ). The mineral dust  
1056 type also includes soil particles (crustal species mixed with organic material) (Zawadowicz et al.,  
1057 2019). The highest total particle number concentration measured by the PALMS ( $218 \text{ cm}^{-3}$ )  
1058 occurred on September 14 (of which  $177 \text{ cm}^{-3}$  consisted of biomass burning and  $34 \text{ cm}^{-3}$  consisted  
1059 of sulfates/organics/nitrates). This biomass burning plume impacted the site for several hours.  
1060 Mineral/soil dust particles were ubiquitous throughout the study, with a concentration of  $0.128 \pm$   
1061  $0.446 \text{ cm}^{-3}$  (median and interquartile range). Anomalous concentrations  $>10 \text{ cm}^{-3}$  observed for a  
1062 few 5-min sample periods are likely due to road dust emitted from site. Dust concentrations were  
1063  $<1 \text{ cm}^{-3}$  for 90% of the PALMS samples. Mineral/soil dust represented a median of 0.3% of  
1064 particles in the  $>0.2 \mu\text{m}$  size range, increasing to 23% and 67% for  $>0.5$  and  $>1.0 \mu\text{m}$  particles  
1065 (Figure 4a). Similarly, mineral dust contributions to total surface area are inconsequential for total  
1066 aerosol (Figure 4b) but dominate in the coarse mode regime for the study (Figure 4c). We revisit  
1067 this result in discussions of parameterization of INPs in Section 3.5.

1069 The daily average number concentration of fluorescing aerosol particles corresponding  
1070 with each of the seven WBS-4A types with diameter  $> 0.5 \mu\text{m}$  is shown in Figure 3(c), and the  
1071 daily average number fraction of each WBS-4A type is shown in Figure 3(d). The dominant types  
1072 of fluorescent aerosol particles throughout the FIN-03 field campaign were types B, AB, and A,  
1073 which on average accounted for  $63.2\% \pm 8.7\%$ ,  $16.0\% \pm 6.3\%$ , and  $12.5\% \pm 3.9\%$  of the particles  
1074 detected by the WBS respectively.

1075 In contrast with the daily average number fraction in each PALMS category, the relative  
1076 contributions of each of the seven WBS-4A particle types did not vary much over the course of  
1077 the study when the WBS-4A was operational, with perhaps the exception that Type AB decreased

Deleted: will

1079 in prevalence from September 18 (42.9%) to September 21 (10.1%). A modest trend from lower  
1080 total fluorescing particle concentrations (0.02 to 0.04 cm<sup>-3</sup> at STP) ~~from September 17 through the~~  
1081 ~~21<sup>st</sup> to higher concentrations (0.07 to 0.15 cm<sup>-3</sup> at STP) from September 22 through the 26<sup>th</sup>.~~ WIBS-  
1082 4A data was not collected on September 13-16, nor on September 27. The first period was  
1083 somewhat critical to evaluating INP relations to bioaerosols, so we note here in advance this  
1084 caveat. Time-resolved size distributions for each WIBS-4A channel, as well as the total particle  
1085 concentration measured across these seven channels, are shown in supplemental Figure S2. FBAP  
1086 assignments related to INP predictions will be discussed in Section 3.5.

Deleted: through

Deleted: 21

Formatted: Superscript

### 1087 3.3 Immersion freezing measurements

1088 A summary of the number concentrations of immersion freezing INPs (*N<sub>INP</sub>*) over the  
1089 course of the field campaign, ~~for all measurements averaged at~~ one degree temperature intervals  
1090 ~~for each instrument~~, is shown in Figure 5. The concentration of INPs detected over this range  
1091 ranged over five orders of magnitude (0.01 to 160 L<sup>-1</sup>). ~~Only two sets of instruments were able to~~  
1092 ~~explore the temperature regimes of -30 °C and colder due their design to permit operation there,~~  
1093 ~~or warmer than -15 °C due to detection limits (controlled by sample volume and drop size used~~  
1094 ~~for immersion freezing).~~ At any one temperature, differences up to a little more than one order of  
1095 magnitude are apparent in comparing average data from individual methods, mirroring results  
1096 presented in previous laboratory and field studies (Hiranuma et al., 2015; DeMott et al., 2017,  
1097 2018; Knopf et al., 2021; [Brasseur et al., 2022](#); Lacher et al., 2024).

Formatted: Font: Italic

Deleted: binned for

1098 As expected, a trend of increasing *N<sub>INP</sub>* with decreasing temperature was observed for the  
1099 FRIDGE-CS, CSU-IS, ~~NCSU-CS (I and F)~~, and CSU-CFDC. ~~Incremental changes in *N<sub>INP</sub>* with~~  
1100 decreasing temperature was similar for all measurements that spanned a broad temperature  
1101 range. ~~The dependence of *N<sub>INP</sub>* on temperature is nearly log-linear from -10 to -27 °C, excepting~~

Formatted: Font: Italic

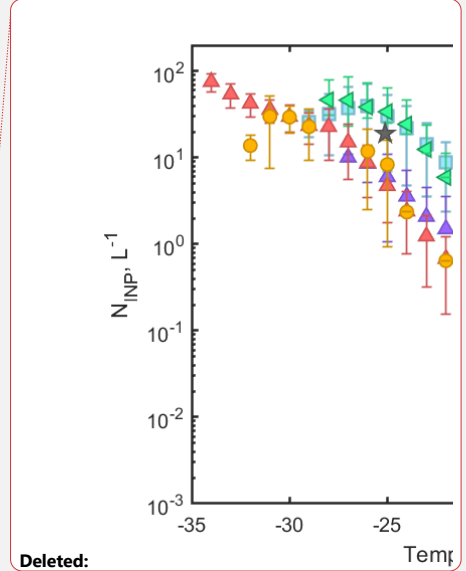
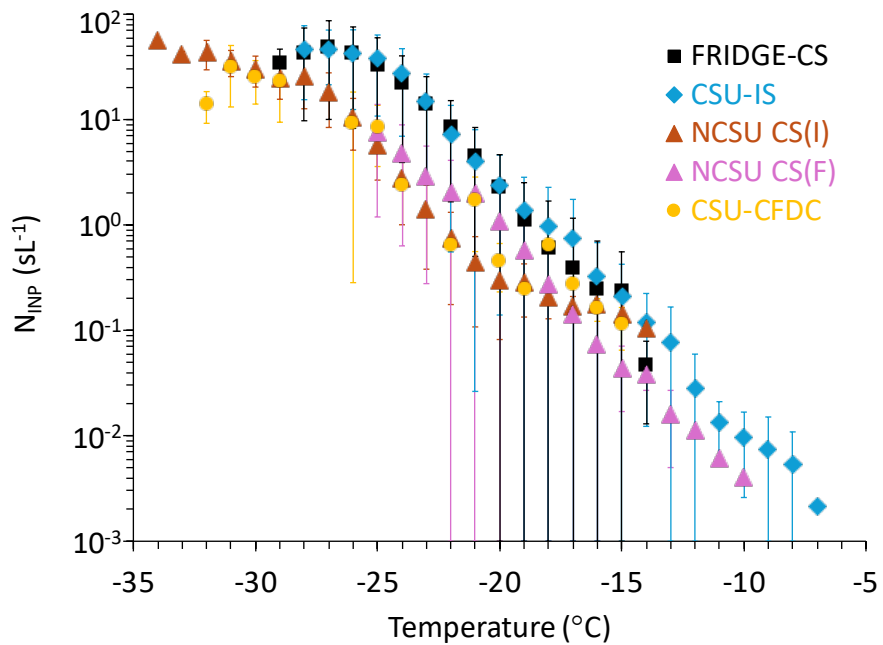
Deleted: NC State

Deleted: The data represented by the single MIT-SPIN processing temperature condition also falls well within the concentration range reported for the other instruments.

Formatted: Font: Italic

Formatted: Subscript

1109 perhaps a steepening of slope from  $-20$  to  $-25$  °C and some lowering of slope below this  
 1110 temperature. This comparability of  $dN_{\text{INP}}/dT$  contrasts with an apparent increasing high bias of  
 1111 drop suspension freezing measurements versus CFDC measurements



1112  
 1113 **Figure 5.** Campaign average immersion freezing INP concentrations ( $\text{sL}^{-1}$ ) in  $1$  °C bins for instruments  
 1114 participating in intercomparison studies. Error bars represent one standard deviation in the measurement  
 1115 means collected at the specified temperature and not measurement uncertainties. The error bars strike the  
 1116 lower axis when the standard deviation exceeded the mean values. The times over which the INP  
 1117 concentration has been averaged for each instrument is explained in the text.  
 1118  
 1119 during comparable sampling at various surface sites (non-mountaintop or free troposphere)  
 1120 found in DeMott et al. (2017) but agrees with FIN-02 laboratory studies (DeMott et al., 2018)

Deleted: star labels indicate

Deleted: se

Deleted: for the FRIDGE-CS data

Deleted: CFDC measurements

1126 and recent atmospheric studies at Puy de Dome (Lacher et al., 2024). INP concentration  
1127 variability at single temperatures, reflected in Figure 5 as a standard deviation of bin means, is  
1128 likely due to variations in aerosol properties affecting INPs in response to production and  
1129 scavenging processes upstream of the site. Nevertheless, generally higher  $N_{INP}$  measurements  
1130 were obtained with the FRIDGE-CS and the CSU-IS than the CSU-CFDC and NCSU-CS (F)  
1131 and NCSU-CS (I) analyses. Such biases in other studies have been attributed to different  
1132 efficiencies in sampling of largest particles (e.g., Lacher et al., 2024; Cornwell et al., 2023), but  
1133 the collection methods for offline measurements in this study were substantially similar, as  
1134 discussed further below. Hence, we cannot attribute measurement differences to a systematic  
1135 source. Comparability of impinger versus filter sampling methods for immersion freezing  
1136 measurements via the NCSU-CS mirrors the findings in DeMott et al. (2017), suggesting that  
1137 particle removal from filters can be highly effective for immersion freezing measurements of  
1138 ambient particles.

1139 To view the data in a more complete manner over the entire project, we explore direct  
1140 comparisons of different instrument data as scatterplots and measurement ratios on temporal  
1141 bases. First, in Figure 6, we show a commonly used representation of large INP project data as  
1142 INP concentrations for four instruments versus one other and segregate the data into broad 4-  
1143 degree temperature ranges. The data used for normalization were from the CSU-IS, though we  
1144 might have used any other. Linear regressions were plotted in Figure 6 to show the overall  
1145 average differences between measurements that are already evident in Figure 5. Figure 6a  
1146 thereby demonstrates the generally good correspondence between the NCSU-CS data of both  
1147 types and the CSU-CFDC data that measure factors of 5 to 8 lower INP concentrations on  
1148 average compared to the CSU-IS, as well as the closer correspondence of the FRIDGE-CS (31%

Deleted: NC State

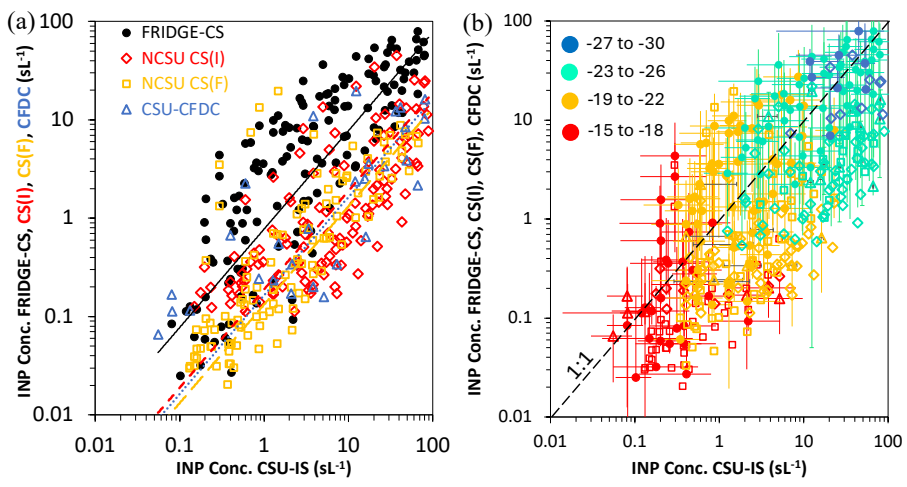
Deleted: NC State

Deleted: NC State



1152 lower) and CSU-IS data. Greatest variations in INP concentrations over the course of the project  
 1153 were focused in the  $-20$  to  $-25$  °C temperature regime (Figure 6b), where variations reached  
 1154 nearly two orders of magnitude. This is not an uncommon observation, also seen in Lacher et al.  
 1155 (2024). Surprising, but not easily understood yet, is the fact that all measurement methods could  
 1156 at times measure equivalently to or more than the CSU-IS.

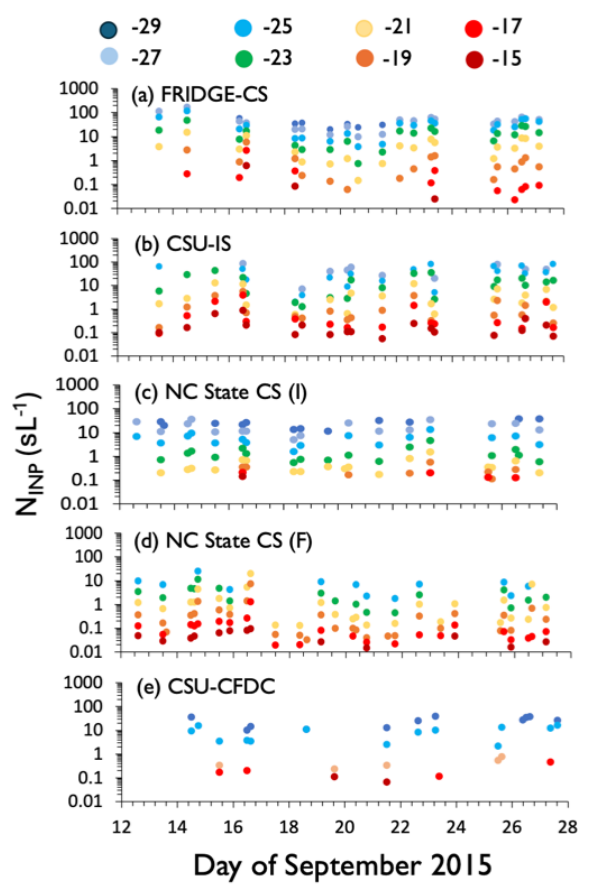
1157



1158

1159 **Figure 6.** (a) INP concentrations for all intercomparison measurement points of FIN-03 from the FRIDGE-  
 1160 CS, NCSU-CS (I), NCSU-CS (F) and CSU-CFDC compared to the INP concentrations from the CSU-IS  
 1161 measurements. Linear regressions with zero intercepts are color coded for each, having slopes of 0.78, 0.19,  
 1162 0.13 and 0.16 for the FRIDGE-CS, NCSU-CS (I) and CSU-CFDC, respectively. (b) The same data are  
 1163 color coded for different temperature ranges in °C and the 1:1 relation is shown. Errors are confidence  
 1164 intervals for FRIDGE-CS, CSU-CFDC, and CSU-IS data. These are not shown for the NCSU-CS data since  
 1165 these are given as temperature errors and would need interpolation to plot as  $N_{\text{INP}}$  errors.

Formatted: Font: 11 pt, Bold  
 Formatted: Font: 11 pt  
 Formatted: Justified, Indent: First line: 0"  
 Formatted: Font: 11 pt  
 Formatted: Font: 11 pt  
 Formatted: Font: 11 pt  
 Formatted: Font: 11 pt



**Deleted:** To compare the operation of these instruments over time, the mean and standard deviation (when applicable) of immersion freezing  $N_{INP}$  were calculated over three-hour

1166  
 1167 **Figure 7.** Time series of immersion-freezing mode INP concentrations ( $sL^{-1}$ ) measured during  
 1168 intercomparison periods by (a) the FRIDGE-CS, (b) the CSU-IS, (c) the NC State CS (I), (d) the NC State  
 1169 CS (F), and (e) the CSU-CFDC. An additional data point from the MIT-SPIN is shown as a square data  
 1170 point in the CSU-CFDC panel. Note that data for the CFDC is plotted only for the most common  
 1171 temperatures of -30, -25, -20 and -15 °C. INP concentrations shown in this figure are those measured  
 1172 within three-hour blocks of time but may capture longer or shorter time periods depending on the specific  
 1173 instrument sampling time that overlapped these periods.

1178  
1179  
1180  
1181  
1182  
1183  
1184  
1185  
1186  
1187  
1188  
1189  
1190  
1191  
1192  
1193  
1194  
1195  
1196  
1197  
1198  
1199  
1200

Temporal data provided further descriptions of instrument comparability. Immersion freezing  $N_{INP}$  in 1 °C bins were compared for periods of the day broken into three-hour intervals in the time series of Figure 7. While absolute INP concentration magnitudes differ, it is not difficult to see comparability of general trends amongst the data sets, albeit with episodic discrepancies that will be discussed further below. For example, all methods measure higher INP concentrations early in the study, a low point around the 18<sup>th</sup> of September and a build up again toward the end of the study. For example, INP concentrations at temperatures > -20 °C were at a maximum during the precipitation period, as might be expected for rainfall production of biological INPs (Huffman et al., 2013; Mignani et al., 2021; Testa et al., 2021; Cornwell et al., 2023), while the strongest differences between the concentrations of INPs active at higher and lower temperatures occurred for all instrumental measurements during the period of warming under high pressure later in the study. The latter observation might be expected for a strong contribution of dust-like INPs, with a steeper  $dN_{INP}/dT$ . These positive points suggesting that the instruments were measuring the same INP cycles was also seen in the study of Lacher et al. (2024), c.f., their Figure 4.

Periods of agreement and discrepancy are clearer in examining the ratios of time-matched and temperature-matched three-hour immersion  $N_{INP}$  values that were calculated for each pair of instruments, as shown in Figure 8. Numbers of overlapping measurement periods, their geometric means, standard deviations and normal 95% confidence intervals of all ratios (all times and temperatures) plotted in each panel of Figure 8 are documented in Table 2. Reiterating what is apparent from campaign-wide results in Figure 5 and 6, Figure 8 indicates the best agreement for short-term periods throughout the study was observed between the FRIDGE-CS

Formatted: Indent: First line: 0.5"

Deleted: periods for each instrument (except for the MIT-SPIN) at 1 °C intervals ( $\pm 0.5$  °C). Means are plotted as a

Deleted: in

Deleted: 6

Formatted: Superscript

Deleted: Although some differences appear in comparing instrument by instrument, as will be discussed, some general observations from the temporal data of Figure 6 are that

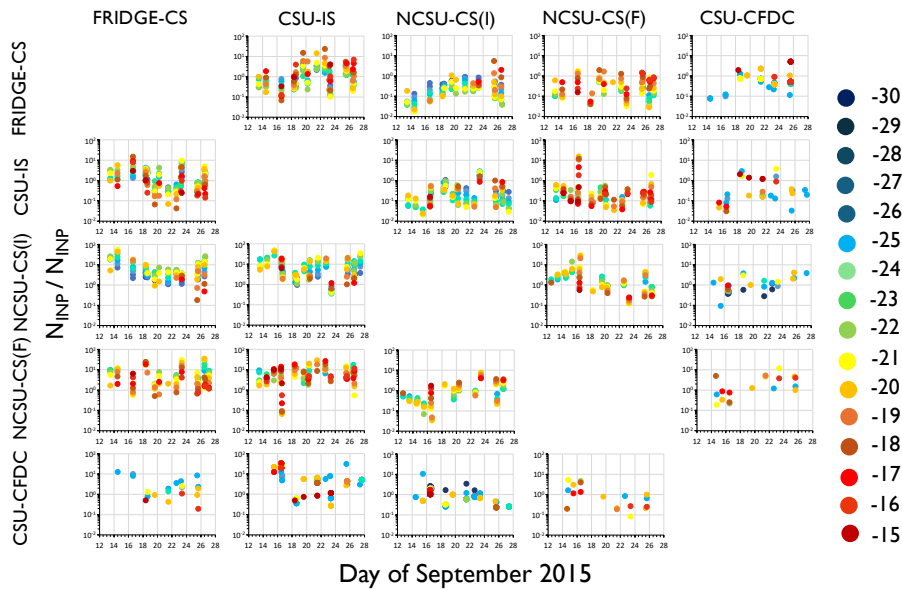
Formatted: Font: Italic

Deleted: ¶

Formatted: Font: Italic

1209 and the CSU-IS, in which only 4 out of 146 3-hour, time- and temperature-matched  $N_{INP}$  (3%)  
 1210 did not agree within an order of magnitude. Nevertheless, discrepancies of a few to several times  
 1211 did occur from September 16<sup>th</sup> onward, focused most often at  $>-22^{\circ}\text{C}$ . These biases flipped in  
 1212 both directions, with the CSU-IS measuring higher from the 19<sup>th</sup> to the 22<sup>nd</sup> and the FRIDGE-CS  
 1213 higher at some other times, notably the 16<sup>th</sup>, 23<sup>rd</sup> and 26<sup>th</sup> of September. None of these periods  
 1214 were distinguished in any discernible manner by weather or aerosol properties. For example,  
 1215 LAS and PALMS concentrations were no more than 20% different from the FIN-03 campaign  
 1216 means during any of these periods. Aerosol surface areas were about a factor of two lower  
 1217 overall during the 19<sup>th</sup> to 22<sup>nd</sup> period than for the period after the 23<sup>rd</sup> (Figure 2), which does not  
 1218 imply a special sampling bias for larger particles for the IS filter that was open to the air, a point  
 1219 we will discuss further below.

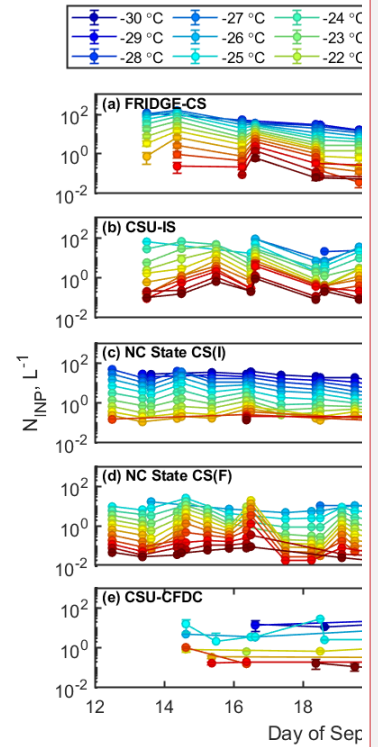
1220



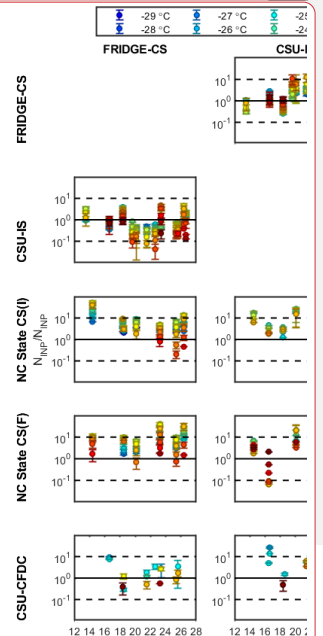
1221

Moved (insertion) [4]

Deleted: than... from the FIN-03 campaign means during any of these periods. Aerosol surface areas were about a factor of two lower overall during the 19<sup>th</sup> to 22<sup>nd</sup> period than for the period after the 23<sup>rd</sup> (Figure 2), which does not imply a special sampling bias for larger particles for the IS filter that was open to the air, a point we will discuss further below. [2]



Deleted:



Deleted:

1252 **Figure 8.** Ratios of the immersion freezing INP concentrations measured by each instrument, to the  
1253 immersion INP concentrations measured by each other instrument (three-hour averages). Each instrument  
1254 (FRIDGE, CSU-IS, NC State-CS (I), NC State-CS (F), and CSU-CFDC) is represented by one of the five  
1255 columns as well as one of the five rows.

1256  
1257 Both the FRIDGE-CS and CSU-IS showed high bias from a few to more than 10 times  
1258 versus NCSU-CS(I) or CS(F), primarily at processing temperatures below  $-20\text{ }^{\circ}\text{C}$ , whereas ratios  
1259 closer to 1 indicated much better agreement at  $-20\text{ }^{\circ}\text{C}$  later in the study. The poorest agreement  
1260 overall was observed for the CSU-IS compared to the NCSU-CS(I), a combination for which 26  
1261 out of 128 (20%) immersion  $N_{\text{INP}}$  means did not agree within an order of magnitude. Agreement  
1262 between the FRIDGE-CS and the NCSU-CS(I) was only slightly better, as 15 out of 108 (14%)  
1263 time-matched  $N_{\text{INP}}$  means did not agree within an order of magnitude. Higher than order of  
1264 magnitude such discrepancies at lower temperatures were markedly present on September 13, 14,  
1265 23 and 26. Based on PALMS data, the 14<sup>th</sup> was richer in compounds from biomass burning,  
1266 poorer in sulfates, organics, and nitrates, and slightly poorer in mineral dust than average, as  
1267 discussed in Section 3.2. The concentration of  $> 0.5\text{ }\mu\text{m}$  particles measured by the LAS during  
1268 this time was also relatively high ( $2.5\text{ cm}^{-3}$  compared to the campaign mean  $0.45\pm 0.62\text{ cm}^{-3}$ ).  
1269 However, the 14<sup>th</sup> is not markedly distinguished overall in the timeline of all INP measurements  
1270 in Figure 7, so perturbations to composition and concentrations of all particle sizes due to the  
1271 biomass burning event did not appear to specially perturb the INP populations. We have already  
1272 noted that the 23<sup>rd</sup> and 26<sup>th</sup> of September had aerosol populations that were not much different  
1273 than the project mean on those days.

Deleted: 7

**Moved up [4]:** and 26<sup>th</sup> of September. None of these periods were distinguished in any discernible manner by weather or aerosol properties. For example, LAS and PALMS concentrations were no more than 20% different than the FIN-03 campaign means during any of these periods. Aerosol surface areas were about a factor of two lower overall during the 19<sup>th</sup> to 22<sup>nd</sup> period than for the period after the 23<sup>rd</sup> (Figure 2), which does not imply a special sampling bias for larger particles for the IS filter that was open to the air, a point we will discuss further below.

**Deleted: ¶**  
Periods of agreement and discrepancy are clearer in examining the ratios of time-matched and temperature-matched three-hour immersion  $N_{\text{INP}}$  values that were calculated for each pair of instruments, as shown in Figure 7. As a positive note, the mean  $N_{\text{INP}}$  reported by different instruments for all temperature conditions taken together generally fell within a span of one order of magnitude. Figure S3 shows the percent of immersion INP measurements in which all instrument pairs agreed within one order of magnitude. This level of agreement compares well with the findings from FIN-02, for which the immersion  $N_{\text{INP}}$  measured by several online and offline instruments agreed within an order of magnitude. This is encouraging given that FIN-02 was a laboratory intercomparison on single composition aerosol samples consisting of particles with diameter  $< 2\text{ }\mu\text{m}$  whereas FIN-03 was a field campaign in which constant changes in the concentration, size distribution, and composition of the ambient aerosol population at Storm Peak Laboratory were all potential factors. This shows that field data can be collected with nearly the same level of accuracy as laboratory experiments. While also mimicking the results of DeMott et al. (2017) for a smaller instrument comparison exercise, agreement was slightly poorer than found in another recent intercomparison where INP concentrations were stated to match within a factor of 5 (Lacher et al., 2024).  
Reiterating what is apparent from campaign-wide results in Figure 5, the best agreement for short-term periods throughout the study as shown in Figure 7 was observed between the FRIDGE-CS and the CSU-IS, in which only one out of seventy-two 3-hour, time- and temperature-matched  $N_{\text{INP}}$  (1.4%) did not agree within an order of magnitude (... [4])

Deleted: NC State

Deleted: was generally very much better

Deleted: NC State

Deleted: 12

Deleted: 44

Deleted: 7

Deleted: NC State

Deleted: 3

Deleted: 52

Deleted: 25

Deleted: 6

1367 The CSU-CFDC INP measurements generally agreed with the other measurements within  
1368 an order of magnitude for data collected on the same day and temperature, excepting a  
1369 particularly low bias versus the CSU-IS at higher temperatures on the 16<sup>th</sup> of September (rain  
1370 and hail day) and at lower temperatures on the 25<sup>th</sup> of the month. Nevertheless, its measurements  
1371 of INP concentration were in best agreement with all methods overall for temperatures > -20 °C,  
1372 albeit for the most limited number of matches (19 to 29). CSU-CFDC INP concentrations also  
1373 tended to be lower than those from the FRIDGE-CS and CSU-IS at temperatures below -20 °C.  
1374 A similar divergence in online versus offline N<sub>INP</sub> measurements in this temperature range was  
1375 reported by DeMott et al (2017) for ground-based sampling, with online measurements tending  
1376 to measure progressively lower INPs than offline integrated filter or impinger collections at  
1377 below -20 °C, approaching one order of magnitude below -25 °C. At the Puy de Dome  
1378 Mountain station (Lacher et al. 2024), only modest and insignificant underestimates were made  
1379 by the CSU-CFDC (also using a 2.5 µm upstream impactor) versus offline INP concentrations  
1380 when all were measured from a PM10 inlet. CSU-CFDC INP measurements were comparable on  
1381 average with measurements from the NCSU-CS(I) and NCSU-CS(F), consistent with the mean  
1382 results shown in Figure 5.

1383 Comparing the timeline of ratios of NCSU-CS(I) to NCSU-CS(F), only 3 out of 87 (3%)  
1384 of the INP concentrations obtained through analysis by the identical off-line apparatus differed  
1385 by more than an order of magnitude.

1386 Despite the discrepancies noted in the time- and temperature-matched data, a more  
1387 positive message from the intercomparison is that the mean N<sub>INP</sub> reported by different  
1388 instruments for all temperature conditions taken together generally fell well within a span of one  
1389 order of magnitude. Figure S3 (values provided in Table 3) shows the percent of immersion INP

Formatted: Superscript

Deleted: and

Formatted: Superscript

Deleted: m

Deleted: gain, with

Deleted: NC State

Deleted: NC State

Deleted: NC State

Deleted: NC State

Deleted: 5

Deleted: 130

Deleted: 4

1400 measurements in which all instrument pairs agreed within one order of magnitude. This is also  
1401 consistent with the representation shown in Figure 6 for which linear regressions imply that the  
1402 CSU-IS measured  $N_{INP}$  a factor of 1.4 to 8 times higher than other methods. Similarly, and  
1403 importantly, the geometric mean ratios for Figure 8 listed in Table 2 were below a factor of about  
1404 5 in all cases. This level of agreement compares well with the findings from FIN-02, for which  
1405 the immersion  $N_{INP}$  measured by several online and offline instruments agreed within an order of  
1406 magnitude. This is encouraging given that FIN-02 was a laboratory intercomparison on single  
1407 composition aerosol samples consisting of particles with diameter  $< 2 \mu\text{m}$  whereas FIN-03 was a  
1408 field campaign in which temporal changes in the concentration, size distribution, and  
1409 composition of INPs at Storm Peak Laboratory were all potential factors. This level of  
1410 correspondence shows that field data can be collected with nearly the same level of accuracy as  
1411 laboratory experiments. While also mimicking the results of DeMott et al. (2017) for a smaller  
1412 instrument comparison exercise, agreement was quite similar to that found in another recent  
1413 intercomparison where INP concentrations measured by multiple systems were found to match  
1414 within a factor of 5 (Lacher et al., 2024).

1415  
1416  
1417  
1418  
1419  
1420  
1421  
1422

1423 **Table 2.** Count number (N), geometric mean, standard deviation (St. dev.), and 95% normal confidence  
 1424 intervals (CI) for the  $N_{WP}$  ratio data of Figure 8 in the main manuscript, including all temperature points.  
 1425 As for that figure, numerator instrument is on the upper horizontal scale and denominator instrument is  
 1426 listed on the vertical scale.

- Formatted: Font: 11 pt
- Formatted: Font: 11 pt
- Formatted: Font: 11 pt
- Formatted: Justified
- Formatted: Font: 11 pt, Italic
- Formatted: Font: 11 pt
- Formatted: Font: 11 pt, Not Bold

		<u>FRIDGE- CS</u>	<u>CSU- IS</u>	<u>NCSU- CS(I)</u>	<u>NCSU- CS(F)</u>	<u>CSU- CFDC</u>
<u>FRIDGE-CS</u>	<u>N</u>		146	107	90	20
	<u>Mean</u>		0.93	0.20	0.26	0.52
	<u>St. dev.</u>		2.86	0.57	0.43	1.12
	<u>CI</u>		0.46	0.10	0.09	0.49
<u>CSU-IS</u>	<u>N</u>	146		128	112	29
	<u>Mean</u>	1.07		0.19	0.21	0.26
	<u>St. dev.</u>	2.41		0.52	2.39	0.92
	<u>CI</u>	0.39		0.09	0.44	0.34
<u>NCSU-CS(I)</u>	<u>N</u>	107	128		83	28
	<u>Mean</u>	4.99	5.40		1.49	0.97
	<u>St. dev.</u>	9.85	9.41		5.03	1.11
	<u>CI</u>	1.87	1.63		1.08	0.41
<u>NCSU-CS(F)</u>	<u>N</u>	94	112	83		18
	<u>Mean</u>	3.81	4.80	0.66		1.37
	<u>St. dev.</u>	7.78	5.47	1.51		2.88
	<u>CI</u>	1.60	1.01	0.32		1.33
<u>CSU-CFDC</u>	<u>N</u>	20	29	28	18	
	<u>Mean</u>	1.91	3.79	1.02	0.73	
	<u>St. dev.</u>	3.54	8.98	1.91	1.61	
	<u>CI</u>	1.55	3.26	0.71	0.74	

1427  
 1428  
 1429  
 1430  
 1431



1432

1433 **Table 3.** Percent agreement within one order of magnitude for all times and temperatures

	$N_{INP}$ (FRIDGE-CS)	$N_{INP}$ (CSU-IS)	$N_{INP}$ (NCSU CS(I))	$N_{INP}$ (NCSU CS(F))	$N_{INP}$ (CSU-CFDC)
$N_{INP}$ (FRIDGE-CS)	100.0				
$N_{INP}$ (CSU-IS)	97.3	100.0			
$N_{INP}$ (NCSU CS(I))	85.9	68.6	100.0		
$N_{INP}$ (NCSU CS(F))	75.0	59.2	96.2	100.0	
$N_{INP}$ (CSU-CFDC)	100.0	87.5	100.0	84.6	100.0

- Formatted: Font: 11 pt, Bold
- Formatted: Font: 11 pt
- Formatted: Font: Italic
- Formatted: Font: Italic
- Formatted: Font: Italic
- Formatted: Font: Italic
- Formatted: Font: Italic
- Formatted: Font: Italic
- Formatted: Font: Italic
- Formatted: Font: Italic
- Formatted: Font: Italic

1434

1435 A possible explanation for  $N_{INP}$  measurement discrepancies that has been tendered in  
 1436 other intercomparison campaigns sampling ambient air is that INPs are highly sensitive to the  
 1437 size range of collected aerosol, and systematic size-dependent differences in collection  
 1438 efficiencies vary for different collection types (DeMott et al., 2017; Knopf et al., 2021; Lacher et  
 1439 al., 2024). For example, Lacher et al. (2024) found significant underestimates of INPs by both  
 1440 online and offline methods measuring from the PM10 inlet versus offline measurements from  
 1441 filter collections made on the laboratory rooftop. In this study, as we have noted above, a  
 1442 similarly consistent difference between rooftop versus laboratory or between online and offline  
 1443 measurements is not found. FRIDGE-CS INP concentration measurements from the turbulent-  
 1444 flow inlet and CSU-IS INP concentration measurements from the rooftop filter agreed within an  
 1445 average of about 30% over the course of the study. The CSU-CFDC INP measurements that  
 1446 were limited and thus biased by its upstream total particle impactor (at 2.5 μm) agreed well on  
 1447 average with the NCSU (F) and (I) measurements, although we may note that if the CSU-CFDC  
 1448 data had been corrected for instrumental loss of particles “out-of-lamina” as found for

- Formatted: Font: Italic
- Formatted: Font: Italic, Subscript
- Deleted: on average
- Deleted: reasonably
- Deleted: NC State
- Deleted: .

1453 measurements on mineral dust (DeMott et al., 2015), INP concentration results would have been  
1454 within a factor of two of the CSU-IS and FRIDGE-CS data. Larger particles do tend to have  
1455 higher likelihood of containing ice nucleation sites, so biases in their collection can lead to  
1456 sometimes large differences in assessed INP concentrations (Mason et al., 2016). Disaggregation  
1457 of the very largest collected particles when placed in water suspensions has also been implicated  
1458 for discrepancies between different substrate collections (DeMott et al., 2017; Lacher et al.,  
1459 2024). For example, if very large aggregates that are preferentially collected by one substrate  
1460 versus another, disaggregation in water could lead to a high bias in ice nucleation sites effective  
1461 at lower temperatures. There may have been additional line losses for the online instruments  
1462 sampling from an inlet and using tubing to transfer particles, though these tend to be of minor  
1463 influence at below the impactor size cut (Knopf et al., 2021). The impinger is known to be less  
1464 efficient for small (<200 nm) and large (>10 µm) particle capture, but unless the relatively light  
1465 to moderate wind conditions at the inlet during FIN-03 conferred some special bias, Hader et al.  
1466 (2014) predict a 50% capture efficiency at near 10 µm. The filter samplers on the rooftop should  
1467 have been equivalent, with the only difference being the orientation of filters for the NCSU  
1468 samples (mounted face-down). The size bias in this configuration is unknown. The FRIDGE  
1469 filter should have captured particles with the same efficiency as the turbulent flow inlet, since  
1470 only a very short line connected the filter to the interior inlet structure in the laboratory. Only if  
1471 very large INPs > 13 µm were dominant by number amongst total INPs, which is unexpected,  
1472 would the FRIDGE filter collection have been expected to differ from the rooftop CSU-IS filter  
1473 collections.

1474 Besides size-dependent sampling biases, the fact that measurements of immersion  
1475 freezing INP concentrations from ambient air are generally uncertain by up to one order of

**Deleted:** ice nucleation efficiency

**Deleted:** An obvious size-based collection bias existed for the online INP instruments, which had impactors upstream to limit particles >2.5 µm (50% cut-size) from entering.

**Deleted:** se

**Deleted:** in

**Deleted:** NC State

**Deleted:** being

**Formatted:** Font: Not Italic

1484 magnitude may result from unquantifiable random or non-random factors, or more likely from  
1485 quantifiable factors that were not fully controlled in this field study nor easily controlled across  
1486 investigating teams in general. Examples of known issues that were only documented after FIN-  
1487 03 relate to inconsistency in sample materials or sample handling and storage (e.g., Barry et al.,  
1488 2021b; Beall et al., 2021).

**Deleted:** In the end, it seems more likely that unquantifiable random and non-random sources of discrepancy, related to such things as sample size, instrument temperature sensor drift, varied instrument cooling rates and inconsistency in sample materials or handling and storage (e.g., Barry et al., 2021b; Beall et al., 2021), may also contribute to the fact that measurements of immersion freezing INP concentrations from ambient air are generally uncertain by up to one order of magnitude, as this study once again supports

### 1489 3.4 Relation of immersion freezing INPs to aerosol properties

1490 While establishing correlations between INPs and aerosol properties were not a focus of  
1491 the intercomparison, the ancillary aerosol data did allow for inspecting some simple linear  
1492 correlation analysis. This provides insight into the size range of greatest relevance for the INP  
1493 intercomparison period. Throughout the campaign, a positive and significant trend between total  
1494 LAS particle concentration (i.e.,  $> 0.1 \mu\text{m}$ ) and  $N_{\text{INP}}$  was observed for FRIDGE-CS ( $R = 0.55-$   
1495  $0.74$  and  $p < 0.05$  for measurements at  $-28 \text{ }^\circ\text{C} < T < -15 \text{ }^\circ\text{C}$ ), but no clear statistically significant  
1496 trend was observed between total LAS particle concentration and  $N_{\text{INP}}$  for the other four  
1497 instruments (Figure S4a). A greater number of significant positive trends were found between the  
1498 concentration of particles with diameter  $> 0.5 \mu\text{m}$  and  $N_{\text{INP}}$ . This was the case for the FRIDGE-  
1499 CS ( $R = 0.54-0.94$  and  $p < 0.05$  for measurements at  $-28 \text{ }^\circ\text{C} < T < -19 \text{ }^\circ\text{C}$ ), CSU IS ( $R = 0.46-$   
1500  $0.72$  and  $p < 0.05$  for measurements at  $-21$  to  $-25 \text{ }^\circ\text{C}$ ), NCSU CS(I) ( $R = 0.46-0.61$  and  $p < 0.05$   
1501 for measurements at  $-29 \text{ }^\circ\text{C} < T < -24 \text{ }^\circ\text{C}$ ), and the NCSU CS(F) ( $R = 0.51-0.64$  and  $p < 0.05$  for  
1502 measurements at  $-26 \text{ }^\circ\text{C} < T < -22 \text{ }^\circ\text{C}$ ).

**Deleted:** NC State

**Deleted:** NC State

1503 No consistent, significant ( $p < 0.05$ ) correlation was found between changes in  
1504 composition (from the PALMS categories and WBS-4A types) and immersion freezing  $N_{\text{INP}}$   
1505 across the range of setpoint temperatures employed during FIN-03 (Figure S4b).

### 1506 3.5 Inferences to INP compositions during FIN-03

1518 To provide context for the discussed intercomparisons and because this study provides  
1519 data needed for testing the relevance of existing parameterizations of ice nucleation in regional  
1520 and global climate models (Andreae & Rosenfeld, 2008; Morris et al., 2011; Seifert et al., 2011),  
1521 we utilize some previously-developed ice nucleation parameterizations for specific compositions  
1522 to diagnose consistency or not with INP compositions in the high altitude environment of FIN-  
1523 03. We examine parameterizations for mineral dust INPs that have different links to larger size  
1524 particle concentrations (DeMott et al., 2015) versus mineral dust surface area (Niemand et al.,  
1525 2012), and biological INPs as linked to fluorescent particle concentrations (Tobo et al., 2013;  
1526 Twohy et al., 2016). Hereafter we will refer to these parameterizations as DeMott 2015,  
1527 Niemand 2012, and Tobo 2013. We also utilize a more direct method of probing INP  
1528 compositions using the [CSU-IS sample treatments discussed in Section 2.2.2](#) and the [CSU-  
1529 CFDC heat treatments of single particles discussed in Section 2.2.1. In relation to these latter  
1530 investigations, we also introduce diagnostic tests of the arable soil dust INP parameterizations of  
1531 Tobo et al. \(2014\)](#).

1532 Each of the above-noted deterministic parameterizations was used to predict  $N_{\text{INP}}$  at  $-30$   
1533  $^{\circ}\text{C}$ ,  $-25$   $^{\circ}\text{C}$ ,  $-20$   $^{\circ}\text{C}$ , and  $-15$   $^{\circ}\text{C}$  using the equations and inputs described in Table 4, and  
1534 summarized below. We do not attempt an analysis using stochastic parameterizations.

1535 1) DeMott 2015 is based on CSU-CFDC laboratory measurements of ice nucleation on  
1536 mineral dust soil samples as well as field data from situations dominated by mineral dusts  
1537 (i.e., dust plumes from major deserts), collected for CFDC operational conditions  
1538 essentially the same as for this study (i.e., simulated immersion freezing conditions at  
1539 105% RH) (DeMott et al., 2015). For FIN-03, aerosol concentrations measured by the  
1540 LAS ( $> 0.5$   $\mu\text{m}$  dry diameter) and converted to STP concentrations were used as the input

Deleted: .

Deleted: 2

1543 for this parameterization for comparison to INP data that is also reported at STP  
 1544 concentrations. Predictions also depend on temperature (Table 4). Since PALMS data  
 1545 indicates that dust particles dominated the coarse mode only at sizes above 1 μm in  
 1546 diameter (Figure 4), we first adjust LAS data accordingly for the percentage of dust  
 1547 particles with diameters > 0.5 μm as input to this parameterization, which we have  
 1548 already stated is 23%. A correction factor (CF) of 3 was also applied (as indicated in  
 1549 Table 4) according to the results in DeMott et al. (2015) which showed that when  
 1550 applying the parameterization to represent immersion freezing dust INP concentrations in  
 1551 a model or in comparison to other immersion freezing methods, this CF is needed to  
 1552 account for CFDC underestimates of immersion freezing INPs (see Methods). The CF is  
 1553 applied in this case because calculations will be compared to the average  $N_{INP}$  from all  
 1554 measurements.

1555 2) The Niemand 2012 parameterization (Table 4) for mineral dust INPs is based entirely  
 1556 from laboratory measurements and incorporates measurements of temperature and  
 1557 particle surface area as the basis for prediction of INPs. It is especially important to limit  
 1558 the size range of aerosols for which this parameterization is applied, because total surface  
 1559 area was dominated by small particles in FIN-03. Therefore, with reference to Figure 4,  
 1560 we will assume that all dust surface area occurs at sizes larger than 0.5 μm and represents  
 1561 50% of that surface area.

Deleted: 2

Deleted: 2

Deleted: 2

1563 **Table 4. Summary of INP parameterizations.**

Param.	Equation	Constants
Mineral dust INPs: Niemand et al. (2012)	$N_{INP}(T_C) \approx n_s(T_C)S_{tot} = (a \exp(b(T_C) + c))(S_{tot})$ $N_{INP}(T_C) = \text{INP concentration (sL}^{-1}\text{) at T (Celsius)}$ $S_{tot}$ in units $\mu\text{m}^2\text{cm}^{-3}$ and $n_s$ in units $\text{m}^{-2}$	$a = 1 \times 10^{-9}$ $b = -0.517$ $c = 8.934$

Deleted: Table 2 Summary of INP parameterizations. Parameterization ... [5]

<u>Mineral dust:</u> <u>DeMott et al. (2015)</u>	$N_{INP}(T_K) = (cf)(n_{a>0.5\mu m})^{(\alpha(273.16-T_K)+\beta)}$ $\exp(\gamma(273.16 - T_K) + \delta)$ <p> <math>N_{INP}(T_K)</math> = INP concentration (sL<sup>-1</sup>) at T (Kelvin)  <math>n_{a&gt;0.5\mu m}</math> = mineral particle number concentration &gt; 0.5 μm (scm<sup>-3</sup>)            cf = 1 (CFDC data comparison) or 3 (other immersion freezing)         </p>	$\alpha = -0.074$ $\beta = 3.8$ $\gamma = 0.414$ $\delta = -9.671$
<u>Fluorescing biological aerosol particle</u> <u>INPs: Tobo et al. (2013)</u>	$N_{INP}(T_k) = (N_{FBAP>0.5\mu m})^{(\alpha'(273.16-T_k)+\beta')}$ $\exp(\gamma'(273.16 - T_k) + \delta')$ <p> <math>N_{INP}</math> = INP concentration (sL<sup>-1</sup>)  <math>N_{FBAP}</math> = FBAP concentration (scm<sup>-3</sup>)         </p>	$\alpha' = -0.108$ $\beta' = 3.8$ $\gamma' = 0$ $\delta' = 4.605$
<u>Fluorescing biological aerosol particle</u> <u>INPs: Cornwell et al. (2023)</u>	$N_{INP}(T_C) = f(T_C)1000N_{FBAP>0.5\mu m}$ <p> <math>f(T_C = -20\text{ °C}) = 0.318</math>  <math>f(T_C = -15\text{ °C}) = 0.016</math> </p>	N/A
<u>Arable soil dust INPs:</u> <u>Tobo et al. (2014)</u>	$N_{INP}(T_C) \approx n_s(T_C)S_{tot} = (a \exp(b(T_C) + c))(S_{tot})$ <p> <math>N_{INP}(T_C)</math> = INP concentration (sL<sup>-1</sup>) at T (Celcius)  <math>S_{tot}</math> in units μm<sup>2</sup>cm<sup>-3</sup> and <math>n_s</math> in units cm<sup>-2</sup> </p>	<u>Total soil:</u> $a = 1 \times 10^{-5}$ $b = -0.4736$ $c = 0.3644$ <u>Inorganics:</u> $a = 1 \times 10^{-5}$ $b = -0.6773$ $c = 7.8436$

1569

1570

1571

1572

1573

1574

1575

1576

1577

1578

3) As discussed earlier, we use two definitions of FBAP at sizes larger than 0.5 μm to and temperature to predict biological INP concentrations based on Tobo 2013 as defined in Section 2.1, presuming to bracket low and high estimates of their links to INPs. We also explore links of higher temperature freezing data (> -20 °C) to FP3 particles, using the same scalings of the relation between FP3 concentrations and INP concentrations as a function of temperature that were established by Cornwell et al. (2023) for a coastal California environment. While we have no reason to expect that these scaling factors listed in Table 4 are valid for the high altitude, continental environment of FIN-03, they are starting points to explore this additional link of certain FBAP particles to INPs.

Deleted: 2

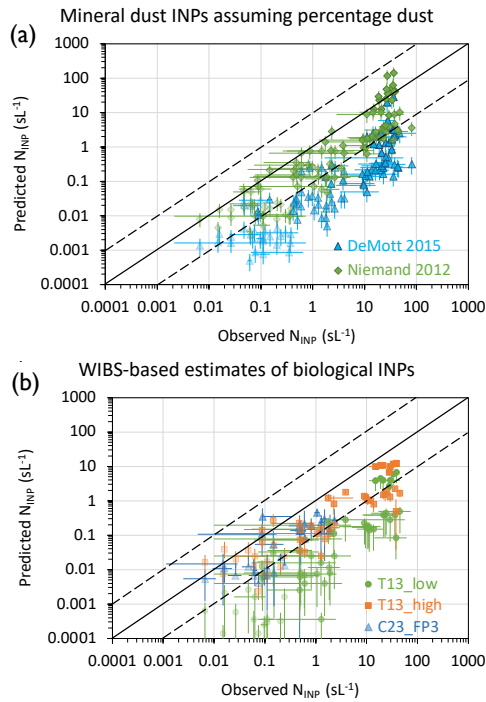
1580 To compare these parameterized values with observations, an overall mean observed  
1581 immersion freezing  $N_{\text{INP}}$  was calculated for each three-hour period based on all the available data  
1582 from all the instruments. This was considered as a reasonable approach since it factors in the  
1583 inherent variability found between methods. Immersion freezing  $N_{\text{INP}}$  was predicted for each  
1584 parameterization using mean WIBS-4A, and LAS data, both at STP concentrations, collected in  
1585 the coincident 3-hour periods of time as the INP data. The observed and predicted immersion  
1586 freezing  $N_{\text{INP}}$  are plotted against each other in Figure 9. Four temperatures of comparison ( $-15$ ,  $-$   
1587  $20$ ,  $-25$  and  $-30$  °C) are presented in Figure 9 for DeMott 2015, Niemand 2012, and Tobo 2013,  
1588 while two temperatures of comparison ( $-15$ ,  $-20$  °C) are used for links to FP3-based prediction  
1589 of biological INPs. Temperatures are indicated via levels of shading of the data points.  
1590 Using the constraint on mineral particles from the combination of PALMS and LAS data for the  
1591 campaign average, **predictions underestimate the mean  $N_{\text{INP}}$  at all temperatures (Figure 9a)**. The  
1592 Niemand 2012 surface-area-based INP estimates come modestly closer to observations,  
1593 averaging 25% of the total INP concentrations for all times and all temperatures, while the  
1594 DeMott 2015 predictions average 4% of INP concentrations, with large variability apparent.  
1595 These results can be expected to be highly sensitive to the assessed average

Deleted: 8

Deleted: 8

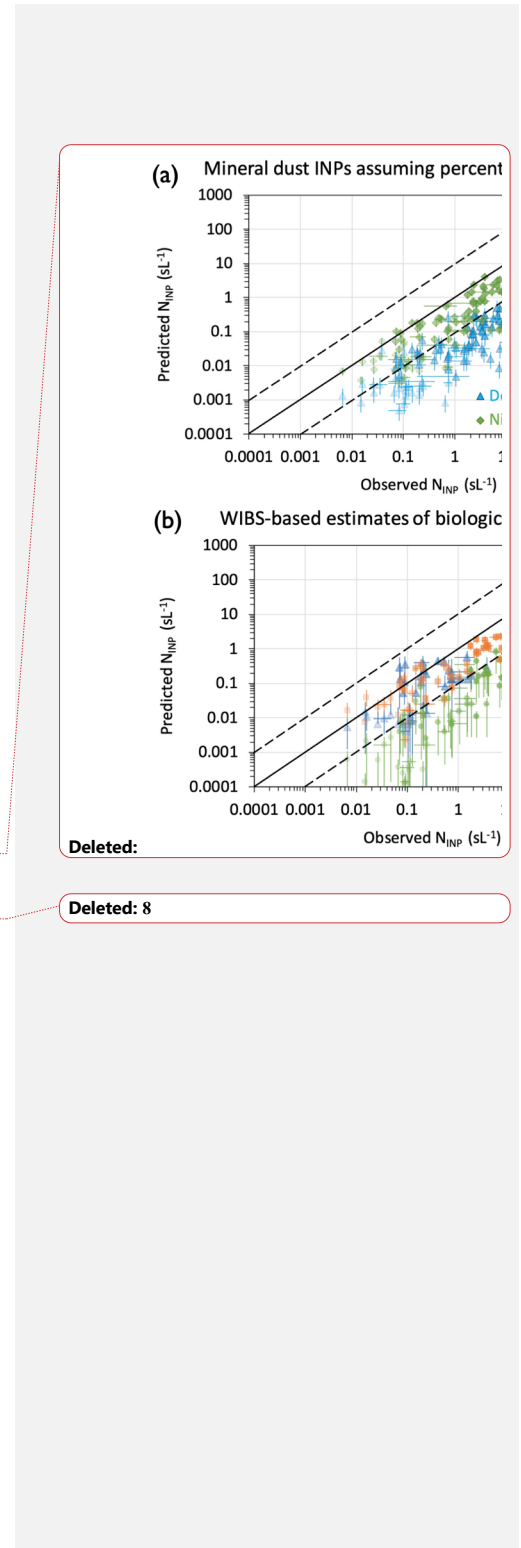
Deleted: predicted INPs underestimate the mean INP concentrations ...

Deleted: 8



1601

1602 **Figure 2.** a) Comparison of mean observed  $N_{\text{INP}}$  (all instrument average) and predicted  $N_{\text{INP}}$  calculated  
 1603 from DeMott et al. (2015) (DeMott 2015) and Niemand et al. (2012) (Niemand 2012) mineral dust INP  
 1604 parameterizations at temperatures -30 °C, -25 °C, -20 °C, and -15 °C (gradations in shading from dark to  
 1605 light) for the PALMS estimated percentages of dust particle number and surface area at sizes above 0.5  
 1606  $\mu\text{m}$ . Mean  $N_{\text{INP}}$  are averaged over three-hour periods and plotted uncertainties are standard deviations.  
 1607 Predicted  $N_{\text{INP}}$  uncertainties are propagated based on 25 % uncertainty in aerosol number and surface area  
 1608 concentrations. b) Comparison of mean observed  $N_{\text{INP}}$  and predicted  $N_{\text{INP}}$  calculated from  
 1609 parameterizations linking to FBAP concentrations from *Tobo et al. (2013)* (T13\_low and T13\_high; see  
 1610 text for description) and from *Cornwell et al. (2023)* (C23\_FP3) following the FP3 particle definition of





1613 *Wright et al.* (2014). Only -15 and -20 °C comparisons are shown for the FP3 prediction. The solid line in  
1614 each plot is the 1:1 line and the dashed lines represent an order of magnitude in both directions.

1615  
1616 mineral particle fraction at sizes above 0.5 µm (varied over the study) and on whether particles  
1617 that have a source from regional soils will be represented only by those with mineral content.

1618 Therefore, for comparison, parameterization results in Figure S5 use the assumption that all  
1619 particles at diameters exceeding 0.5 µm were dust particles. In this case, a somewhat unrealistic  
1620 maximum assumption on soil dust numbers and surface area that considers all particles and  
1621 compositions in this size range as emanating from dust, Niemand 2012 estimates a dust source

1622 for 50% and DeMott 2015 estimates 25% of observed INPs on average. Thus, the predictions of  
1623 the two parameterizations become more closely aligned for assumption of more overall mineral

1624 dust particles in the size range larger than 0.5 µm. Discrepancy has been noted previously in  
1625 applying these parameterizations to link to the aerosol model in an Earth System model for the  
1626 Southern Ocean region (McCluskey et al., 2023). In that case, calculations were based on aerosol

1627 model derived dust distributions and occurred under very low dust loading scenarios where  
1628 neither parameterization has been firmly tested in the laboratory or field. Under both

1629 assumptions on mineral particle number, since DeMott 2015 was developed based on CFDC  
1630 measurements for particles < 2.5 µm in the field and laboratory, a low bias compared to

1631 Niemand 2012 might be expected in comparison to average immersion freezing data that  
1632 includes larger particles.

1633 The timeline of predicted  $N_{INP}$  for the two dust parameterizations in comparison to mean

1634 observed  $N_{INP}$  is shown in Figure 10 for the same temperatures used in Figure 9. These analyses

1635 emphasize that 1) INP observations do not show a special enhancement during the biomass

1636 burning event at the start of FIN-03, and hence closer agreement of the dust parameterizations

Deleted: using an

Deleted: are presented in Figure S5

Deleted: admittedly

Deleted: mineral

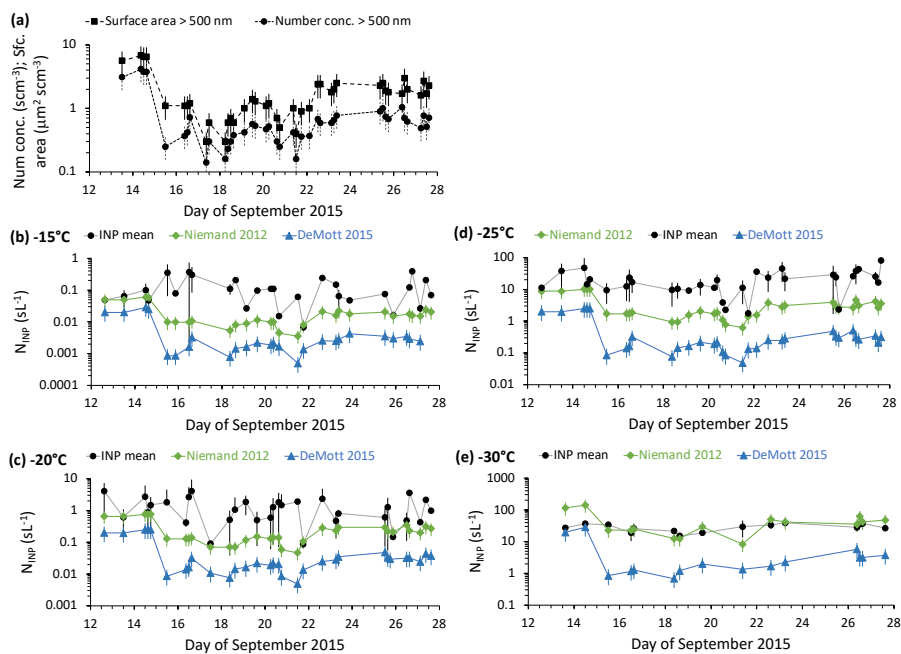
Deleted: ¶

Deleted: 9

Deleted: 8

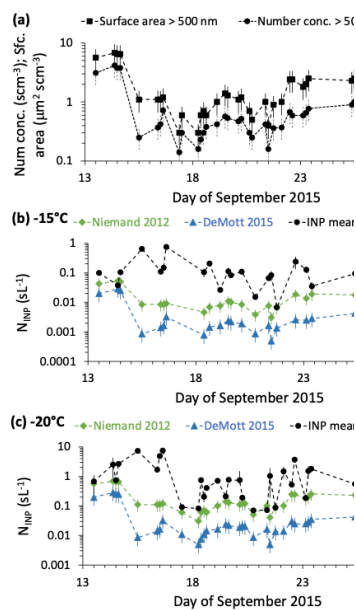
1644 with observations at that time is likely an artifact of attributing dust-like INP activation  
 1645 properties to the dominant biomass burning compositions at that time; 2) the structure of the  
 1646 timeline of predicted  $N_{INP}$  resembles that of the observed  $N_{INP}$  only below  $-20\text{ }^{\circ}\text{C}$ , as expected  
 1647 for a dominance of dust-like INPs; and 3) the predictions fare less well in describing the  
 1648 observed INP populations at  $> -20\text{ }^{\circ}\text{C}$  where biological INPs may be expected to have greater  
 1649 influence. Thus, these analyses overall suggest the presence of a dust-like immersion freezing  
 1650 INP type active at lower temperatures during FIN-03, but that the typical INP efficiency (INP as  
 1651 a function of dust concentration and temperature) attributed to mineral dust underestimates the  
 1652 freezing behavior of INPs overall during the period of study.

1653



1654

Deleted: the predicted  $N_{INP}$  trends better with observed  $N_{INP}$  at temperatures <

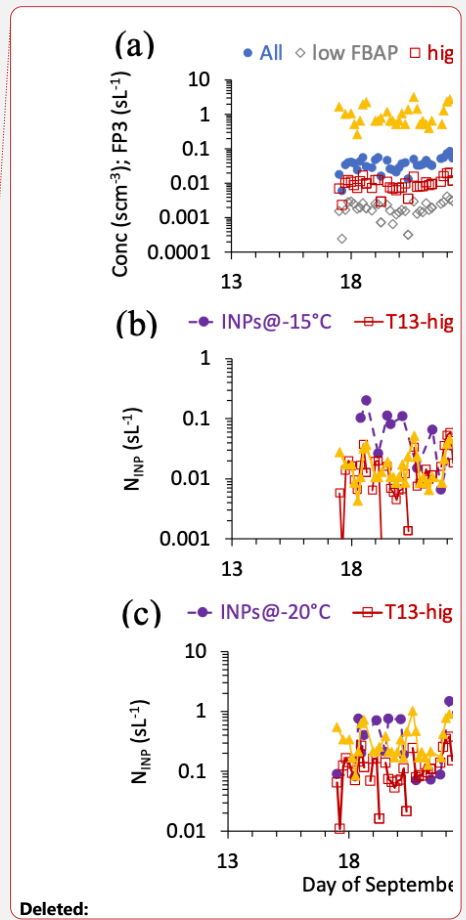
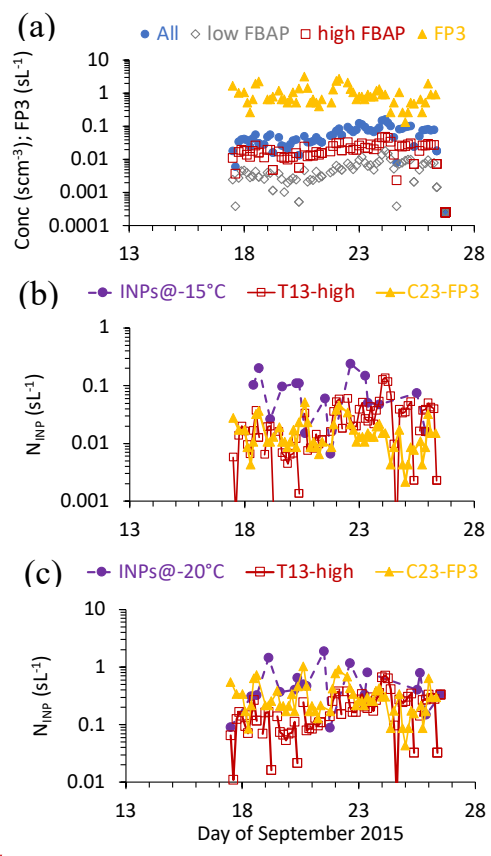


Deleted:

1658 **Figure 10.** Time series of aerosol number concentration and surface area (3-h averages at STP) in a), and  
 1659 observed mean measured immersion freezing  $N_{INP}$  (INP mean) plotted with predicted  $N_{INP}$  from the  
 1660 mineral dust parameterizations of Niemand 2012 and DeMott 2015 as described in the main text (all  
 1661 three-hour averages at STP) at temperatures of -15, -20, -25, and -30 °C in b) to e), respectively. Lines are  
 1662 intended only to connect data points and do not imply knowledge of intermediate values. Uncertainties  
 1663 mark one standard deviation above and below the mean values of all parameters.

Deleted: 9

Deleted: Dashed l



1664

1668 **Figure 11.** a) Timelines of WIBS-based fluorescent particles assignments (all fluorescing in any channel,  
1669 low and high FBAP, and FP3 particles), as defined in the text, during FIN-03. b) INP observed mean  
1670 concentrations and biological INP parameterization predictions linked to high FBAP following Tobo et  
1671 al. (2013) (T13-high) and FP3 particles following Cornwell et al. (2023) at -15 °C in b) and -20 °C in c).

Deleted: 10

1672  
1673 For FIN-03, the Tobo 2013 parameterization of biological INPs consistently  
1674 underpredicted  $N_{INP}$ , independent of the WIBS FBAP definition used, denoted as T13\_low and  
1675 T13\_high in the scatterplot comparison of measured versus predicted values (at all times and  
1676 temperatures) in Figure 9b and the timeline comparisons at -15 and -20 °C shown in Figure 11,  
1677 Figure 11 also

Deleted: 8  
Deleted: 0  
Deleted: 0

1678 shows the timeline of WIBS total fluorescent particle concentrations, the high and low FBAP  
1679 concentrations, and FP3 concentrations. The higher FBAP prediction of INPs falls much closer  
1680 to the observations than the low FBAP prediction in Figure 9b and shares some proximal  
1681 equivalence to observations at -15 to -20 °C at times. This result is like that found by Twohy et  
1682 al. (2016) for air over the site where Tobo et al. (2013) collected their data, with the higher  
1683 FBAP estimate bounding the upper end of measured immersion freezing INP concentrations at

Deleted: 8

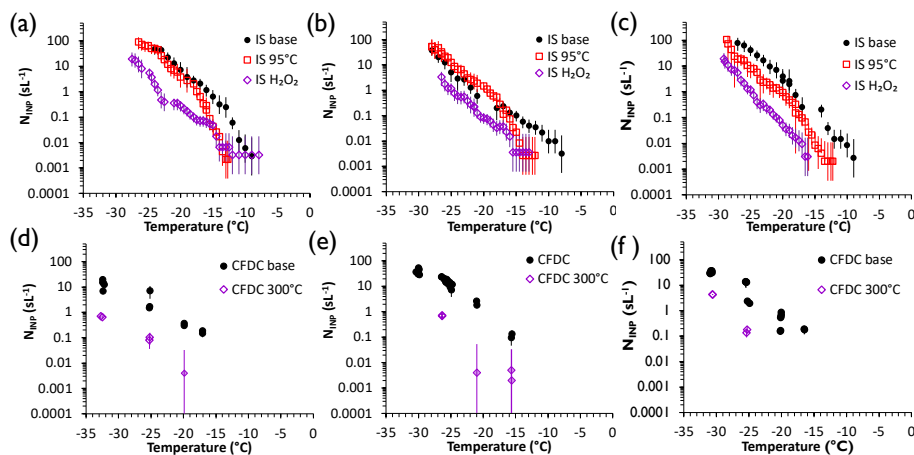
1684 temperatures > -20 °C. Also notable in Figure 9b and Figure 11, is that the C13-FP3 INP  
1685 concentration predictions filled a similar space as the T13\_high estimates, coming closest  
1686 together at -20 °C. While these results suggest that biological INP parameterizations can explain  
1687 the higher temperature INP concentrations observed during FIN-03, with caveats on the large  
1688 and likely not fully quantifiable uncertainty in such predictions, the temporal analysis indicates  
1689 that there is no consistent temporal agreement between predicted and measured INPs, even if  
1690 different scaling factors were applied to the predictions. Predictions at -20 °C show better

Deleted: 8  
Deleted: 0

Deleted: ¶  
(Figure S6)

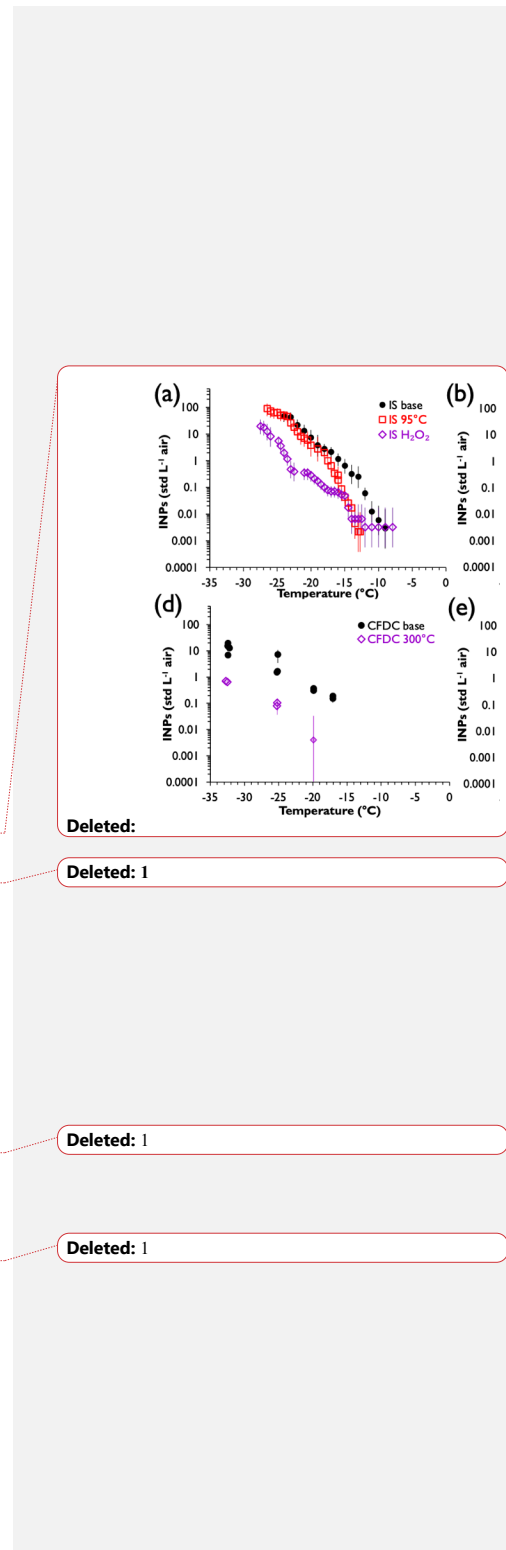
Deleted: ¶  
Deleted: again  
Deleted: the best

1703 overall agreement, while those at  $-15\text{ }^{\circ}\text{C}$  suggest that the Cornwell et al. (2023) scaling factor  
 1704 should be higher for the SPL site at the time of FIN-03 to better describe mean values of  
 1705 biological INP concentrations using the FP3 particle signal.  
 1706



1707  
 1708 **Figure 12.** Summary of treated IS filter suspensions using heat and peroxide (a, b, c) and dry heat-treated  
 1709 CSU CFDC single particle data (d, e, f), for September 15, 23 and 25 (a-c, d-f, respectively). Error bars  
 1710 represent 95% confidence intervals for individual experimental spectra for the CSU-IS and for individual  
 1711 CSU CFDC measurements.

1712 The results of CSU-IS and CSU-CFDC treatments on INP concentrations measured for  
 1713 three (of 21 overall) intercomparison time periods are shown in Figure 12, for examination of  
 1714 consistency with the results of the diagnostic parameterization analysis just discussed. In Figure  
 1715 12a-c, it is seen that thermal treatments indicated the strong contribution of inferred biological  
 1716 INPs primarily at temperatures higher than about  $-20\text{ }^{\circ}\text{C}$ , but that peroxide digestion of organic  
 1717 compounds lowered INP activity at all tested temperatures by an order of magnitude on average.



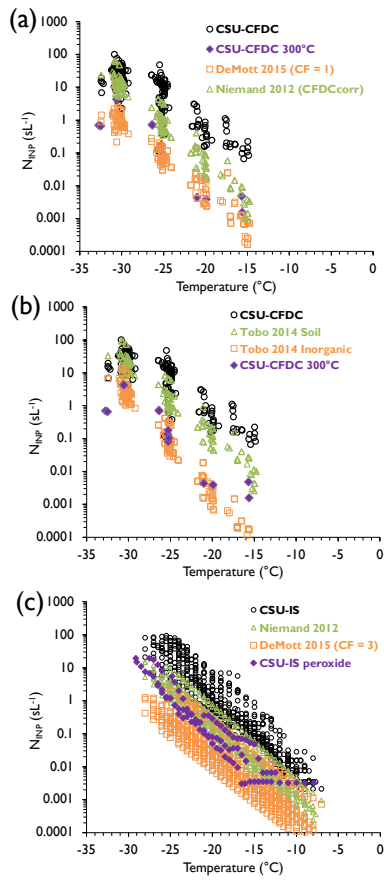
1722 Similar reductions of INPs measured for single particles by the CSU-CFDC following dry  
1723 heating (Figure 12d-e) demonstrate strong consistency with the IS results for bulk immersion  
1724 freezing on the dominance of organic INP compositions, even though CSU-CFDC measured  
1725 unamended INP concentrations were always lower. The CSU-IS heat treatment results (Figure  
1726 12a-c) suggest that biological INPs may have been ubiquitous during FIN-03 at temperatures  
1727 above  $-20^{\circ}\text{C}$ , and extended to lower temperatures at times, as indicated by the results from  
1728 September 25. This is broadly consistent with the parameterization results based on FBAP  
1729 measurements, although the Tobo 2013 and FP3 parameterizations did not capture all the  
1730 influence of apparent biological INPs during the study. Whether for size-limited ( $< 2.5\ \mu\text{m}$ ) as in  
1731 CSU-CFDC measurements, or bulk aerosol collected for CSU-IS immersion freezing  
1732 measurements, the inferred INP compositions that were typically dominated by organics at  
1733 temperatures  $< -20^{\circ}\text{C}$  could reflect origins from arable soil dusts (Testa et al., 2021) that  
1734 surround the region of study. Biomass burning aerosols also have influence as organic INPs  
1735 (Schill et al, 2020; Barry et al., 2021a). However, while biomass burning type particles were  
1736 noted as a prevalent composition in FIN-03, these types of potential INPs likely cannot explain  
1737 INP concentrations in FIN-03 because Barry et al. (2021a) showed that Western U.S. biomass  
1738 burning INPs have active site densities about 3 orders of magnitude lower than those attributed  
1739 to dust particles that also were ubiquitous at modest number concentrations during FIN-03.  
1740 Furthermore, the strong biomass burning event noted on September 14 had only modest, if any,  
1741 apparent impacts on INP concentrations despite greatly elevated aerosol concentrations and  
1742 surface areas, as already mentioned above (Figure 10).

Deleted: 1

Deleted: 1

Deleted: 9

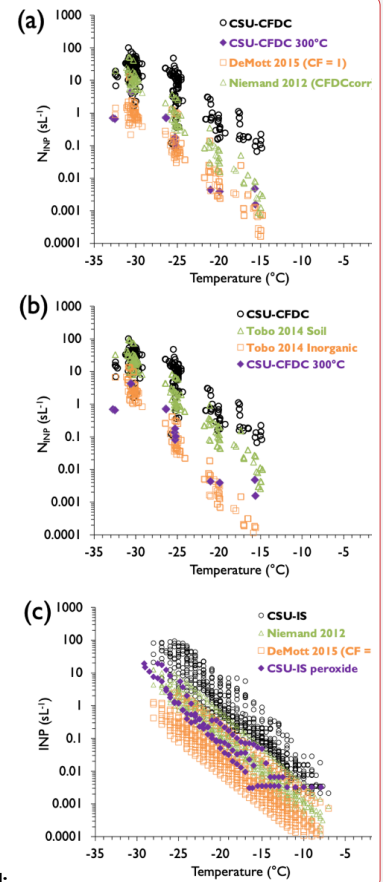
1746 Finally, in Figure 13, we address whether the treatment results support the conclusion of  
 1747 the diagnostic parameterization analysis suggesting that inorganic INPs (mineral particles in  
 1748 particular) were of minor influence during FIN-03.



1749  
 1750 **Figure 13.** a) Comparison of all untreated CSU CFDC data (black circles), cases after passing through the  
 1751 upstream 300  $^{\circ}C$  tube heater (purple diamonds), and calculations from the DeMott 2015 dust  
 1752 parameterization in (orange squares) and with CF = 1 as appropriate for a direct comparison to CSU

Deleted: 2

Deleted: We introduce the additional parameterization of Tobo et al. (2014) (Tobo 2014) for arable soil dust INPs as part of this discussion. Tobo et al. (2014) parameterized the ice nucleation behavior of soil dusts from Wyoming, regionally proximal to the FIN-03 site at SPL, specifically using the CSU CFDC and the dry heat method at



Deleted:

Deleted: 12

1762 CFDC data (see text). b) The same exercise as in a) but using predictions of total soil organic INP  
1763 concentrations and inorganic INP concentrations within soil INPs, both from Tobo et al. (2014). c) The  
1764 same exercise but for all CSU-IS data and the cases with peroxide digestion. In this case, CF = 3 must be  
1765 used in DeMott 2015 and the mineral dust INP prediction of Niemand 2012 is also shown.

1766  
1767 For this purpose, we introduce results for the parameterization of Tobo et al. (2014) (hereafter,  
1768 Tobo 2014) for arable soil dust INPs listed in Table 4. Tobo et al. (2014) parameterized the ice  
1769 nucleation behavior of soil dusts from Wyoming, regionally proximal to the FIN-03 site at SPL,  
1770 specifically using the and the CSU-CFDC dry heat method at 300 °C to indicate organic versus  
1771 inorganic INP contributions from such soil particles. A caveat is that their results were for dusts  
1772 generated in the laboratory and size-selected at 600 nm. This parameterization, like Niemand

1773 2012, is based on the surface area of dust particles and so we apply the same assumptions as  
1774 before to restrict to the proportion of dust larger than 0.5 µm. Since the CSU-CFDC is also  
1775 restricted to measuring INPs at diameters below 2.5 µm, we apply a correction factor to the  
1776 surface area to account for the fact that the surface area at below this size was 90% of the project  
1777 average total surface area. No significant impact of the treatments is assumed on aerosol  
1778 concentrations or surface area at sizes above 0.5 µm in Figure 13.

1779 Figures 13a and 13b focus on specific comparisons to CSU-CFDC data. In Figure 13a, it  
1780 is seen that INP concentrations predicted by the DeMott 2015 parameterization for sampling  
1781 periods during the entire campaign show remarkable agreement with the 300 °C CSU-CFDC  
1782 data on selected days when applying CF = 1 in the parameterization, as is appropriate for a direct  
1783 comparison to CSU-CFDC instrument data that is uncorrected for the underestimates that led to  
1784 selecting CF = 3 for atmospheric modeling studies. In Figure 13 b, it is shown that the Tobo  
1785 2014 parameterizations for untreated soil dusts and the inorganic remnants also give very good

Deleted: 300 °C to indicate organic versus inorganic INP contributions from such soil particles.

Deleted: ¶

Deleted: 2

Deleted: 2

Deleted: 2

Deleted: 2

Deleted: 12



1794 agreement with CFDC untreated and treated  $N_{INP}$  data, supporting the likely important influence  
1795 of such arable soil dusts during FIN-03. Predictions for untreated soils do not quite reach the  
1796 level of the observed INPs, but this could be explained by the additional contribution of  
1797 biological INPs that has already been discussed.

1798 In Figure 13c, direct comparisons of the Niemand 2012 and DeMott 2015 predictions for  
1799 mineral dust INPs for the entire project are shown in comparison to the CSU-IS untreated and  
1800 H<sub>2</sub>O<sub>2</sub> treated data on selected days. The DeMott 2015 prediction of INP concentrations uses CF  
1801 = 3 in this case, as appropriate. The same discrepancy between the DeMott 2015 and Niemand  
1802 2012 predictions as discussed already regarding Figure 9a appears in this comparison.

1803 Nevertheless, it is seen that both parameterizations grossly underestimate untreated CSU-IS INP  
1804 concentrations and the treated CSU-IS results fall between the predicted values, agreeing better  
1805 with the Niemand 2012 parameterization. While one might wish to allude to the fact that the IS  
1806 filters sample particle sizes, to 10 µm and possibly larger that may have higher ice nucleation  
1807 efficiencies, while the CSU-CFDC was restricted to sampling particles <2.5 µm as a source for  
1808 the lower DeMott 2015 estimate in comparison to CSU-IS data, we have already addressed that  
1809 there was no general consistency in INP concentrations for methods that sampled similar size  
1810 particles overall. The best that can be stated is that the parameterization exercises and treatment  
1811 data strongly support that inorganic INPs were of weak influence during FIN-03 and that arable  
1812 soil dusts and biological INPs accounted for the strongest influences during sampling, akin to the  
1813 findings of Testa et al. (2021).

### 1814 3.6 Observations of INPs in the deposition nucleation regime

1815 Measurements of deposition nucleation  $N_{INP}$  are summarized in Figures 14 and 15,  
1816 FRIDGE-DC nucleation substrates were collected for 1 to 5 periods on many days during FIN-03

Deleted: 2

Deleted: 8

Deleted: 13

Deleted: 4.

Deleted: FRIDGE-DEP

1822 and processed at 5-degree interval temperatures from -15 to -30 °C, and for setpoint humidity of  
 1823 95% and 99% RH (uncertainties to 2%). Data collected at 102% via the standard FRIDGE  
 1824 methods are not included herein. CSU-CFDC and MIT-SPIN deposition data were collected  
 1825 nominally at 95% RH with an uncertainty of about 2.5% RH, and at a range of temperatures on  
 1826 different days. Mean values and standard deviation error bars of the ~~FRIDGE-DC~~ data are  
 1827 shown in Figure 14a and median values of ~~FRIDGE-DC~~  $N_{INP}$  (with interquartile values as error  
 1828 bars) are shown in Figure 14b. Standard deviations were large over the course of the study for  
 1829 comprehensive ~~FRIDGE-DC~~ data when binned at 5-degree interval temperatures. Nevertheless,  
 1830 average concentrations of deposition INPs measured by the ~~FRIDGE-DC~~

Deleted: FRIDGE-DEP

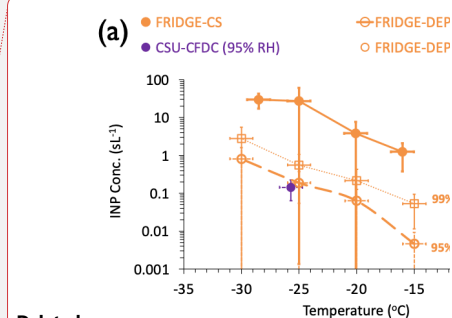
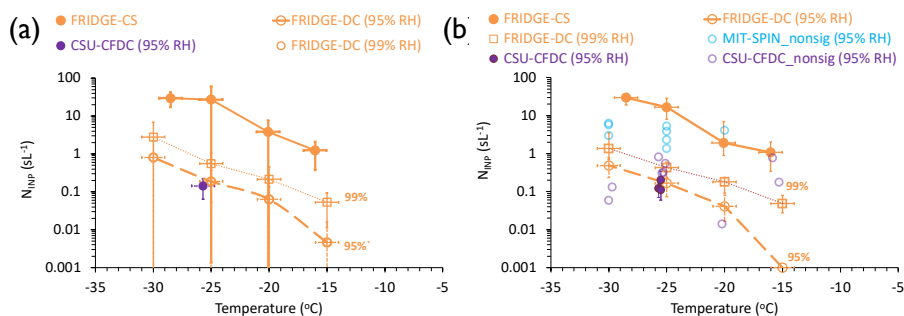
Deleted: 3

Deleted: FRIDGE-DEP

Deleted: 3

Deleted: FRIDGE-DEP

Deleted: FRIDGE-DEP



Deleted:

Deleted: 3

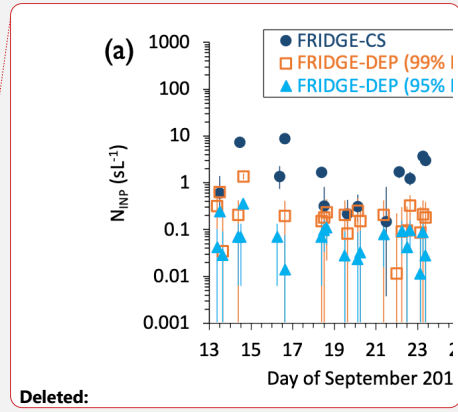
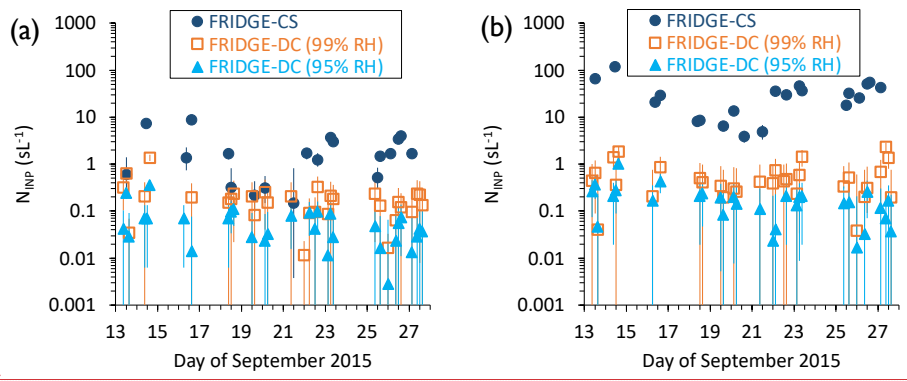
Deleted: FRIDGE-DEP

1832 **Figure 14.** Summary of deposition-mode  $N_{INP}$  ( $sL^{-1}$ ) as a function of temperature. In a), mean ~~FRIDGE-~~  
 1833 ~~DC~~ data at 95% (open orange circles) and 99% (open orange squares) RH are shown along with mean  
 1834 immersion freezing data from the FRIDGE-CS (filled orange circles) and the mean for the few cases of  
 1835 statistically significant CSU-CFDC data (filled purple circle) at 95% RH. Error bars are one standard  
 1836 deviation of the means. In b), median ~~FRIDGE-DC~~ data are shown and error bars for these are the 95%  
 1837 confidence intervals. The significant CSU-CFDC measurement points at 95% RH are also shown with  
 1838 their 95% confidence intervals. Data measured at 95% RH from the CSU-CFDC and MIT-SPIN that were

Deleted: FRIDGE-DEP

1849 positively valued, but failed significance testing are shown without errors as open purple and open blue  
 1850 circles, respectively.  
 1851  
 1852 indicated a consistent 3-5 factor increase between 95 and 99% RH over the range of  
 1853 temperatures investigated.  $N_{INP}$  differences at the two RH values were slightly smaller for  
 1854 median values (Figure 14b), and the median values are slightly lower than the means. Finally,  
 1855 FRIDGE-CS values are plotted in each panel of Figure 14, indicating that FRIDGE-DC  $N_{INP}$   
 1856 concentrations averaged for 99% RH are factors 10 to 30 lower than average immersion freezing  
 1857  $N_{INP}$  concentrations, depending on temperature.

Deleted: concentration  
 Formatted: Font: Italic  
 Deleted: 3  
 Deleted: 3  
 Deleted: FRIDGE-DEP  
 Formatted: Font: Italic



1858 **Figure 15.** Time series of FRIDGE-CS (immersion freezing) and FRIDGE-DC (deposition)  $N_{INP}$   
 1859 measured at a) -20 °C, and b) -25 °C. Data are from individual filters or wafer collections and error bars  
 1860 are 95% confidence intervals.  
 1861

Deleted: 4  
 Deleted: FRIDGE-DEP

1862 One day of significant data was obtained for the CSU-CFDC deposition measurements  
 1863 while using the aerosol concentrator, on September 14, containing three different time periods.  
 1864 These are averaged to create the only online data point represented as a mean in Figure 14a. The  
 1865 individual period measurements from this day, with confidence intervals as errors, are shown for

Deleted: 3

1874 the CSU-CFDC in Figure 14b. Thereby it is seen that these measurements at close to  $-25\text{ }^{\circ}\text{C}$   
1875 agree very well with the mean FRIDGE deposition  $N_{\text{INP}}$  at  $-25\text{ }^{\circ}\text{C}$  and 95% RH. No  
1876 measurements of significance were achieved with the MIT-SPIN when operating in the  
1877 deposition regime. In fact, the most common CSU-CFDC and MIT-SPIN deposition nucleation  
1878  $N_{\text{INP}}$  results were below instrument detection limits, not meeting the test for significance despite  
1879 being positively valued, as shown for all periods from 6 common days of such observations  
1880 represented in Figure 14b. Understanding that these data represent a failure to collect  
1881 statistically-defensible data, the non-significant data generally scatter about the significant CSU-  
1882 CFDC data and the FRIDGE-DC data at 95% RH, with a higher bias for the MIT-SPIN data.  
1883 This indicates the difficulty for online continuous flow instruments to capture low deposition  
1884  $N_{\text{INP}}$  concentration data that fall below  $1\text{ sL}^{-1}$  at most times, considering the FRIDGE-DC data as  
1885 the standard. Higher sample volumes and limited background frost conditions are needed to  
1886 sense these low atmospheric INP concentrations.

1887 Time series of the FRIDGE-DC measurements at  $-20\text{ }^{\circ}\text{C}$  and  $-25\text{ }^{\circ}\text{C}$  are shown in Figure  
1888 15. Deposition-mode  $N_{\text{INP}}$  has been averaged over three-hour periods for this analysis. The  
1889 FRIDGE immersion freezing data is included in this figure to allow for direct comparison  
1890 temporally. Immersion freezing  $N_{\text{INP}}$  generally exceeded deposition-mode  $N_{\text{INP}}$  when both types  
1891 of measurements were collected by the two FRIDGE operational methods within the same period  
1892 (or during adjacent time periods). This difference ranged from 0 to 2 orders of magnitude, with  
1893 the largest differences seen at  $-25\text{ }^{\circ}\text{C}$  and a period of insignificant differences between the  
1894 operational mode results seen only from the 18<sup>th</sup> to the 22<sup>nd</sup> of September at  $-20\text{ }^{\circ}\text{C}$  (Figure 15a).

1895 Based on these FRIDGE-CS and FRIDGE-DC results, immersion-mode ice nucleation  
1896 dominates at most times at mixed-phase cloud temperatures. Nevertheless, deposition-mode ice

Deleted: 3

Deleted: 3

Deleted: FRIDGE-DEP

Deleted: FRIDGE-DEP

Deleted: FRIDGE-DEP

Deleted: 14

Deleted: 14a

Deleted: FRIDGE-DEP

1905 nucleation contributes modestly to the pool of INP at mixed-phase cloud temperatures in the  
1906 atmosphere, and thus may bear consideration for parameterization in atmospheric models. The  
1907 ability of online ice nucleation instruments to measure  $N_{\text{INP}}$  in the deposition mode in  
1908 correspondence to offline measurements has not been confirmed due to the mentioned inability  
1909 of the online instruments used in FIN-03 to capture the low deposition nucleation  $N_{\text{INP}}$   
1910 concentrations. More work should be carried out on measurements of INPs in the deposition  
1911 mode to understand variabilities in time and their relation to INP size and composition, as well as  
1912 to resolve if online measurements can be improved. For the time being, the substrate methods  
1913 appear to be recommended for ambient atmospheric measurements in the realm below water  
1914 saturation at mixed-phase cloud temperatures.

1915

#### 1916 4. Summary and conclusions

1917 FIN-03 was an ice nucleation instrument intercomparison conducted in the challenging  
1918 environment of the high-altitude mountaintop field setting. Two online systems (CSU-CFDC,  
1919 MIT-SPIN) and three offline systems (FRIDGE, CSU-IS, ~~NCSU-CS~~) were represented in FIN-  
1920 03. The immersion freezing INP concentrations measured in FIN-03 by one or more instruments  
1921 spanned a dynamic range of over five orders of magnitude ( $10^{-3}$  to  $\approx 10^2 \text{ L}^{-1}$ ) over the temperature  
1922 range  ~~$-34$~~  °C to  ~~$-7$~~  °C. Intercomparisons for two or more measurements were made from  $-30$  to  
1923  $-15$  °C. Agreement within one order of magnitude in immersion freezing  $N_{\text{INP}}$  was generally  
1924 observed between all ice nucleation instruments measuring immersion INP concentrations at any  
1925 given temperature if measurement and sampling times were matched to within 3 hours. Better  
1926 than one order of magnitude agreement was found at temperatures lower than  $-25$  °C and higher  
1927 than  $-18$  °C, with occasional deviations larger than an order of magnitude in the temperature

Deleted: NC State

Deleted: ~

Deleted: 5

Deleted: 5

1932 range  $-25\text{ }^{\circ}\text{C}$  to  $-18\text{ }^{\circ}\text{C}$ . Always better than an approximate 5x factor agreement was found  
1933 between average ratios of the  $N_{\text{INP}}$  measured by pairs of instruments for all times of sampling  
1934 We do not have a full understanding of what controls better or worse agreement at different  
1935 times or different temperatures, though some factors have been previously discussed in  
1936 documenting FIN-02 laboratory studies (DeMott et al., 2018). In this study, there was some  
1937 inference that the different filters and impinger used did not equally capture particles in all size  
1938 ranges, which is something to improve on in future studies. A review of handling and storage  
1939 protocols for consistency amongst groups could also help isolate the role of such factors. Given  
1940 the constant changes in the concentration, size distribution and composition of the ambient  
1941 aerosol population, inevitable with any field campaign, ~~the~~ level of agreement found represents  
1942 state-of-the-art, at least as judged based on recent laboratory and other field comparisons using  
1943 similar instrumentation that appear to show 5x factor agreements (e.g., Knopf et al., 2021;  
1944 Brasseur et al., 2022; Lacher et al., 2024).

1945 Although FIN-03 was not conducted as an aerosol/INP closure study per se, ancillary  
1946 data on aerosol sizes and compositions as recommended in more recent discussions of needs for  
1947 true closure exercises (Knopf et al., 2021; Burrows et al., 2022) were purposefully collected for  
1948 integration into analyses. This included explicit measurements of the aerosol size distribution,  
1949 and single particle measurements of aerosol chemical and biological composition. These  
1950 measurements allowed inferences to be made about INP compositions that provided context for  
1951 the period of study and establish an example for future intercomparison and long-term  
1952 measurement efforts. Through comparing INP data to some current parameterizations describing  
1953 biological, mineral and soil dust INPs, and additional direct investigations of INP composition  
1954 via certain pre-treatments to remove biological and organic immersion-freezing INPs, these

Formatted: Font: Italic

Formatted: Font: Italic, Subscript

Formatted: Font: Italic

Deleted: is

1956 investigations revealed ubiquitous biological and organic-influenced soil-dust-like INP  
1957 influences that mimic those found over other continental regions (Knopf et al., 2021; Testa et al.,  
1958 2021; Lacher et al., 2024). Biological INPs were indicated via selected immersion freezing heat  
1959 treatments to be dominant at  $> -20$  °C, although of potential influence at all mixed-phase  
1960 temperatures. Prediction of these based on parameterizations that utilize single particle  
1961 fluorescence data (Tobo et al., 2013; Wright et al., 2014; Cornwell et al., 2023) suggest the  
1962 average utility of such parameterizations but these were unable to predict the full temporal  
1963 variation of biological INPs. This suggests that local variations of these INPs, which may in fact  
1964 represent multiple biological particle types, is an area that requires more effort. Based on  
1965 relatively good consistency between predicted and measured mineral influences on immersion-  
1966 freezing  $N_{\text{INP}}$  concentrations, strictly mineral or other inorganic components of INPs were  
1967 suggested to have a modest contribution to total INP concentrations at most times and at the  
1968 freezing temperatures probed during this study. As in most prior studies, the mineral influence  
1969 became stronger at the lowest temperatures assessed. In contrast, it was found by comparison to  
1970 a parameterization based on proximally regional soil particles that arable soil INPs likely  
1971 explained the second most important contribution (behind biological INPs) of INPs during FIN-  
1972 03, those emanating from other organic particle components that may have been internally mixed  
1973 with minerals. Biomass burning influences were possible but appear to have not contributed  
1974 greatly to the climatology of INPs during the study. It was critically important in arriving at these  
1975 conclusions to have single particle aerosol composition data, from a mass spectrometer that  
1976 could discern the sizes and fractional contribution of minerals and from a laser-based single  
1977 particle fluorescence measurement to estimate the biological character of particles. Nevertheless,  
1978 there is a limit beyond the instrumentation complex here utilized in that INPs may always

1979 ~~constitute a subset of the aerosol different in composition and size than the predominant aerosol.~~  
1980 ~~Knowledge advance may require improvement in methods that link INP and compositional~~  
1981 ~~measurements on single particles to specifically isolate these factors. Hence,~~ a great amount of  
1982 work is still needed to generally parameterize the mixed INP populations that may occur  
1983 temporally in the atmosphere at higher altitude sites like SPL, or anywhere for that matter.  
1984 Importantly, FIN-03 included an assessment of the separate relative contributions of  
1985 deposition and immersion freezing INP concentrations, one of the few existing data sets of this  
1986 kind. The offline ~~FRIDGE-DC~~ method was used to acquire comprehensive deposition  $N_{INP}$   
1987 measurements in dependence on RH (95 and 99%), while the CSU-CFDC and MIT-SPIN  
1988 instruments attempted focused deposition nucleation measurements at (nominally) 95% RH on  
1989 several days. ~~The deposition INP concentration obtained by FRIDGE-DC increased from 95%~~  
1990 ~~RH to 99% RH on average by a factor of 3.3.~~ Also, deposition  $N_{INP}$  were nearly always lower  
1991 than immersion freezing  $N_{INP}$  ~~for the temperatures assessed.~~ Deposition INP concentrations at  
1992 most times at 99% RH (always at 95% RH) were lower by an order of magnitude than  
1993 immersion freezing INP concentrations at  $-20\text{ }^{\circ}\text{C}$  and by more than an order of magnitude at  $-25$   
1994  $^{\circ}\text{C}$ . For the online instruments, only limited periods of deposition INP measurements ~~with the~~  
1995 ~~CSU-CFDC~~ achieved statistical significance. While these data were in good agreement with  
1996 ~~FRIDGE-DC~~ data at  $-25\text{ }^{\circ}\text{C}$  and 95% RH, the most striking result was that all other  
1997 measurement periods for the CSU-CFDC and MIT-SPIN gave measurements that were not  
1998 significant at the 95% confidence level. Thus, currently, offline methods for measuring  
1999 deposition INPs appear to offer the best chance for success in measuring the lower  
2000 concentrations of INPs that activate below water saturation in the mixed-phase temperature  
2001 regime. It would be useful to make such assessments at a variety of sites to confirm

**Deleted:** FRIDGE-DEP

**Formatted:** Font: Not Italic

**Deleted:** As expected, FRIDGE-DEP measurements indicated factor of a few increases in deposition  $N_{INP}$  concentrations between 95 to 99% RH

**Deleted:** concentrations

**Formatted:** Font: Italic

**Deleted:** concentrations

**Formatted:** Font: Italic

**Deleted:** on one day

**Deleted:** from the CSU-CFDC data

**Deleted:** FRIDGE-DEP



2011 measurements made during FIN-03 on the relative contributions and variability of INPs active in  
2012 these conditions toward ice formation in clouds. Additional instrument developments for online  
2013 measurements of these, and future intercomparisons, will be useful.

2014 In summary, the ~~agreements amongst instruments during FIN-03, within factors ranging~~  
2015 ~~from nearly 1 to up to 5.5 times on average between individual measurements and rarely~~  
2016 ~~exceeding one order of magnitude in short time periods, match those found in the FIN-02~~  
2017 laboratory studies. ~~These represented state-of-the-art for measurements at the time of FIN-03 and~~  
2018 ~~taken together with further improvements since this time as reflected in recent studies (Knopf et~~  
2019 ~~al., 2021; Brasseur et al., 2022; Lacher et al., 2024) demonstrate steady improvement in the~~  
2020 community's collective ability to detect and quantify atmospheric ice nucleation. There was not a  
2021 clear divide between the ability of online and offline systems to measure ~~immersion freezing~~ INP  
2022 concentrations from the data collected in this study, although the need to carefully consider  
2023 aerosol sampling efficiencies for different instruments was highlighted as a potential issue, ~~one~~  
2024 requiring close attention in future studies. In principle, both types of instruments show excellent  
2025 promise for future field studies. For full closure studies of ice nucleation by atmospheric  
2026 aerosols, methods for identifying INP composition as demonstrated herein and recommended by  
2027 other recent discussions in Knopf et al. (2021) and Burrows et al. (2022) are critical for  
2028 understanding and improving INP measurements overall.

2029 ~~There is a clear need in the future to extend measurement comparisons to the~~  
2030 ~~atmospherically-relevant and critically important temperature range higher than -15 °C. The low~~  
2031 ~~atmospheric number concentrations of INPs existing at times at these temperatures is a~~  
2032 ~~significant challenge for such, reflected in this study by the inability to measure INP~~  
2033 ~~concentrations above detection limits at the SPL site even for 3-to-4-hour filter collections at~~

Deleted: relative

Deleted: that

Deleted:

Deleted: are encouraging and represent

Deleted: in this study

Deleted: and

2040 temperatures higher than  $-7^{\circ}\text{C}$ . Longer sample times and higher volume collections can improve  
2041 this situation, but introduce other technical challenges and do not appear possible for online  
2042 instruments.

2043 We also herein do not address the relevance of INP measurements overall for  
2044 understanding ice formation in clouds, where secondary processes may come into play. This is  
2045 an additional topic for critical investigation, given a degree of confidence now established in  
2046 measuring INPs. However, the fact that 5-factor to order of magnitude correspondence between  
2047 measurements equate to  $3.5$  to  $5^{\circ}\text{C}$  temperature uncertainties in assessment of INPs is something  
2048 that also deserves scrutiny from the cloud modeling community concerning if this is satisfactory,  
2049 and if not, what level of correspondence should the INP research community be seeking.  
2050

Formatted: Font: Not Italic

Formatted: Font: Not Italic

2051 **Data availability** All data used for the figures in this paper can be accessed at  
2052 <https://radar.kit.edu/radar/en/dataset/eGhfvcOhsOyADZXXN> (persistent  
2053 doi:10.35097/eGhfvcOhsOyADZXXN)

#### 2054 **Author contributions**

2055 Paul J. DeMott, Jessica A. Mirrielees and Sarah D. Brooks wrote the paper with assistance from  
2056 all teams and authors contributing information on instrument descriptions and comments on all  
2057 results and conclusions, with contributions from Jake Zenker on some data analysis. Paul J.  
2058 DeMott, Ezra J.T. Levin, Thea Schiebel, Kaitlyn Suski, and Tom Hill provided data and analyses  
2059 from the CSU-CFDC and IS instruments. Daniel J. Cziczo, Martin J. Wolfe, Sarvesh Garimella,  
2060 and Maria Zawadowicz provided MIT-SPIN team measurements and analyses. Markus D.  
2061 Petters and Sarah S. Petters provided data and analysis for the ~~NCSU~~-CS instrument. Heinz G.  
2062 Bingemer, Jann Schrod, and Daniel Weber provided data and analyses for the FRIDGE  
2063 instrument. Anne Perring provided data and analyses for the WIBS-4A. Karl Froyd provided  
2064 data and analyses for the LAS and PALMS. Anna Gannet Hallar and Ian McCubbin oversaw  
2065 field operations, coordinated with visiting teams at Storm Peak Laboratory, and provided  
2066 nephelometer and meteorological measurements. Paul J. DeMott, Daniel J. Cziczo, Ottmar  
2067 Möhler contributed to organize the campaign in connection with the other FIN activities.  
2068

#### 2069 **Competing interests**

2070 The contact author has declared that none of the authors has any competing interests.

2071

2072

Deleted: NC State

2074 **Acknowledgements**

2075 Partial financial support for this project was provided by the U.S. National Science  
2076 Foundation, Grant No. AGS-1339264 and U.S. Department of Energy's Atmospheric System  
2077 Research, an Office of Science, Office of Biological and Environmental Research program,  
2078 under grant no. DE-SC0014487. Paul J. DeMott, Ezra J.T. Levin, Thea Schiebel, Kaitlyn Suski,  
2079 and Tom Hill acknowledge partial and in-kind research support during FIN-03 from NSF grant  
2080 no. AGS-1358495. Markus Petters acknowledges partial and in-kind support during FIN-03 from  
2081 NSF grant no. AGS-1450690. Jann Schrod acknowledges research support from the European  
2082 Union's Seventh Framework Programme (FP7/2007-2013) project BACCHUS under grant  
2083 agreement no. 603445. Heinz G. Bingemer and Daniel Weber acknowledge research support  
2084 under DFG grant BI 462/3-2. Thea Schiebel and Ottmar Möhler received support through the  
2085 German Science Foundation Projects INUIT and INUIT-2 (MO 668/4-1 and MO 668/4-2). Anne  
2086 Perring acknowledges support from the NOAA Health of the Atmosphere Program and the  
2087 NOAA Atmospheric Composition and Climate Program. Special thanks to Romy Fösig (Ullrich)  
2088 for assistance with data archival.

2089

2090

2091 **References**

- 2092 Alsante, A. N., Thornton, D. C. O., & Brooks, S. D.: Ice nucleation catalyzed by the  
2093 photosynthesis enzyme RuBisCO and other abundant biomolecules. *Communications*  
2094 *Earth & Environment*, 4(1). doi:10.1038/s43247-023-00707-7, 2023.
- 2095 Agresti, A. and Coull, B. A.: Approximate is better than "exact" for interval estimation of  
2096 binomial proportions, *The American Statistician*, 52, 119-126,  
2097 <https://doi.org/10.1080/00031305.1998.10480550>, 1998.
- 2098 Andreae, M. O., & Rosenfeld, D.: Aerosol-cloud-precipitation interactions. Part 1. The nature  
2099 and sources of cloud-active aerosols. *Earth-Science Reviews*, 89(1-2), 13-41.  
2100 <https://doi.org/10.1016/j.earscirev.2008.03.001>, 2008.
- 2101 Andrews, E., and Coauthors, 2019: Overview of the NOAA/ESRL Federated Aerosol  
2102 Network. *Bull. Amer. Meteor. Soc.*, 100, 123–135, <https://doi.org/10.1175/BAMS-D-17-0175.1>.
- 2103
- 2104 Ardon-Dryer, K., & Levin, Z.: Ground-based measurements of immersion freezing in the eastern  
2105 Mediterranean. *Atmospheric Chemistry and Physics*, 14(10), 5217-5231.  
2106 <https://doi.org/10.5194/acp-14-5217-2014>, 2014.
- 2107 Barry, K. R., Hill, T. C. J., Levin, E. J. T., Twohy, C. H., Moore, K. A., Weller, Z. D., Toohey, D. W., Reeves,  
2108 M., Campos, T., Geiss, R., Fischer, E. V., Kreidenweis, S. M., and DeMott, P. J.: Observations of ice  
2109 nucleating particles in the free troposphere from western US wildfires. *Journal of Geophysical*  
2110 *Research: Atmospheres*, 126, e2020JD033752. <https://doi.org/10.1029/2020JD033752>, 2021a.
- 2111 Barry, K. R., Hill, T. C. J., Jentsch, C., Moffett, B. E., Stratmann, F., and DeMott, P. J.: Pragmatic protocols  
2112 for working cleanly when measuring ice nucleating particles, *Atmospheric Research*, 250, 105419,  
2113 <https://doi.org/10.1016/j.atmosres.2020.105419>, 2021b.
- 2114 Beall, C. M., Lucero, D., Hill, T. C. J., DeMott, P. J., Stokes, M. D., and Prather, K. A.: Best  
2115 practices for precipitation sample storage for offline studies of ice nucleation in marine  
2116 and coastal environments, *Atmos. Meas. Tech.*, 13, 6473–6486,  
2117 <https://doi.org/10.5194/amt-13-6473-2020>, 2020.
- 2118 Boose, Y., Sierau, B., Isabel García, M., Rodríguez, S., Alastuey, A., Linke, C., Schnaiter, M.,  
2119 Kupiszewski, P., Kanji, Z. A., and Lohmann, U.: Ice nucleating particles in the Saharan  
2120 Air Layer. *Atmospheric Chemistry and Physics*, 16(14), 9067-9087.  
2121 <https://doi.org/10.5194/acp-16-9067-2016>, 2016.
- 2122 Boucher, O., Randall, D., Artaxo, P., Bretherton, C., Feingold, G., Forster, P., Kerminen, V.-M.,  
2123 Kondo, Y., Liao, H., Lohmann, U., Rasch, P., Satheesh, S. K., Sherwood, S., Stevens, B.,  
2124 and Zhang, X. Y.: *Clouds and Aerosols. In: Climate Change 2013: The Physical Science*  
2125 *Basis. Contribution of Working Group I to the Fifth Assessment Report of the*  
2126 *Intergovernmental Panel on Climate Change*. Retrieved from Cambridge, United  
2127 Kingdom and New York, NY, USA, 2013.
- 2128 Brasseur, Z., Castarède, D., Thomson, E. S., Adams, M. P., Drossaert van Dusseldorp, S.,  
2129 Heikkilä, P., Korhonen, K., Lampilahti, J., Paramonov, M., Schneider, J., Vogel, F., Wu,  
2130 Y., Abbott, J. P. D., Atanasova, N. S., Bamford, D. H., Bertozzi, B., Boyer, M., Brus, D.,  
2131 Daily, M. I., Fösig, R., Gute, E., Harrison, A. D., Hietala, P., Höhler, K., Kanji, Z. A.,  
2132 Keskinen, J., Lacher, L., Lampimäki, M., Levula, J., Manninen, A., Nadolny, J., Peltola,  
2133 M., Porter, G. C. E., Poutanen, P., Proske, U., Schorr, T., Silas Umo, N., Stenszky, J.,  
2134 Virtanen, A., Moisseev, D., Kulmala, M., Murray, B. J., Petäjä, T., Möhler, O., and

Formatted: Font: Not Italic

Formatted: Font: Not Bold

Formatted: Font: Not Italic

Formatted: Font: Not Bold

Formatted: Font: Bold

Deleted: ¶

Formatted: Underline

2136 [Duplissy, J.: Measurement report: Introduction to the HyICE-2018 campaign for](#)  
 2137 [measurements of ice-nucleating particles and instrument inter-comparison in the Hyytiälä](#)  
 2138 [boreal forest. \*Atmospheric Chemistry and Physics\*, 22\(8\), 5117–5145.](#)  
 2139 <https://doi.org/10.5194/acp-22-5117-2022>, 2022.

2140 [Burrows, S. M., McCluskey, C. S., Cornwell, G., Steinke, I., Zhang, K., Zhao, B., Zawadowicz,](#)  
 2141 [M., Raman, A., Kulkarni, G., China, S., Zelenyuk, A. and DeMott, P. J.: Ice-nucleating](#)  
 2142 [particles that impact clouds and climate: Observational and modeling research needs,](#)  
 2143 [\*Reviews of Geophysics\*, 60, e2021RG000745. https://doi.org/10.1029/2021RG000745,](#)  
 2144 [2022.](#)

2145 [Collaud Coen, M., Andrews, E., Aliaga, D., Andrade, M., Angelov, H., Bukowiecki, N., Ealo,](#)  
 2146 [M., Fialho, P., Flentje, H., Hallar, A. G., Hooda, R., Kalapov, I., Krejci, R., Lin, N.-H.,](#)  
 2147 [Marinoni, A., Ming, J., Nguyen, N. A., Pandolfi, M., Pont, V., Ries, L., Rodríguez, S.,](#)  
 2148 [Schauer, G., Sellegri, K., Sharma, S., Sun, J., Tunved, P., Velasquez, P., and Ruffieux,](#)  
 2149 [D.: Identification of topographic features influencing aerosol observations at high altitude](#)  
 2150 [stations: Identification of topographic features influencing aerosol observations at high](#)  
 2151 [altitude stations. \*Atmospheric Chemistry and Physics\*, 18\(16\), 12289–12313.](#)  
 2152 <https://doi.org/10.5194/acp-18-12289-2018>, 2018.

2153 [Coluzza, I., Creamean, J., Rossi, M. J., Wex, H., Alpert, P. A., Bianco, V., Boose, Y., Dellago,](#)  
 2154 [C., Felgitsch, L., Fröhlich-Nowoisky, J., Herrmann, H., Jungblut, S., Kanji, Z. A., Menzl,](#)  
 2155 [G., Moffett, B., Moritz, C., Mutzel, A., Pöschl, U., Schauperl, M., Scheel, J., Stopelli, E.,](#)  
 2156 [Stratmann, F., Grothe, H., and Schmale, D. G.: Perspectives on the Future of Ice](#)  
 2157 [Nucleation Research: Research Needs and Unanswered Questions Identified from Two](#)  
 2158 [International Workshops. \*Atmosphere\*, 8\(8\). https://doi.org/10.3390/atmos8080138](#), 2017.

2159 [Cornwell, G. C., McCluskey, C. S., Hill, T. C. J., Levin, E. J. T., Rothfuss, N. E., Taia, S.-L.,](#)  
 2160 [Petters, M. D., DeMott, P. J., Martin, A., Kreidenweis, S. M., Prather, K. A. and](#)  
 2161 [Burrows, S. M.: Bioaerosols are the dominant source of warm-temperature immersion-](#)  
 2162 [mode INPs and drive uncertainties in INP predictability in the ambient atmosphere.](#)  
 2163 [\*Science Advances\*, 9, eadg3715, https://doi.org/10.1126/sciadv.adg3715](#), 2023.

2164 [Cornwell, G. C., McCluskey, C. S., Levin, E. J. T., Suski, K. J., DeMott, P. J., Kreidenweis, S.](#)  
 2165 [M., & Prather, K. A.: Direct online mass spectrometry measurements of ice nucleating](#)  
 2166 [particles at a California coastal site. \*Journal of Geophysical Research: Atmospheres\*, 124,](#)  
 2167 [12,157–12,172. https://doi.org/10.1029/2019JD030466](#), 2019.

2168 [Creamean, J. M., Suski, K. J., Rosenfeld, D., Cazorla, A., DeMott, P. J., Sullivan, R. C., White,](#)  
 2169 [A. B., Ralph, F. M., Minnis, P., Comstock, J. M., Tomlinson, J. M., and Prather, K. A.:](#)  
 2170 [Dust and biological aerosols from the Sahara and Asia influence precipitation in the](#)  
 2171 [western U.S. \*Science\*, 339\(6127\), 1572–1578. https://doi.org/10.1126/science.1227279](#),

2172 2013.

2173 [David, R. O., Fahrni, J., Marcolli, C., Mahrt, F., Brühwiler, D., and Kanji, Z. A: The role of](#)  
 2174 [contact angle and pore width on pore condensation and freezing. \*Atmos. Chem. Phys.\*, 20,](#)  
 2175 [9419–9440, https://doi.org/10.5194/acp-20-9419-2020](#), 2020.

2176 [David, R. O., Cascajo-Castresana, M., Brennan, K. P., Rösch, M., Els, N., Werz, J., Weichlinger,](#)  
 2177 [V., Boynton, L. S., Bogler, S., Borduas-Dedekind, N., Marcolli, C., and Kanji, Z. A.:](#)  
 2178 [Development of the DRoplet Ice Nuclei Counter Zurich \(DRINCZ\): validation and](#)  
 2179 [application to field-collected snow samples, \*Atmos. Meas. Tech.\*, 12, 6865–6888,](#)  
 2180 <https://doi.org/10.5194/amt-12-6865-2019>, 2019.

Formatted: Font: Italic

2181 DeMott, P. J., Mohler, O., Cziczo, D. J., Hiranuma, N., Petters, M. D., Petters, S. S., Belosi, F.,  
 2182 Bingemer, H. G., Brooks, S. D., Budke, C., Burkert-Kohn, M., Collier, K. N.,  
 2183 Danielczok, A., Eppers, O., Felgitsch, L., Garimella, S., Grothe, H., Herenz, P., Hill, T.  
 2184 C. J., Höhler, K., Kanji, Z. A., Kiselev, A., Koop, T., Kristensen, T. B., Krüger, K.,  
 2185 Kulkarni, G., Levin, E. J. T., Murray, B. J., Nicosia, A., O'Sullivan, D., Peckhaus, A.,  
 2186 Polen, M. J., Price, H. C., Reicher, N., Rothenberg, D. A., Rudich, Y., Santachiara, G.,  
 2187 Schiebel, T., Schrod, J., Seifried, T. M., Stratmann, F., Sullivan, R. C., Suski, K. J.,  
 2188 Szakáll, M., Taylor, H. P., Ullrich, R., Vergara-Temprado, J., Wagner, R., Whale, T. F.,  
 2189 Weber, D., Welti, A., Wilson, T. W., Wolf, M. J., Zenker, J.: The Fifth International  
 2190 Workshop on Ice Nucleation phase 2 (FIN-02): laboratory intercomparison of ice  
 2191 nucleation measurements. *Atmospheric Measurement Techniques*, 11(11), 6231-6257.  
 2192 <https://doi.org/10.5194/amt-11-6231-2018>, 2018.  
 2193 DeMott, P. J., Hill, T. C. J., Petters, M. D., Bertram, A. K., Tobo, Y., Mason, R. H., Suski, K. J.,  
 2194 McCluskey, C. S., Levin, E. J. T., Schill, G. P., Boose, Y., Rauker, A. M., Miller, A. J.,  
 2195 Zaragoza, J., Rocci, K., Rothfuss, N. E., Taylor, H. P., Hader, J. D., Chou, C., Huffman,  
 2196 J. A., Pöschl, U., Prenni, A. J., and Kreidenweis, S. M.: Comparative measurements of  
 2197 ambient atmospheric concentrations of ice nucleating particles using multiple immersion  
 2198 freezing methods and a continuous flow diffusion chamber, *Atmos. Chem. Phys.*, 17,  
 2199 11227–11245, <https://doi.org/10.5194/acp-17-11227-2017>, 2017.  
 2200 DeMott, P. J., Prenni, A. J., McMeeking, G. R., Sullivan, R. C., Petters, M. D., Tobo, Y.,  
 2201 Niemand, M., Möhler, O., Snider, J. R., Wang, Z., and Kreidenweis, S. M.: Integrating  
 2202 laboratory and field data to quantify the immersion freezing ice nucleation activity of  
 2203 mineral dust particles. *Atmospheric Chemistry and Physics*, 15(1), 393-409.  
 2204 <https://doi.org/10.5194/acp-15-393-2015>, 2015.  
 2205 DeMott, P. J., Mohler, O., Stetzer, O., Vali, G., Levin, Z., Petters, M. D., Murakami, M., Leisner,  
 2206 T., Bundke, U., Klein, H., Kanji, Z. A., Cotton, R. Jones, H., Petters, M. D., Prenni, A.,  
 2207 Benz, S. Brinkmann, M., Rzesanke, D., Saathoff, H. Nicolet, M., Gallavardin, S., Saito,  
 2208 A., Nillius, B., Bingemer, H., Abbatt, J., Ardon, K., Ganor, E., Georgakopoulos, D. G.,  
 2209 and Saunders, C.: Resurgence in ice nuclei measurement research. *Bulletin of the*  
 2210 *American Meteorological Society*, 92(12), 1623-+. [https://doi.org/10.1175/bams-d-10-](https://doi.org/10.1175/bams-d-10-3119.1)  
 2211 [3119.1](https://doi.org/10.1175/bams-d-10-3119.1), 2011  
 2212 DeMott, P. J., Prenni, A. J., Liu, X., Kreidenweis, S. M., Petters, M. D., Twohy, C. H.,  
 2213 Richardson, M. S., Eidhammer, T., Kreidenweis, S. M., and Rogers, D. C.: Predicting  
 2214 global atmospheric ice nuclei distributions and their impacts on climate. *Proceedings of*  
 2215 *the National Academy of Sciences of the United States of America*, 107(25), 11217-  
 2216 11222. <https://doi.org/10.1073/pnas.0910818107>,  
 2217 Durant, A. J., and Shaw, R. A.: Evaporation freezing by contact nucleation inside-out.  
 2218 *Geophysical Research Letters*, 32(20). <https://doi.org/10.1029/2005gl024175>, 2005.  
 2219 Eidhammer, T., DeMott, P. J., Prenni, A. J., Petters, M. D., Twohy, C. H., Rogers, D. C., Stith,  
 2220 J., Heymsfield, A., Wang, Z., Haimov, S., French, J., Pratt, K., Prather, K., Murphy, S.,  
 2221 Seinfeld, J., Subramanian, R. and Kreidenweis, S. M.: Ice initiation by aerosol particles:  
 2222 Measured and predicted ice nuclei concentrations versus measured ice crystal  
 2223 concentrations in an orographic wave cloud. *J. Atmos. Sci.*, 67, 2417–2436.  
 2224 <https://doi.org/10.1175/2010JAS3266.1>, 2010.

2225 Fornea, A. P., Brooks, S. D., Dooley, J. B., and Saha, A.: Heterogeneous freezing of ice on  
2226 atmospheric aerosols containing ash, soot, and soil. *Journal of Geophysical Research:*  
2227 *Atmospheres*, 114(D13). <https://doi.org/10.1029/2009jd011958>, 2009.

2228 Froyd, K.D., Yu, P., Schill, G.P. *et al.* Dominant role of mineral dust in cirrus cloud formation  
2229 revealed by global-scale measurements. *Nat. Geosci.* **15**, 177–183.  
2230 <https://doi.org/10.1038/s41561-022-00901-w>, 2022.

2231 Froyd, K. D., Murphy, D. M., Brock, C. A., Campuzano-Jost, P., Dibb, J. E., Jimenez, J.-L.,  
2232 Kupc, A., Middlebrook, A. M., Schill, G. P., Thornhill, K. L., Williamson, C. J., Wilson,  
2233 J. C., and Ziemba, L. D.: A new method to quantify mineral dust and other aerosol  
2234 species from aircraft platforms using single-particle mass spectrometry. *Atmospheric*  
2235 *Measurement Techniques*, 12(11), 6209-6239. <https://doi.org/10.5194/amt-12-6209-2019>,  
2236 2019.

2237 Gabey, A. M., Gallagher, M. W., Whitehead, J., Dorsey, J. R., Kaye, P. H., and Stanley, W. R.:  
2238 Measurements and comparison of primary biological aerosol above and below a tropical  
2239 forest canopy using a dual channel fluorescence spectrometer. *Atmospheric Chemistry*  
2240 *and Physics*, 10(10), 4453-4466. <https://doi.org/10.5194/acp-10-4453-2010>, 2010.

2241 Garimella, S., Kristensen, T. B., Ignatius, K., Welti, A., Voigtländer, J., Kulkarni, G. R., Sagan,  
2242 F., Kok, G. L., Dorsey, J., Nichman, L., Rothenberg, D. A., Rösch, M., Kirchgäßner, A.  
2243 C. R., Ladkin, R., Wex, H., Wilson, T. W., Ladino, L. A., Abbatt, J. P. D., Stetzer, O.,  
2244 Lohmann, U., Stratmann, F., and Cziczo, D. J.: The SPectrometer for Ice Nuclei (SPIN):  
2245 an instrument to investigate ice nucleation. *Atmospheric Measurement Techniques*, 9(7),  
2246 2781-2795. <https://doi.org/10.5194/amt-9-2781-2016>, 2016.

2247 Garimella, S., Rothenberg, D. A., Wolf, M. J., David, R. O., Kanji, Z. A., Wang, C., Rösch, M.,  
2248 and Cziczo, D. J.: Uncertainty in counting ice nucleating particles with continuous flow  
2249 diffusion chambers. *Atmospheric Chemistry and Physics*, 17(17), 10855-10864.  
2250 <https://doi.org/10.5194/acp-17-10855-2017>, 2017.

2251 Hader, J. D., Wright, T. P., & Petters, M. D.: Contribution of pollen to atmospheric ice nuclei  
2252 concentrations. *Atmospheric Chemistry and Physics*, 14(11), 5433-  
2253 5449. <https://doi.org/10.5194/acp-14-5433-2014>, 2014.

2254 Healy, D. A., Huffman, J. A., O'Connor, D. J., Pöhlker, C., Pöschl, U., & Sodeau, J. R.: Ambient  
2255 measurements of biological aerosol particles near Killarney, Ireland: a comparison  
2256 between real-time fluorescence and microscopy techniques. *Atmospheric Chemistry and*  
2257 *Physics*, 14(15), 8055-8069. <https://doi.org/10.5194/acp-14-8055-2014>, 2014.

2258 Hallar, A. G., G. Chirokova, I. McCubbin, T. H. Painter, C. Wiedinmyer, and C.  
2259 Dodson: Atmospheric bioaerosols transported via dust storms in the western United  
2260 States, *Geophys. Res. Lett.*, 38, L17801, <https://doi.org/10.1029/2011GL048166>, 2011.

2261 Healy, D. A., Huffman, J. A., O'Connor, D. J., Pöhlker, C., Pöschl, U., & Sodeau, J. R.: Ambient  
2262 measurements of biological aerosol particles near Killarney, Ireland: a comparison  
2263 between real-time fluorescence and microscopy techniques. *Atmospheric Chemistry and*  
2264 *Physics*, 14(15), 8055-8069. <https://doi.org/10.5194/acp-14-8055-2014>, 2014.

2265 Hiranuma, N., Augustin-Bauditz, S., Bingemer, H., Budke, C., Curtius, J., Danielczok, A., Diehl,  
2266 K., Dreischmeier, K., Ebert, M., Frank, F., Hoffmann, N., Kandler, K., Kiselev, A.,  
2267 Koop, T., Leisner, T., Möhler, O., Nillius, B., Peckhaus, A., Rose, D., Weinbruch, S.,  
2268 Wex, H., Boose, Y., DeMott, P. J., Hader, J. D., Hill, T. C. J., Kanji, Z. A., Kulkarni, G.,  
2269 Levin, E. J. T., McCluskey, C. S., Murakami, M., Murray, B. J., Niedermeier, D., Petters,  
2270 M. D., O'Sullivan, D., Saito, A., Schill, G. P., Tajiri, T., Tolbert, M. A., Welti, A., Whale,



2271 T. F., Wright, T. P., and Yamashita, K.: A comprehensive laboratory study on the  
 2272 immersion freezing behavior of illite NX particles: a comparison of 17 ice nucleation  
 2273 measurement techniques, *Atmospheric Chemistry and Physics*, 15(5), 2489-2518.  
 2274 <https://doi.org/10.5194/acp-15-2489-2015>, 2015.

2275 Huffman, J. A., Prenni, A. J., DeMott, P. J., Pöhlker, C., Mason, R. H., Robinson, N. H.,  
 2276 Fröhlich-Nowoisky, J., Tobo, Y., Després, V. R., Garcia, E., Gochis, D. J., Harris, E.,  
 2277 Müller-Germann, I., Ruzene, C., Schmer, B., Sinha, B., Day, D. A., Andreae, M. O.,  
 2278 Jimenez, J. L., Gallagher, M., Kreidenweis, S. M., Bertram, A. K., and Pöschl, U.: High  
 2279 concentrations of biological aerosol particles and ice nuclei during and after rain.  
 2280 *Atmospheric Chemistry and Physics*, 13(13), 6151-6164. <https://doi.org/10.5194/acp-13-6151-2013>, 2013.

2282 Jones, H. M., Flynn, M. J., DeMott, P. J., and Mohler, O.: Manchester Ice Nucleus Counter  
 2283 (MINC) measurements from the 2007 International workshop on Comparing Ice  
 2284 nucleation Measuring Systems (ICIS-2007). *Atmospheric Chemistry and Physics*, 11(1),  
 2285 53-65. <https://doi.org/10.5194/acp-11-53-2011>, 2011.

2286 Kanji, Z. A., DeMott, P. J., Mohler, O., and Abbatt, J. P. D.: Results from the University of  
 2287 Toronto continuous flow diffusion chamber at ICIS 2007: instrument intercomparison  
 2288 and ice onsets for different aerosol types. *Atmospheric Chemistry and Physics*, 11(1), 31-  
 2289 41. <https://doi.org/10.5194/acp-11-31-2011>, 2011.

2290 Kanji, Z. A., Ladino, L. A., Wex, H., Boose, Y., Burkert-Kohn, M., Cziczo, D. J., & Krämer, M.:  
 2291 Overview of Ice Nucleating Particles. In D. Baumgardner, G. M. McFarquhar, & A. J.  
 2292 Heymsfield (Eds.), *Ice Formation and Evolution in Clouds and Precipitation:  
 2293 Measurement and Modeling Challenges, Meteorological Monographs*, 58, 1.1-1.33.  
 2294 <https://doi.org/10.1175/amsmonographs-d-16-0006.1>, 2017.

2295 Kaye, P. H., Stanley, W. R., Hirst, E., Foot, E. V., Baxter, K. L., and Barrington, S. J.: Single  
 2296 particle multichannel bio-aerosol fluorescence sensor. *Optics Express*, 13(10), 3583-  
 2297 3593. <https://doi.org/10.1364/OPEX.13.003583>, 2005.

2298 Knopf, D. A., Barry, K. R., Brubaker, T. A., Jahl, L. G., Jankowski, K. A. L., Li, J., Lu, Y.,  
 2299 Monroe, L. W., Moore, K. A., Rivera-Adorno, F. A., Saucedo, K. A., Shi, Y., Tomlin, J.  
 2300 M., Vepuri, H. S. K., Wang, P., Lata, N. N., Levin, E. J. T., Creamean, J. M., Hill, T. C.  
 2301 J., China, S., Alpert, P. A., Moffet, R. C., Hiranuma, N., Sullivan, R. C., Fridlind, A. M.,  
 2302 West, M., Riemer, N., Laskin, A., DeMott, P. J., & Liu, X. (2021). Aerosol–Ice  
 2303 Formation Closure: A Southern Great Plains Field Campaign, *Bulletin of the American  
 2304 Meteorological Society*, 102(10), E1952-E197, <https://doi.org/10.1175/BAMS-D-20-0151.1>

2305  
 2306 Kulkarni, G. and Kok, G (2012): Mobile Ice Nucleus Spectrometer, Pacific Northwest National  
 2307 Laboratory, Richland, WA, 13 pg.

2308 Lacher, L., Adams, M. P., Barry, K., Bertozzi, B., Bingemer, H., Boffo, C., Bras, Y., Büttner, N.,  
 2309 Castarede, D., Cziczo, D. J., DeMott, P. J., Fösig, R., Goodell, M., Höhler, K., Hill, T. C.  
 2310 J., Jentzsch, C., Ladino, L. A., Levin, E. J. T., Mertes, S., Möhler, O., Moore, K. A.,  
 2311 Murray, B. J., Nadolny, J., Pfeuffer, T., Picard, D., Ramírez-Romero, C., Ribeiro, M.,  
 2312 Richter, S., Schrod, J., Sellegri, K., Stratmann, F., Swanson, B. E., Thomson, E., Wex,  
 2313 H., Wolf, M., and Freney, E.: The Puy de Dôme ICe Nucleation Intercomparison  
 2314 Campaign (PICNIC): Comparison between online and offline methods in ambient air,  
 2315 *Atmos. Chem. Phys.*, 24, 2651–2678, <https://doi.org/10.5194/acp-24-2651-2024>, 2024.

Formatted: Font: Italic

2316 Levin, E. J. T., DeMott, P. J., Suski, K. J., Boose, Y., Hill, T. C. J., McCluskey, C. S., Schill, G.  
 2317 P., Rocci, K., Al-Mashat, H., Kristensen, L. J., Cornwell, G. C., Prather, K. A.,  
 2318 Tomlinson, J. M., Mei, F., Hubbe, J., Pekour, M. S., Sullivan, R. J., Leung L. R., and  
 2319 Kreidenweis, S. M.: Characteristics of ice nucleating particles in and around California  
 2320 winter storms, *Journal of Geophysical Research: Atmospheres*, **124**, 11,530-11,551,  
 2321 <https://doi.org/10.1029/2019JD030831>, 2019.  
 2322 Lohmann, U., and Feichter, J.: Global indirect aerosol effects: a review. *Atmospheric Chemistry  
 2323 and Physics*, **5**, 715-737. <https://doi.org/10.5194/acp-5-715-2005>, 2005.  
 2324 Marcolli, C., Deposition nucleation viewed as homogeneous or immersion freezing in pores and  
 2325 cavities. *Atmospheric Chemistry and Physics*, **14**(4), 2071-2104.  
 2326 <https://doi.org/10.5194/acp-14-2071-2014>, 2014.  
 2327 Mason, R. H., Si, M., Chou, C., Irish, V. E., Dickie, R., Elizondo, P., Wong, R., Brintnell, M.,  
 2328 Elsasser, M., Lassar, W. M., Pierce, K. M., Leaitch, W. R., MacDonald, A. M., Platt, A.,  
 2329 Toom-Saunty, D., Sarda-Estève, R., Schiller, C. L., Suski, K. J., Hill, T. C. J., Abbatt, J.  
 2330 P. D., Huffman, J. A., DeMott, P. J., and Bertram, A. K.: Size-resolved measurements of  
 2331 ice-nucleating particles at six locations in North America and one in Europe. *Atmos.  
 2332 Chem. Phys.*, **16**, 1637–1651, <https://doi.org/10.5194/acp-16-1637-2016>, 2016.  
 2333 McCluskey, C. S., Gettelman, A., Bardeen, C. G., DeMott, P. J., Moore, K. A., Kreidenweis, S.  
 2334 M., Hill, T. C. J., Barry, K. R., Twohy., C. H., Toohey, D. W., Rainwater, B., Jensen, J.  
 2335 B., Reeves, J. M., Alexander, S. P. and McFarquhar, G. M.: Simulating Southern Ocean  
 2336 aerosol and ice nucleating particles in the Community Earth System Model version 2.  
 2337 *Journal of Geophysical Research: Atmospheres*, **128**, e2022JD036955, 2023.  
 2338 <https://doi.org/10.1029/2022JD036955>, 2023.  
 2339 McCluskey, C. S., Hill, T. C. J., Humphries, R. S., Rauker, A. M., Moreau, S., Stratton, P. G.,  
 2340 Chambers, S. D., Williams, A. G., McRobert, I., Ward, J., Keywood, M. D., Harnwell,  
 2341 J., Ponsonby, W., Loh, Z.M., Krummel, P. B., Protat, A., Kreidenweis, S.M., and  
 2342 DeMott, P. J.: Observations of ice nucleating particles over Southern Ocean waters.  
 2343 *Geophysical Research Letters*, **45**, 11,989–11,997,  
 2344 <https://doi.org/10.1029/2018GL079981>, 2018.  
 2345 Möhler, O., Adams, M., Lacher, L., Vogel, F., Nadolny, J., Ullrich, R., Boffo, C., Pfeuffer, T.,  
 2346 Hobl, A., Weiß, M., Vepuri, H. S. K., Hiranuma, N., and Murray, B. J.: The Portable Ice  
 2347 Nucleation Experiment (PINE): a new online instrument for laboratory studies and  
 2348 automated long-term field observations of ice-nucleating particles. *Atmospheric  
 2349 Measurement Techniques*, **14**(2), 1143-1166. <https://doi.org/10.5194/amt-14-1143-2021>,  
 2350 2021.  
 2351 Morris, C. E., Sands, D. C., Bardin, M., Jaenicke, R., Vogel, B., Leyronas, C., Ariya, P. A., and  
 2352 Psenner, R.: Microbiology and atmospheric processes: research challenges concerning  
 2353 the impact of airborne micro-organisms on the atmosphere and climate. *Biogeosciences*,  
 2354 **8**, 17. <https://doi.org/10.5194/bg-8-17-2011>, 2011.  
 2355 Murray, B. J., O'Sullivan, D., Atkinson, J. D., & Webb, M. E: Ice nucleation by particles  
 2356 immersed in supercooled cloud droplets. *Chemical Society Reviews*, **41**(19), 6519-6554.  
 2357 <https://doi.org/10.1039/C2CS35200A>, 2012.  
 2358 Niemand, M., Mohler, O., Vogel, B., Vogel, H., Hoose, C., Connolly, P., Klein, H. Bingemer,  
 2359 H., DeMott, P. J., Skrotzki, J., and Leisner, T.: A Particle-Surface-Area-Based  
 2360 Parameterization of Immersion Freezing on Desert Dust Particles. *Journal of the  
 2361 Atmospheric Sciences*, **69**(10), 3077-3092. <https://doi.org/10.1175/jas-d-11-0249.1>, 2012.

- 2362 Perring, A. E., Schwarz, J. P., Baumgardner, D., Hernandez, M. T., Spracklen, D. V., Heald, C.  
 2363 L., Gao, R. S., Kok, G., McMeeking, G. R., McQuaid, J. B., and Fahey, D. W.:  
 2364 Airborne observations of regional variation in fluorescent aerosol across the United  
 2365 States. *Journal of Geophysical Research-Atmospheres*, 120(3), 1153-1170.  
 2366 <https://doi.org/10.1002/2014jd022495>, 2015.
- 2367 Petersen, R. C., Hallar, A. G., McCubbin, I. B., Ogren, J. A., Andrews, E., Lowenthal, D.,  
 2368 Gorder, R., Purcell, R., Sleeth, D., and Novosselov, I.: Numerical, wind-tunnel, and  
 2369 atmospheric evaluation of a turbulent ground-based inlet sampling system, *Aerosol*  
 2370 *Science and Technology*, 53 (6), 712-727,  
 2371 <https://doi.org/10.1080/02786826.2019.1602718>, 2019.
- 2372 Petters, M. D., and Wright, T. P.: Revisiting ice nucleation from precipitation samples.  
 2373 *Geophysical Research Letters*, 42(20), 8758-8766. doi:10.1002/2015gl065733, 2015.
- 2374 Pöhlker, C., Huffman, J. A., and Pöschl, U.: Autofluorescence of atmospheric bioaerosols –  
 2375 fluorescent biomolecules and potential interferences. *Atmospheric Measurement*  
 2376 *Techniques*, 5(1), 37-71. <https://doi.org/10.5194/amt-5-37-2012>, 2012.
- 2377 Rogers, D.C.: Development of a continuous flow thermal gradient diffusion chamber for ice  
 2378 nucleation studies. *Atmos. Res.*, 22, 149-181, [https://doi.org/10.1016/0169-8095\(88\)90005-1](https://doi.org/10.1016/0169-8095(88)90005-1), 1988.
- 2380 Rogers, D. C., DeMott, P. J., Kreidenweis S. M., and Chen, Y.: A continuous flow diffusion  
 2381 chamber for airborne measurements of ice nuclei, *J. Atmos. Oceanic Technol.*, 18, 725-  
 2382 741, [https://doi.org/10.1175/1520-0426\(2001\)018<0725:ACFDCF>2.0.CO;2](https://doi.org/10.1175/1520-0426(2001)018<0725:ACFDCF>2.0.CO;2), 2001.
- 2383 Schill, G. P., DeMott, P. J., Emerson, E. W., Rauker, A. M. C., Kodros, J. K., Suski, K. J., Hill,  
 2384 T. C. J., Levin, E. J. T., Pierce, J. R., Farmer, D. K., and Kreidenweis, S. M.: The  
 2385 contribution of black carbon to global ice nucleating particle concentrations relevant to  
 2386 mixed-phase clouds. *Proceedings of the National Academy of Sciences*, 117 (37), 22705–  
 2387 22711, <https://doi.org/10.1073/pnas.2001674117>, 2020.
- 2388 Schrod, J., Danielczok, A., Weber, D., Ebert, M., Thomson, E. S., and Bingemer, H. G.: Re-  
 2389 evaluating the Frankfurt isothermal static diffusion chamber for ice nucleation, *Atmos.*  
 2390 *Meas. Tech.*, 9, 1313–1324, <https://doi.org/10.5194/amt-9-1313-2016>, 2016.
- 2391 Schrod, J., Thomson, E. S., Weber, D., Kossmann, J., Pöhlker, C., Saturno, J., Ditas, F., Artaxo,  
 2392 P., Clouard, V., Saurel, J.-M., Ebert, M., Curtius, J., and Bingemer, H. G.: Long-term  
 2393 deposition and condensation ice-nucleating particle measurements from four stations  
 2394 across the globe, *Atmos. Chem. Phys.*, 20, 15983–16006, <https://doi.org/10.5194/acp-20-15983-2020>, 2020.
- 2396 Seifert, P., Ansmann, A., Groß, S., Freudenthaler, V., Heinold, B., Hiebsch, A., Mattis, I.,  
 2397 Schmidt, J., Schnell, F., Tesche, M., Wandinger, U., and Wiegner, M.: Ice formation in  
 2398 ash-influenced clouds after the eruption of the Eyjafjallajökull volcano in April 2010.  
 2399 *Journal of Geophysical Research: Atmospheres*, 116(D20).  
 2400 <https://doi.org/10.1029/2011jd015702>, 2011.
- 2401 [Shen, X., Bell, D. M., Coe, H., Hiranuma, N., Mahrt, F., Marsden, N. A., Mohr, C., Murphy, D.](#)  
 2402 [M., Saathoff, H., Schneider, J., Wilson, J., Zawadowicz, M. A., Zelenyuk, A., DeMott, P.](#)  
 2403 [J., Möhler, O., and Cziczo, D. J.: Measurement report: The Fifth International Workshop](#)  
 2404 [on Ice Nucleation phase 1 \(FIN-01\): intercomparison of single-particle mass](#)  
 2405 [spectrometers, \*Atmos. Chem. Phys.\*, 24, 10869–10891, \[https://doi.org/10.5194/acp-24-\]\(https://doi.org/10.5194/acp-24-10869-2024\)](#)  
 2406 [10869-2024, 2024.](#)

**Deleted:** ¶

**Formatted:** Normal, Indent: Left: 0", Hanging: 0.5",  
 Border: Top: (No border), Bottom: (No border), Left: (No  
 border), Right: (No border), Between : (No border)

**Formatted:** Font: Italic

- 2408 Suski, K. J., Hill, T. C. J., Levin, E. J. T., Miller, A., DeMott, P. J., and Kreidenweis, S. M.: Agricultural  
 2409 harvesting emissions of ice-nucleating particles, *Atmos. Chem. Phys.*, **18**, 13755-13771,  
 2410 <https://doi.org/10.5194/acp-18-13755-2018>.
- 2411 Testa, B., Hill, T. C. J., Marsden, N. A., Barry, K. R., Hume, C. C., Bian, Q., Uetake, J., Hare,  
 2412 H., Perkins, R. J., Möhler, O., Kreidenweis, S. M. and DeMott, P. J.: Ice nucleating  
 2413 particles in the boundary layer of the Sierras de Córdoba, Argentina, during the Cloud,  
 2414 Aerosol, and Complex Terrain Interactions experiment, *Journal of Geophysical  
 2415 Research: Atmospheres* **126**, e2021JD03518, <https://doi.org/10.1029/2021JD035186>,  
 2416 2021.
- 2417 *Thomson, D. S., Schein, M. E., and Murphy, D. M.: Particle analysis by laser mass spectrometry*  
 2418 *WB-57 instrument overview, Aerosol Sci. Technol.*, **33**, 153–169,  
 2419 <https://doi.org/10.1080/027868200410903>, 2000.
- 2420 Tobo, Y., DeMott, P. J., Hill, T. C. J., Prenni, A. J., Swoboda-Colberg, N. G., Franc, G. C., and  
 2421 Kreidenweis, S. M.: Organic matter matters for ice nuclei of agricultural soil origin.  
 2422 *Atmos. Chem. Phys.*, **14**, 8521–8531, <https://doi.org/10.5194/acp-14-8521-2014>, 2014.
- 2423 Tobo, Y., Prenni, A. J., DeMott, P. J., Huffman, J. A., McCluskey, C. S., Tian, G. X., Pöhlker,  
 2424 C., Pöschl, U., and Kreidenweis, S. M.: Biological aerosol particles as a key determinant  
 2425 of ice nuclei populations in a forest ecosystem. *Journal of Geophysical Research-  
 2426 Atmospheres*, **118**(17), 10100-10110. <https://doi.org/10.1002/jgrd.50801>, 2013.
- 2427 Ullrich, R., Hoose, C., Möhler, O., Niemand, M., Wagner, R., Höhler, K., Hiranuma, N.,  
 2428 Saathoff, H., and Leisner, T.: A New Ice Nucleation Active Site Parameterization for  
 2429 Desert Dust and Soot. *Journal of the Atmospheric Sciences*, **74**(3), 699-717.  
 2430 <https://doi.org/10.1175/jas-d-16-0074.1>, 2017.
- 2431 Willeke, K., Lin, X., and Grinshpun, S. A.: Improved Aerosol Collection by Combined  
 2432 Impaction and Centrifugal Motion, *Aerosol. Sci. Tech.*, **28**(5), 439–456.  
 2433 <https://doi.org/10.1080/02786829808965536>, 1998.
- 2434 Wright, T. P., & Petters, M. D.: The role of time in heterogeneous freezing nucleation. *Journal of  
 2435 Geophysical Research: Atmospheres*, **118**, 3731–3743.  
 2436 <https://doi.org/10.1002/jgrd.503652013>, 2013.
- 2437 Wright, T. P., Hader, J. D., McMeeking, G. R., and Petters, M.D.: High Relative Humidity as a  
 2438 Trigger for Widespread Release of Ice Nuclei, *Aerosol Science and Technology*, **48** (11),  
 2439 i-v. <https://doi.org/10.1080/02786826.2014.968244>, 2014.
- 2440 Wright, T. P., Petters, M. D., Hader, J. D., Morton, T., & Holder, A. L.: Minimal cooling rate  
 2441 dependence of ice nuclei activity in the immersion mode. *Journal of Geophysical  
 2442 Research: Atmospheres*, **118**, 10,535–10,543. <https://doi.org/10.1002/jgrd.50810>, 2013.
- 2443 Vali, G., DeMott, P. J., Möhler, O. and Whale, T. F.: Technical Note: A proposal for ice nucleation  
 2444 terminology, *Atmos. Chem. Phys.*, **15**, 10263–10270, <https://doi.org/10.5194/acp-15-10263-2015>,  
 2445 2015.
- 2446 Vali, G.: Nucleation terminology. *Journal of Aerosol Science*, **16**(6), 575-576,  
 2447 [https://doi.org/10.1016/0021-8502\(85\)90009-6](https://doi.org/10.1016/0021-8502(85)90009-6), 1985.
- 2448 Vali, G.: Quantitative evaluation of experimental results on the heterogeneous freezing  
 2449 nucleation of supercooled liquids. *J. Atmos. Sci.*, **28**, 402–409,  
 2450 [https://doi.org/10.1175/1520-0469\(1971\)028<0402:QEOERA>2.0.CO;2](https://doi.org/10.1175/1520-0469(1971)028<0402:QEOERA>2.0.CO;2), 1971.
- 2451 Wagner, R., Kiselev, A., Mohler, O., Saathoff, H., & Steinke, I.: Pre-activation of ice-nucleating  
 2452 particles by the pore condensation and freezing mechanism. *Atmospheric Chemistry and  
 2453 Physics*, **16**(4), 2025-2042. <https://doi.org/10.5194/acp-16-2025-2016>, 2016.

Formatted: Font: Not Bold

Formatted: Font: Italic

2454 Wex, H., Augustin-Bauditz, S., Boose, Y., Budke, C., Curtius, J., Diehl, K., Dreyer, A., Frank,  
2455 F., Hartmann, S., Hiranuma, N., Jantsch, E., Kanji, Z. A., Kiselev, A., Koop, T., Möhler,  
2456 O., Niedermeier, D., Nillius, B., Rösch, M., Rose, D., Schmidt, C., Steinke, I., and  
2457 Stratmann, F.: Intercomparing different devices for the investigation of ice nucleating  
2458 particles using Snomax (R) as test substance. *Atmospheric Chemistry and Physics*, 15(3),  
2459 1463-1485. <https://doi.org/10.5194/acp-15-1463-2015>, 2015.

2460 Willeke, K., Lin, X., and Grinshpun, S. A.: Improved Aerosol Collection by Combined  
2461 Impaction and Centrifugal Motion, *Aerosol. Sci. Tech.*, 28(5), 439–456.  
2462 <https://doi.org/10.1080/02786829808965536>, 1998.

2463 Wright, T. P., & Petters, M. D.: The role of time in heterogeneous freezing nucleation. *Journal of*  
2464 *Geophysical Research: Atmospheres*, 118, 3731–3743.  
2465 <https://doi.org/10.1002/jgrd.503652013>, 2013.

2466 Wright, T. P., Hader, J. D., McMeeking, G. R., and Petters, M.D.: High Relative Humidity as a  
2467 Trigger for Widespread Release of Ice Nuclei, *Aerosol Science and Technology*, 48 (11),  
2468 i-v. <https://doi.org/10.1080/02786826.2014.968244>, 2014.

2469 Wright, T. P., Petters, M. D., Hader, J. D., Morton, T., & Holder, A. L.: Minimal cooling rate  
2470 dependence of ice nuclei activity in the immersion mode. *Journal of Geophysical*  
2471 *Research: Atmospheres*, 118, 10,535–10,543. <https://doi.org/10.1002/jgrd.50810>, 2013.

2472 Yadav, S., Venezia, R. E., Paerl, R. W., & Petters, M. D.: Characterization of ice-nucleating  
2473 particles over Northern India. *Journal of Geophysical Research:*  
2474 *Atmospheres*, 124, 10467–10482. <https://doi.org/10.1029/2019JD030702>, 2019.

2475 Zawadowicz, M. A., Froyd, K. D., Murphy, D. M., and Cziczo, D. J.: Improved identification of  
2476 primary biological aerosol particles using single-particle mass spectrometry. *Atmospheric*  
2477 *Chemistry and Physics*, 17(11), 7193-7212. <https://doi.org/10.5194/acp-17-7193-2017>,  
2478 2017.

2479 Zawadowicz, M. A., Froyd, K. D., Perring, A. E., Murphy, D. M., Spracklen, D. V., Heald, C.  
2480 L., Buseck, P. R., and Cziczo, D. J.: Model-measurement consistency and limits of  
2481 bioaerosol abundance over the continental United States. *Atmospheric Chemistry and*  
2482 *Physics*, 19(22), 13859-13870. <https://doi.org/10.5194/acp-19-13859-2019>, 2019.

2483 Zenker, J., Collier, K. N., Xu, G., Yang, P., Levin, E. J. T., Suski, K. J., DeMott, P. J., and  
2484 Brooks, S. D.: Using depolarization to quantify ice nucleating particle concentrations: a  
2485 new method, *Atmos. Meas. Tech.*, 10, 4639–4657, [https://doi.org/10.5194/amt-10-4639-](https://doi.org/10.5194/amt-10-4639-2017)  
2486 [2017](https://doi.org/10.5194/amt-10-4639-2017), 2017.

2487

2488

**Page 16: [1] Deleted** **Paul DeMott** **10/14/24 12:03:00 PM**

**Page 44: [2] Deleted** **Paul DeMott** **11/5/24 10:40:00 AM**

**Page 44: [2] Deleted** **Paul DeMott** **11/5/24 10:40:00 AM**

**Page 44: [3] Deleted** **Paul DeMott** **10/10/24 1:41:00 PM**

**Page 45: [4] Deleted** **Paul DeMott** **11/3/24 8:00:00 PM**

**Page 53: [5] Deleted** **Paul DeMott** **11/14/24 8:11:00 AM**

# Field Intercomparison of Ice Nucleation Measurements: The Fifth International Workshop on Ice Nucleation Phase 3 (FIN-03)

## Supporting Information

Paul J. DeMott<sup>1</sup>, Jessica A. Mirrielees<sup>2,a</sup>, Sarah Suda Petters<sup>3,b</sup>, Daniel J. Cziczo<sup>4,c</sup>, Markus D. Petters<sup>3,d</sup>, Heinz G. Bingemer<sup>5</sup>, Thomas C. J. Hill<sup>1</sup>, Karl Froyd<sup>6,7,e</sup>, Sarvesh Garimella<sup>4,f</sup>, A. Gannet Hallar<sup>8,9</sup>, Ezra J.T. Levin<sup>1,g</sup>, Ian B. McCubbin<sup>8,9</sup>, Anne E. Perring<sup>7,h</sup>, Christopher N. Rapp<sup>c</sup>, Thea Schiebel<sup>10,i</sup>, Jann Schrod<sup>5</sup>, Kaitlyn J. Suski<sup>1j</sup>, Daniel Weber<sup>5,k</sup>, Martin J. Wolfe<sup>3,l</sup>, Maria Zawadowicz<sup>3,m</sup>, Jake Zenker<sup>2,n</sup>, Ottmar Möhler<sup>10</sup> and Sarah D. Brooks<sup>2</sup>

<sup>1</sup>Department of Atmospheric Science, Colorado State University, Fort Collins, CO, USA

<sup>2</sup>Department of Atmospheric Sciences, Texas A&M University, College Station, TX, USA

<sup>3</sup>Department of Marine, Earth and Atmospheric Sciences, North Carolina State University, Raleigh, NC, USA

<sup>4</sup>Department of Earth, Atmospheric and Planetary Sciences, Massachusetts Institute of Technology, Cambridge, MA, USA

<sup>5</sup>Institute for Atmospheric and Environmental Sciences, Goethe University Frankfurt, 60438 Frankfurt am Main, Germany

<sup>6</sup>NOAA Earth System Research Laboratory, Boulder, CO, USA

<sup>7</sup>CIRES, University of Colorado, Boulder, CO, USA

<sup>8</sup>Storm Peak Laboratory, Department of Atmospheric Sciences, University of Utah, Salt Lake City, Utah, USA

<sup>9</sup>Department of Atmospheric Sciences, University of Utah, Salt Lake City, Utah, USA

<sup>10</sup>Institute of Meteorology and Climate Research (IMK-AAF), Karlsruhe Institute of Technology (KIT), Eggenstein-Leopoldshafen, Germany

<sup>a</sup>now at: Chemistry Department, University of Michigan, Ann Arbor, MI

<sup>b</sup>now at: Center for Environmental Research and Technology, University of California, Riverside, Riverside, CA, USA

<sup>c</sup>now at: Department of Earth, Atmospheric, and Planetary Sciences, Purdue University, West Lafayette, IN, USA

<sup>d</sup>now at: Riverside, Department of Chemical and Environmental Engineering, University of California, Riverside, CA, USA

<sup>e</sup>now at: Air Innova, Boulder, CO, USA

<sup>f</sup>now at: ACME AtronOmatic, LLC, Portland, OR, USA

<sup>g</sup>now at: Colorado Department of Public Health and Environment, Denver CO, USA

<sup>h</sup>now at: Department of Chemistry, Colgate University, Hamilton, NY, USA

<sup>i</sup>now at: Faculty 8- Mathematics and Physics, University of Stuttgart, Stuttgart, Germany

<sup>j</sup>now at: Rainmaker Technology Corporation, El Segundo, CA, USA

<sup>k</sup>now at: Federal Waterways Engineering and Research Institute, Karlsruhe, Germany

<sup>l</sup>now at: Yale Center for Law and Policy, New Haven, CT, USA

<sup>m</sup>now at: Brookhaven National Laboratory, Richland, WA, USA

<sup>n</sup>now at: Sandia National Laboratories, Albuquerque, NM, USA

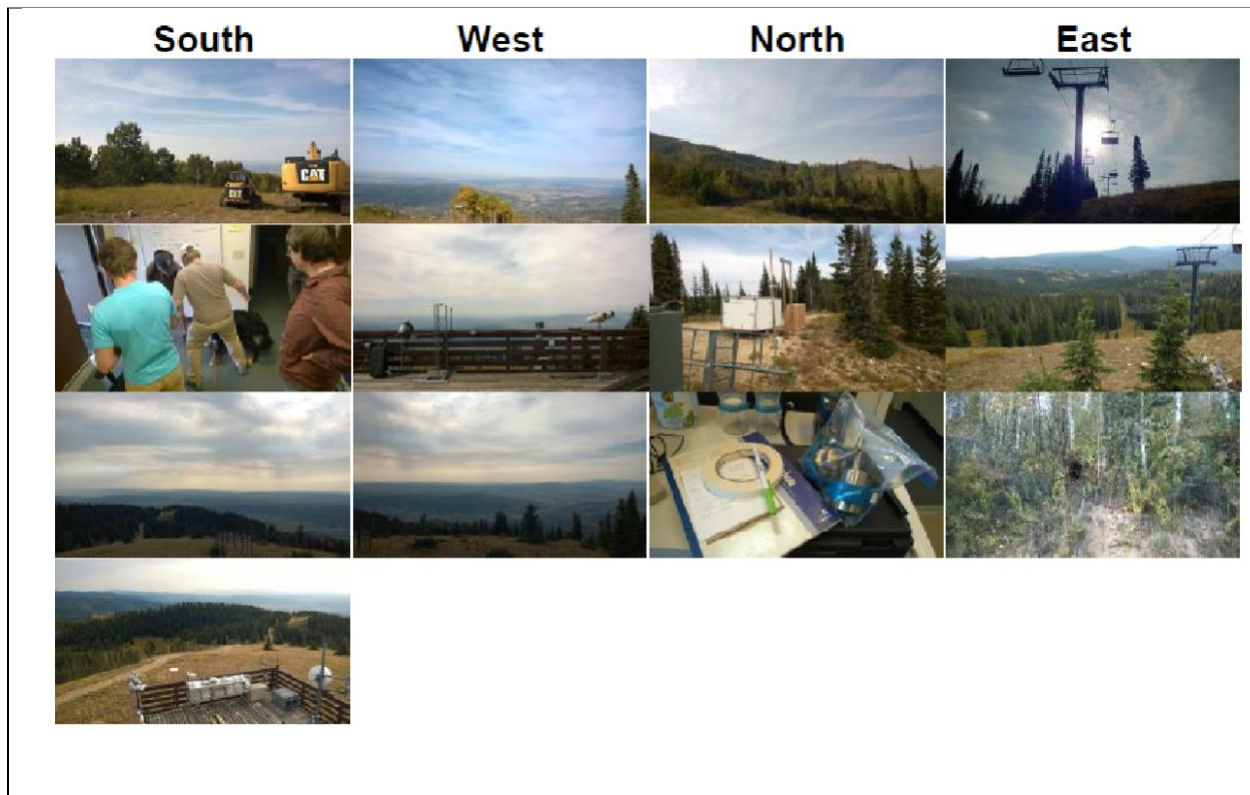
Correspondence: Paul J. DeMott ([Paul.Demott@colostate.edu](mailto:Paul.Demott@colostate.edu))

## S1. Weather conditions and photos

Photographs shown here are available at <https://sspetters.github.io/fin03/index.html> or upon request to Sarah Petters.







**Date: September 13, 2015**

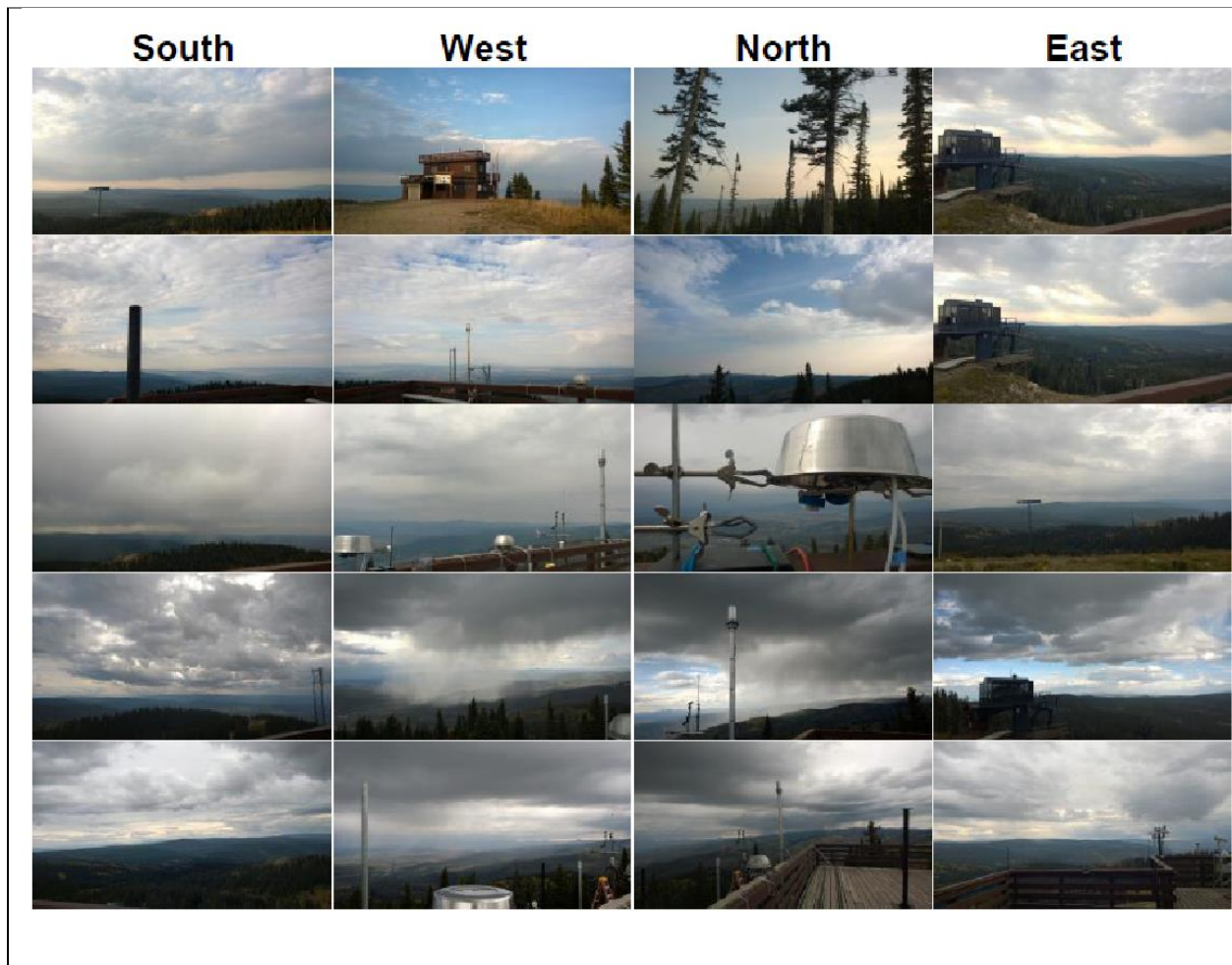
**Observations**

Clouds arriving. The road was again dusty in the morning (not pictured). Brown haze layer is present.

Stronger winds from West in the daytime (10 AM - 4 PM).

1 PM: Very hazy now, thicker cirrostratus

3 PM: Very breezy. 70-80% coverage with altostratus.



**Date: September 14, 2015**

**Observations**

Arrival of rain. Wind picked up after 6pm.

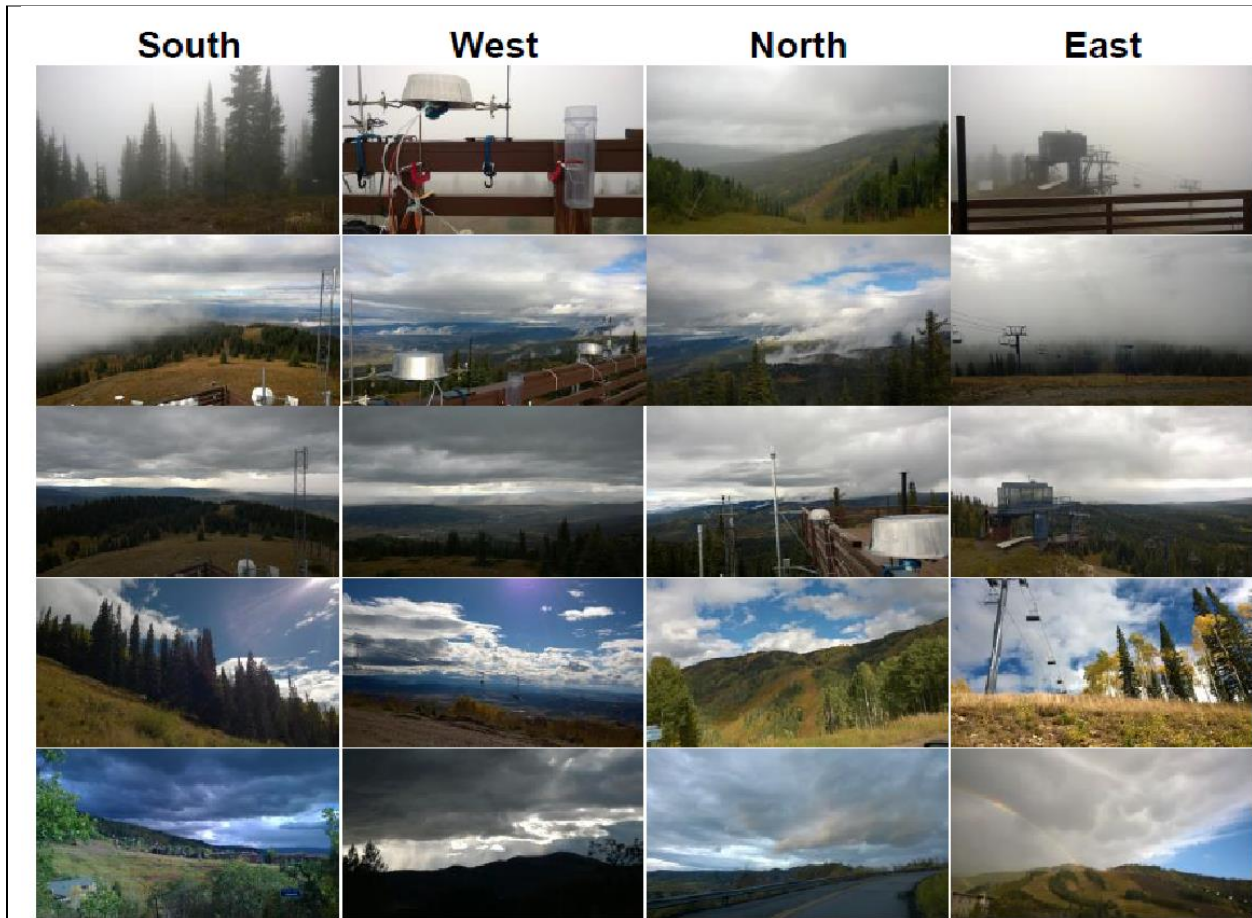
8-8:30 AM: Wind from direction of anvil cloud; transition to overcast; continued wind, clouds break up

8:45-9 AM: Vehicles arriving on dirt road; 8:50 AM: Sun breaking behind Skilift, patches of broken stratocumulus

9 AM: Clear in valley, hazy; 10:28,10:58 AM: Vehicles on dirt road; 1:20-1:50 PM: Wind dies, first drops of rain; rain stops

5:02 PM: Rain (8 minutes); 5:30 PM: Meeting. For road dust, later arrivals will park lower on road;

6:11 PM: Rain begins again, stays



**Date: September 15, 2015**

**Observations**

Rain predicted through 2:30 PM, "elective downtime" today (intercomparison cancelled due to road conditions).

1:35 PM: Rain

1:45 PM: Raining quite hard, sideways

2:10 PM: Separation of cloud layers



**Date: September 16, 2015**

**Observations**

Rain intermittently.

8:44 AM: Rain approaching; wind coming from downpour to west; 9 AM: Rain has begun and stopped

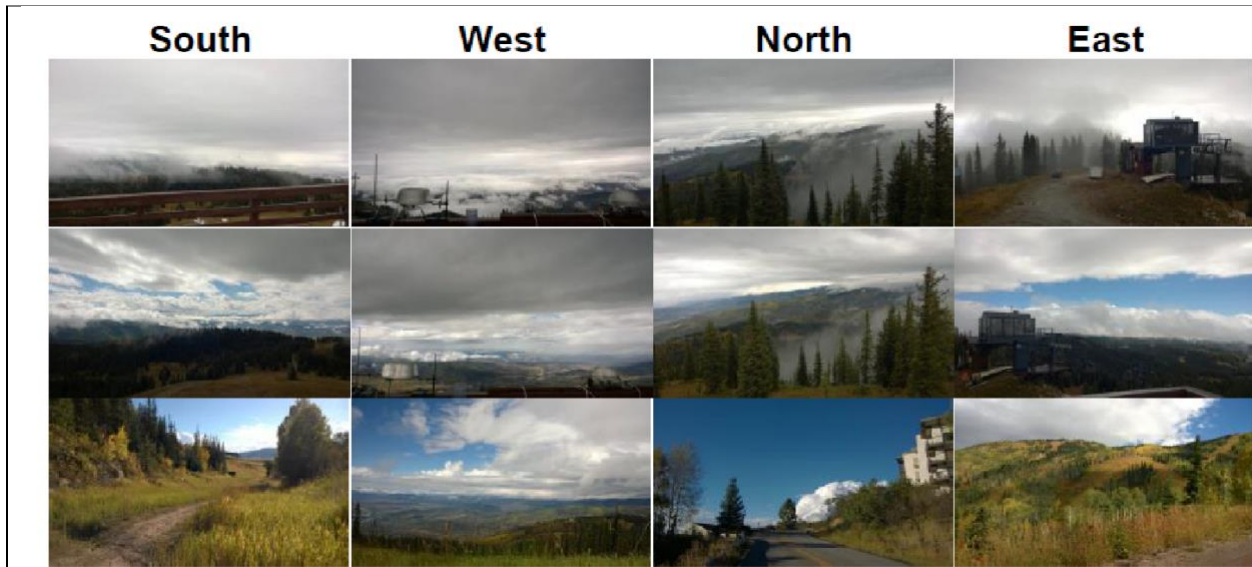
9 AM: Meeting: Bike race on dirt road over weekend; Free troposphere peaks at 6am; Starting this weekend there will be smoke from California on the West wind; Children will visit on Monday

1:06 PM: Raining again; 3:18 PM: 1-mm hail, roundish, for a couple of minutes; 3:25 PM: Small amount of rain

3:40 PM: Intercomparison cancelled; SPIN background issues; 3:41 PM: Hail again, 5 minutes

4:40 PM: Rain has stopped in valley, patchy cumulus

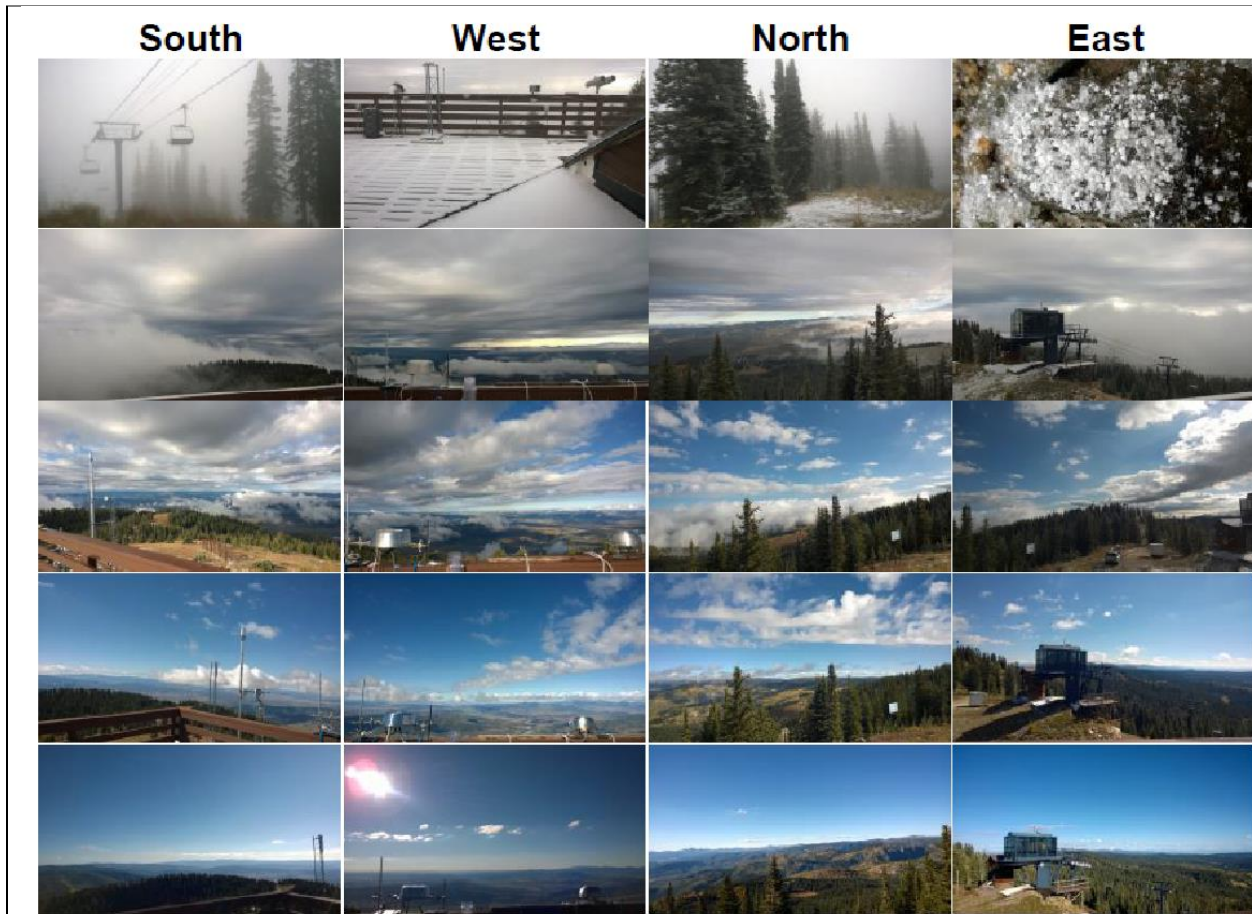
5:05 PM: 2 minutes of hail



**Date: September 17, 2015**

**Observations**

Site closed after half day due to weather.  
10 AM: Arrive in fog/rain/snow; everything is wet  
10:30 AM: Rain has stopped  
11 AM: Snow and sleet again  
12:40 PM: Still raining



**Date: September 18, 2015**

**Observations**

Early snow, clear later.


8 AM: Arrive in snow/graupel; 8:20 AM: Snow depth 1/2 inch; 8:26 AM: Fog arrives, visibility low

9 AM: Sun is out; power plant plumes clearly visible in valley

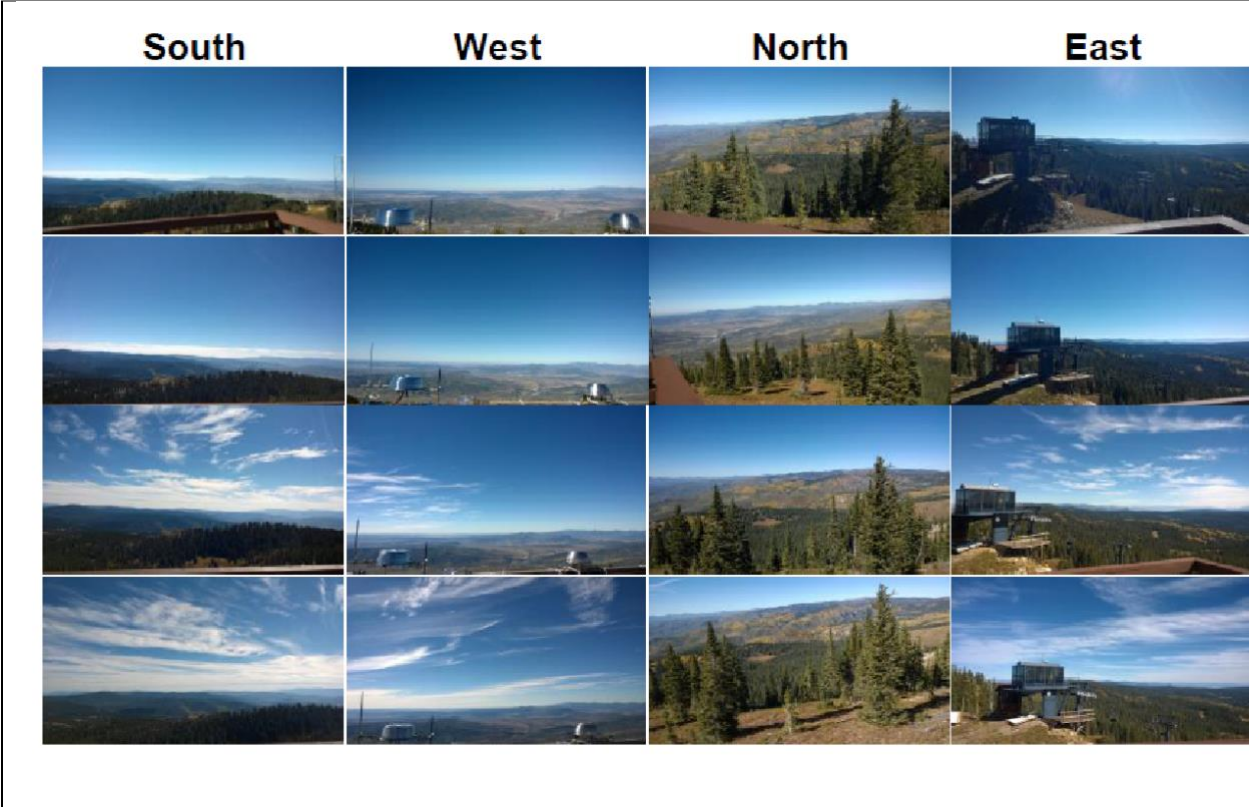
10:32 AM: Clear sky above high cloud, clumpy low cumulus (much lower than past couple days), generally clear above, sunny, RH 51%

11:38 AM: Sunny, scattered cumulus in valley. Upper level cumulus height above mountain is constant (to East)

1:00 PM: Vehicles departing; 2:40 PM: Sunny, small amount of haze; 3:25 PM: Vehicles; 4:15 PM: Vehicle

<b>South</b>	<b>West</b>	<b>North</b>	<b>East</b>
			
<b>Date: September 19, 2015</b>			
<b>Observations</b>			
Winds from West 10am-9pm. No precipitation was anticipated. 12 PM: No rain/snow overnight			

<b>No photos taken</b>
Date: September 20, 2015
Observations
<b>None</b>

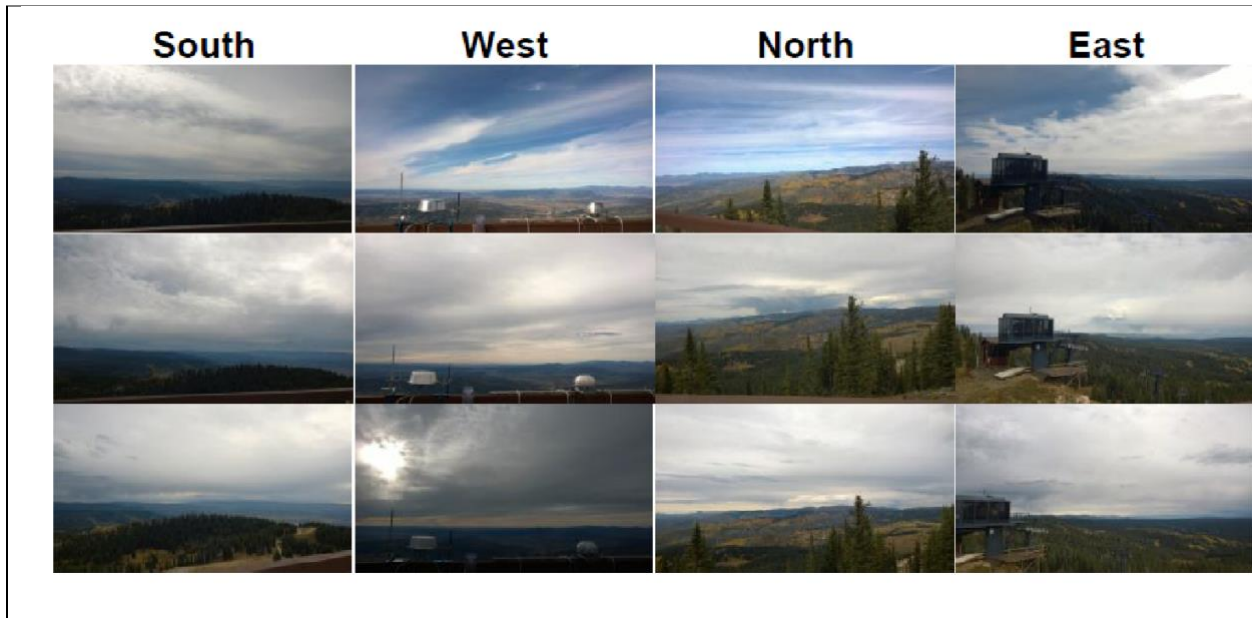


**Date: September 21, 2015**

**Observations**

Clear with high clouds.  
 10 AM: Clear and slightly hazy  
 11 AM: Vehicles





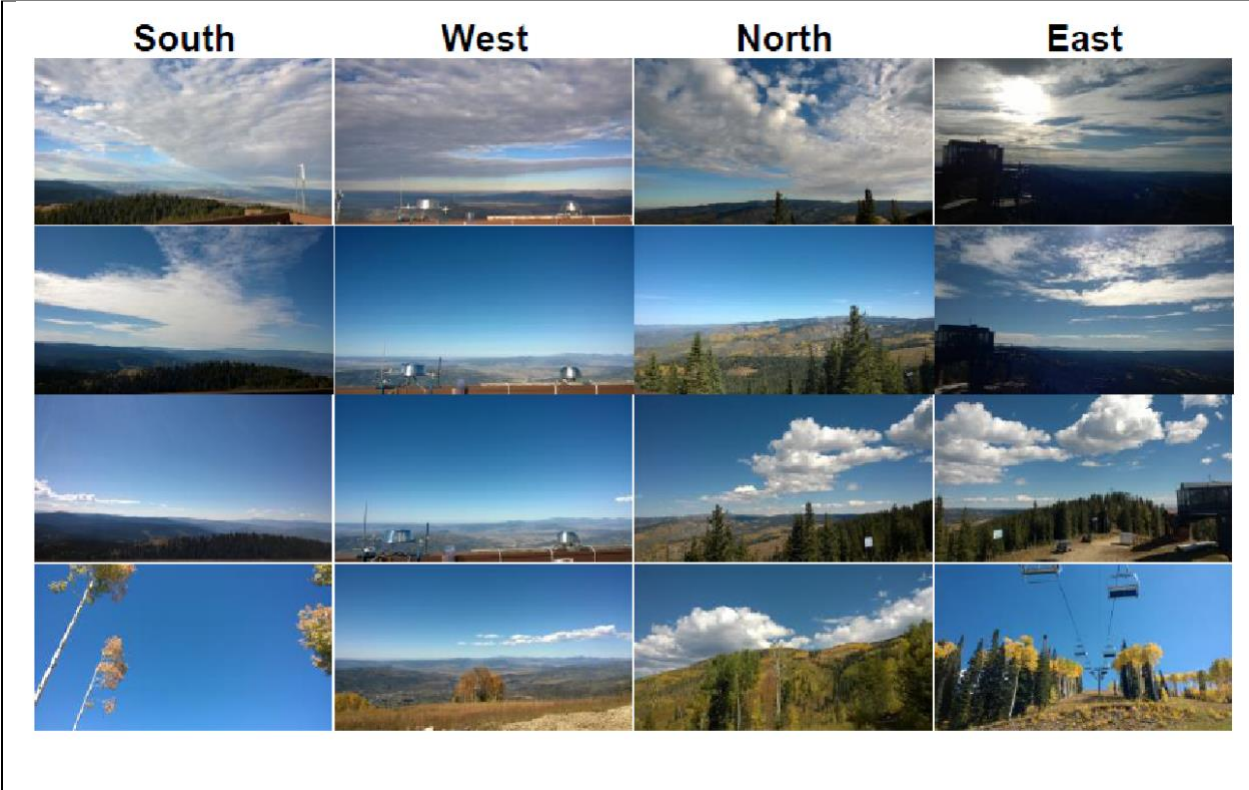
**Date: September 22, 2015**

**Observations**

Overcast without rain.

2 PM: Hazy with a couple of clouds downwind; Ian goes to block road after some discussions with Forest Service

3:48 PM: Virga descending on horizon; wind has died; thunderstorm downwind



**Date: September 23, 2015**

**Observations**

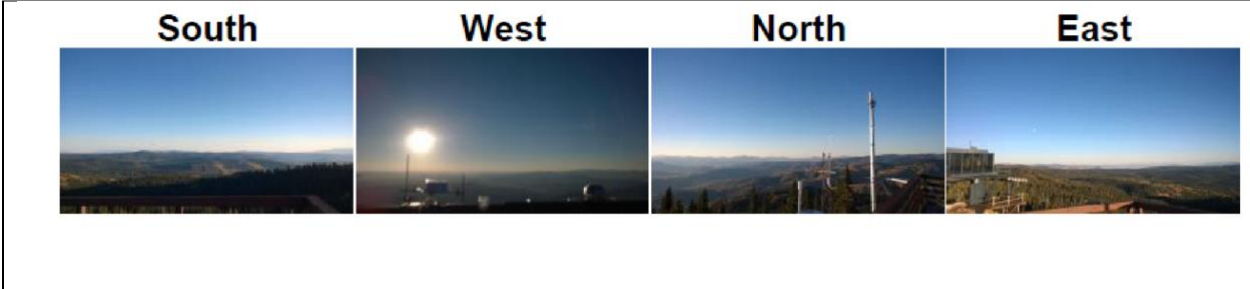
Breezy, scattered clouds.



**Date: September 24, 2015**

**Observations**

None (mandatory downtime)



**Date: September 25, 2015**

**Observations**

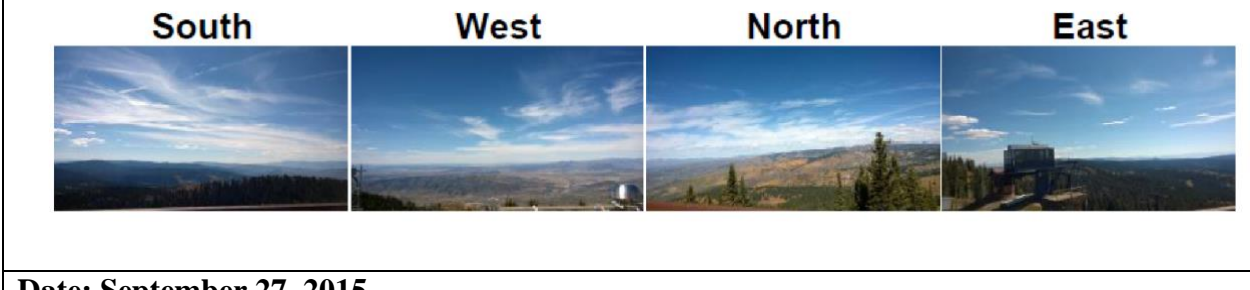
Hazy day. Wind from NW after 10am.  
 8 AM: Sunny and hazy  
 11:30 AM: Fairly hazy  
 6:20 PM: Very hazy, slight breeze, no clouds



**Date: September 26, 2015**

**Observations**

Scattered high clouds.



**Date: September 27, 2015**

**Observations**

Scattered high clouds.

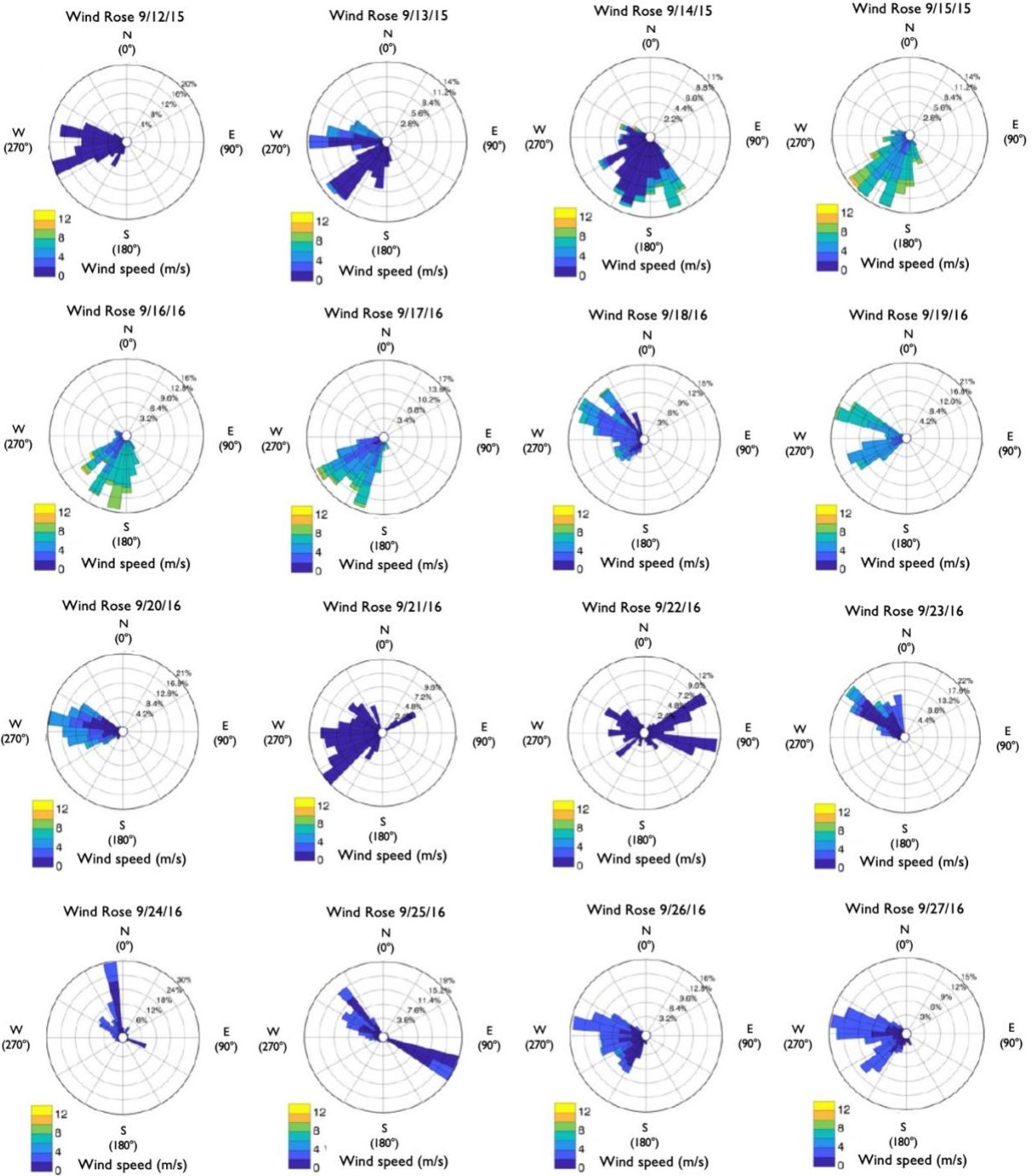


**Figure S1.** Wind roses displaying wind speed throughout FIN-03.

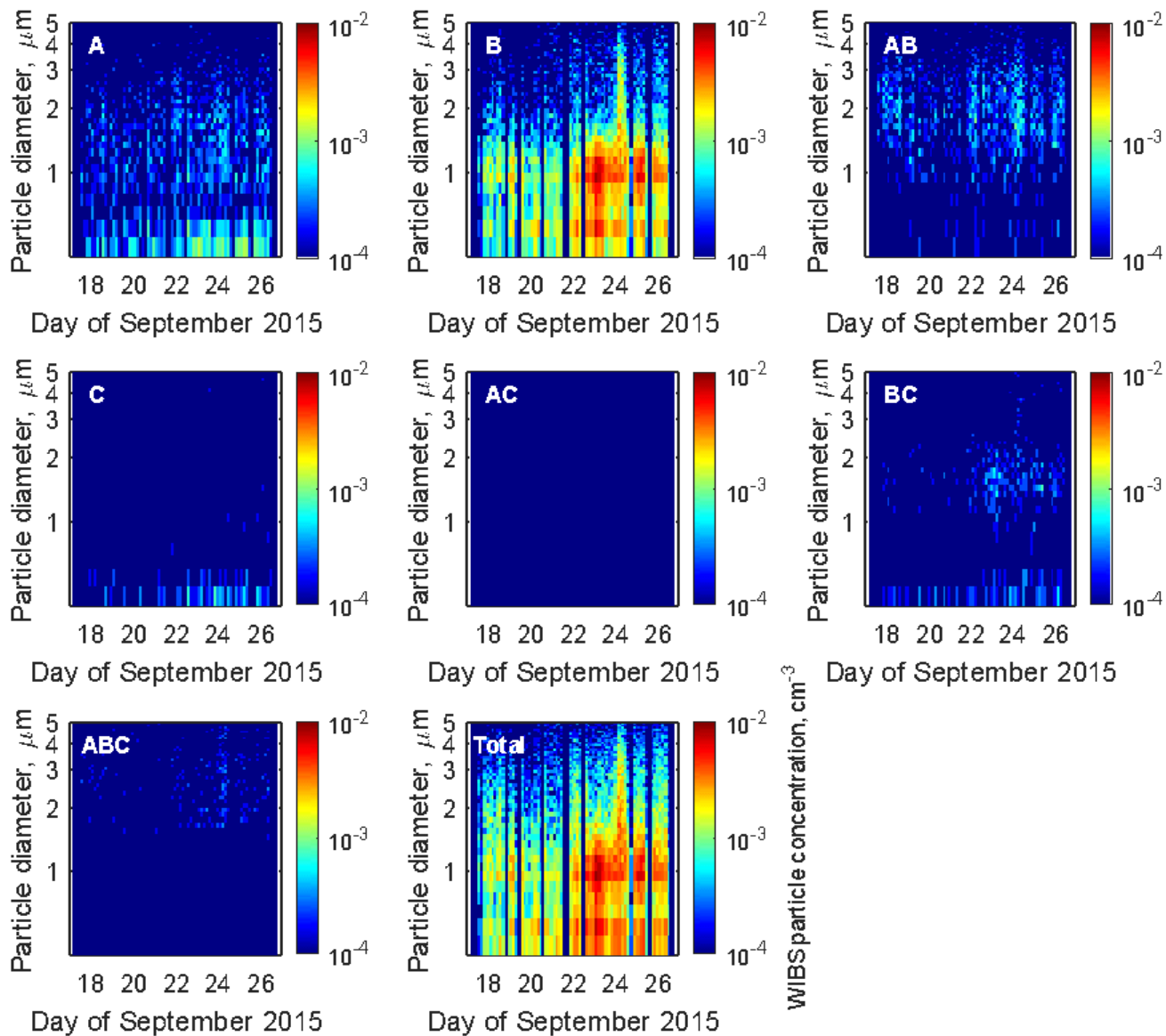


**Figure S2.** WBS time series heatmaps by particle type (A, B, AB, C, AC, BC, and ABC) as well as total (all fluorescing particles measured by the WBS which are categorized into one of the seven types). The WBS measures the concentration of particles with diameter 0.4 - 20  $\mu\text{m}$ , but the y-axis has been truncated at 5  $\mu\text{m}$  to show more detail in the range that held most particles.

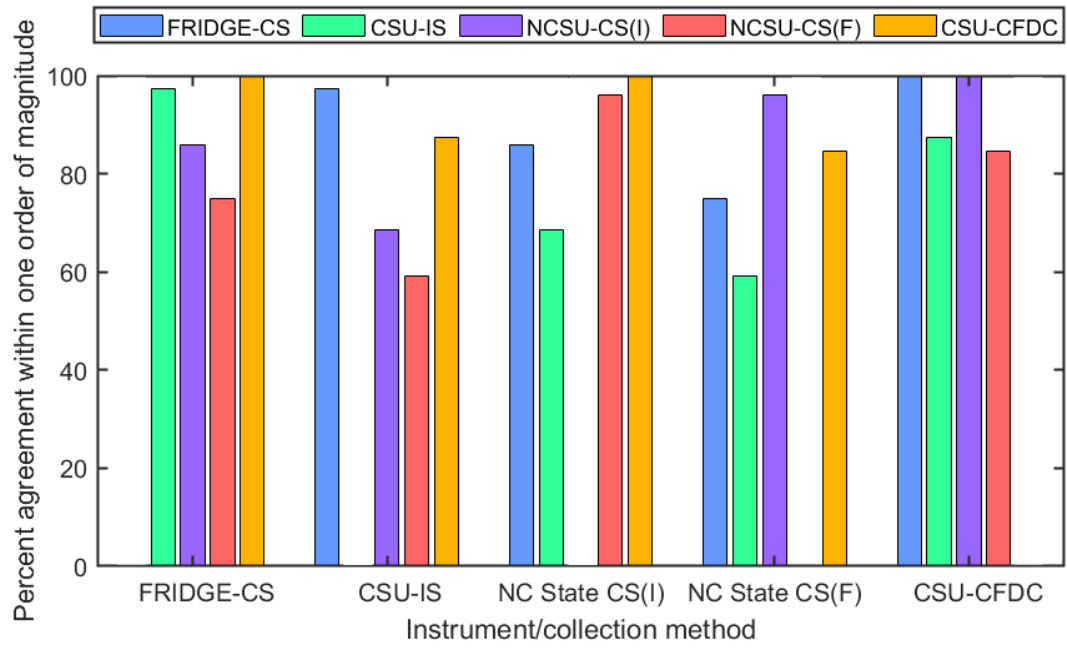


**Figure S3.** The percent of immersion INP measurements in which all instrument pairs agreed within one order of magnitude are shown for each pair of ice nucleation instruments.

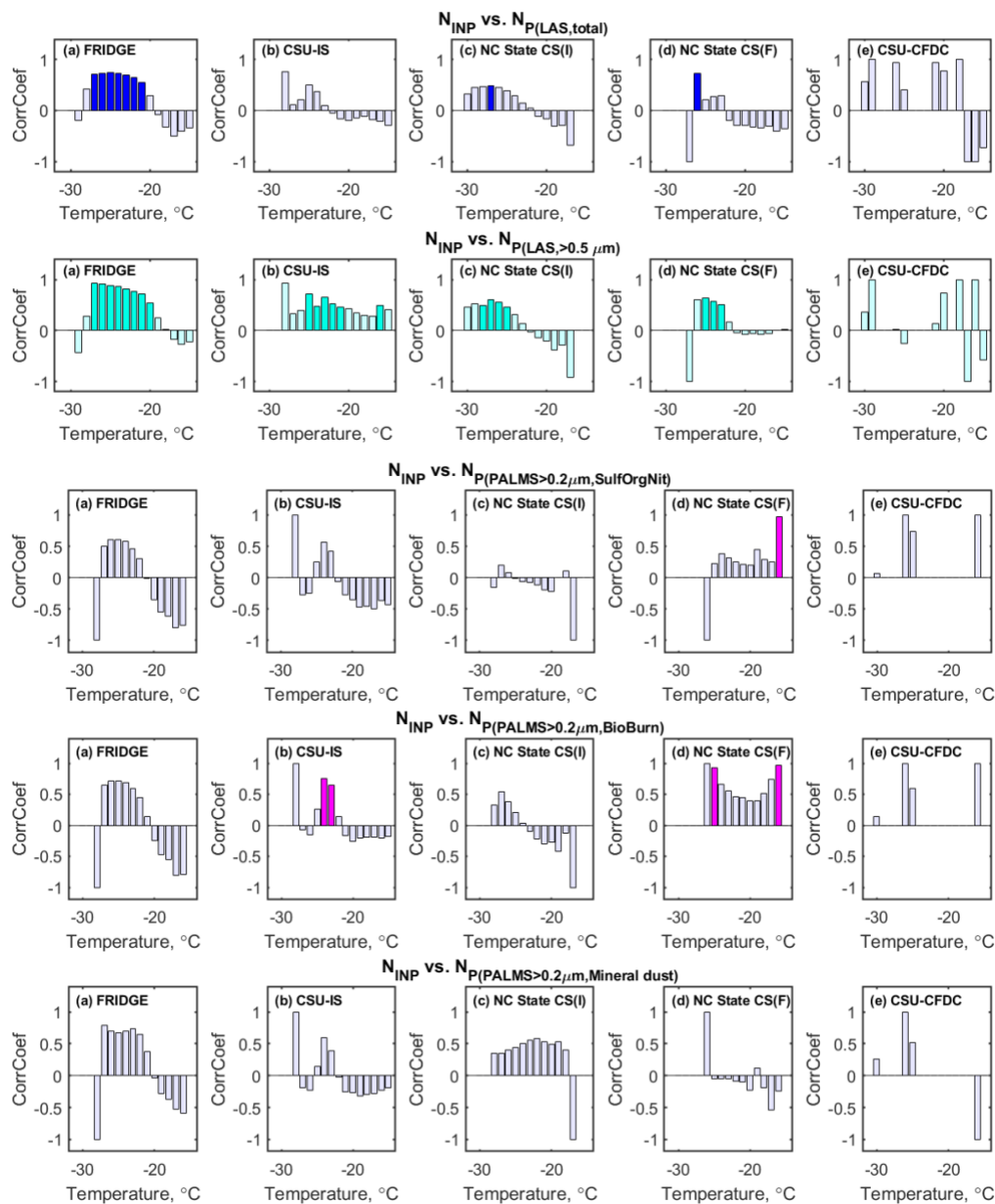


**Figure S4a.** Correlation coefficients in 1°C temperature bins for INPs measured by different methods with aerosol number concentrations from the LAS in all size bins and at sizes  $> 0.5 \mu m$ , and with number concentrations of PALMS sulfate/organic/nitrate, biomass burning and mineral dust particle types at sizes  $> 0.2 \mu m$  (Bright-colored bar =  $p < 0.05$ , Light-colored bar =  $p > 0.10$  or  $p = NaN$  when there were too few samples per bin to derive the p-value)

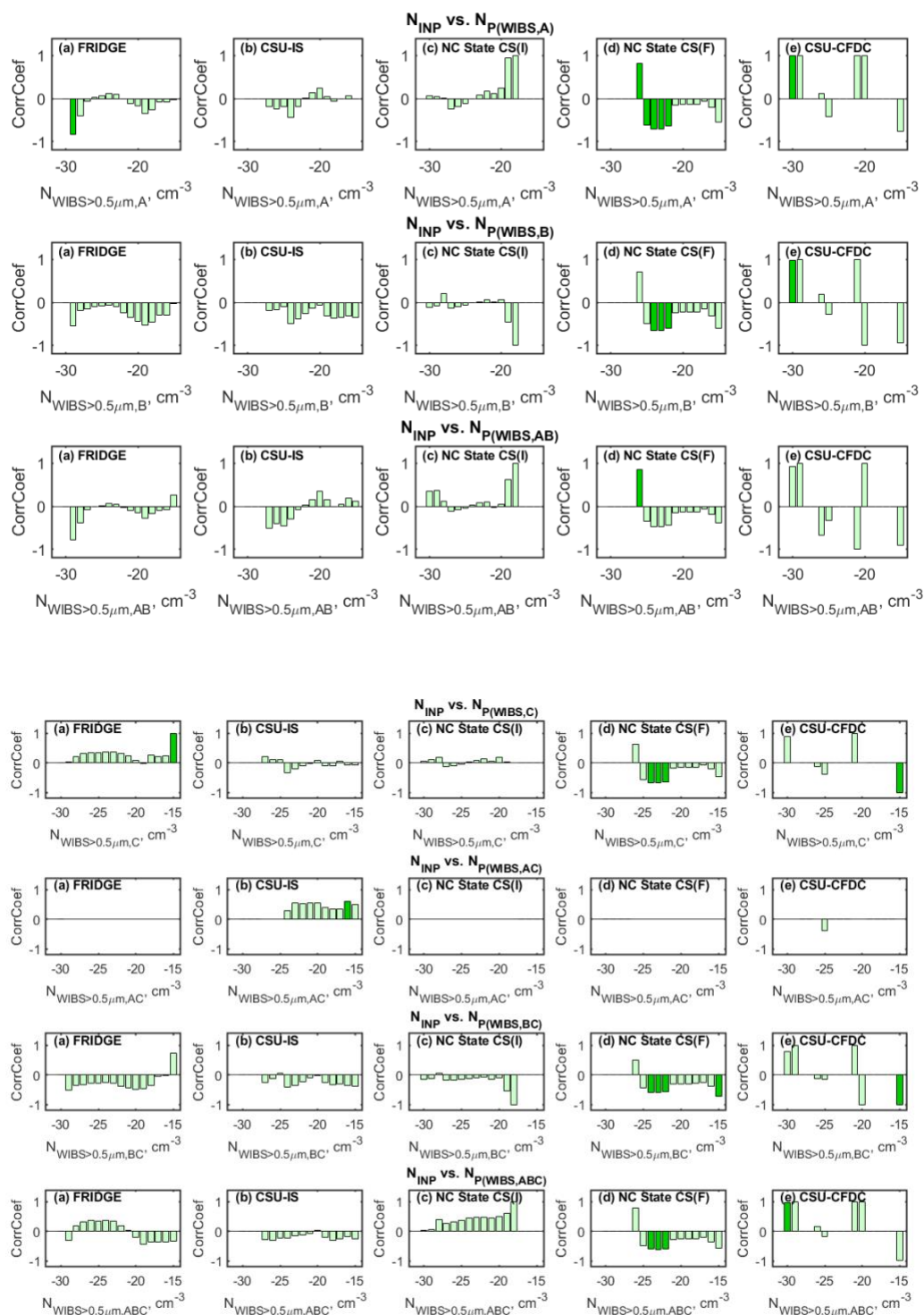


**Figure S4b.** Correlation coefficients in  $1^\circ\text{C}$  temperature bins for INPs measured by different methods with WBS category concentrations at sizes  $> 0.5 \mu\text{m}$  (Bright-colored bar =  $p < 0.05$ , Light-colored bar =  $p > 0.10$  or  $p = \text{NaN}$ )



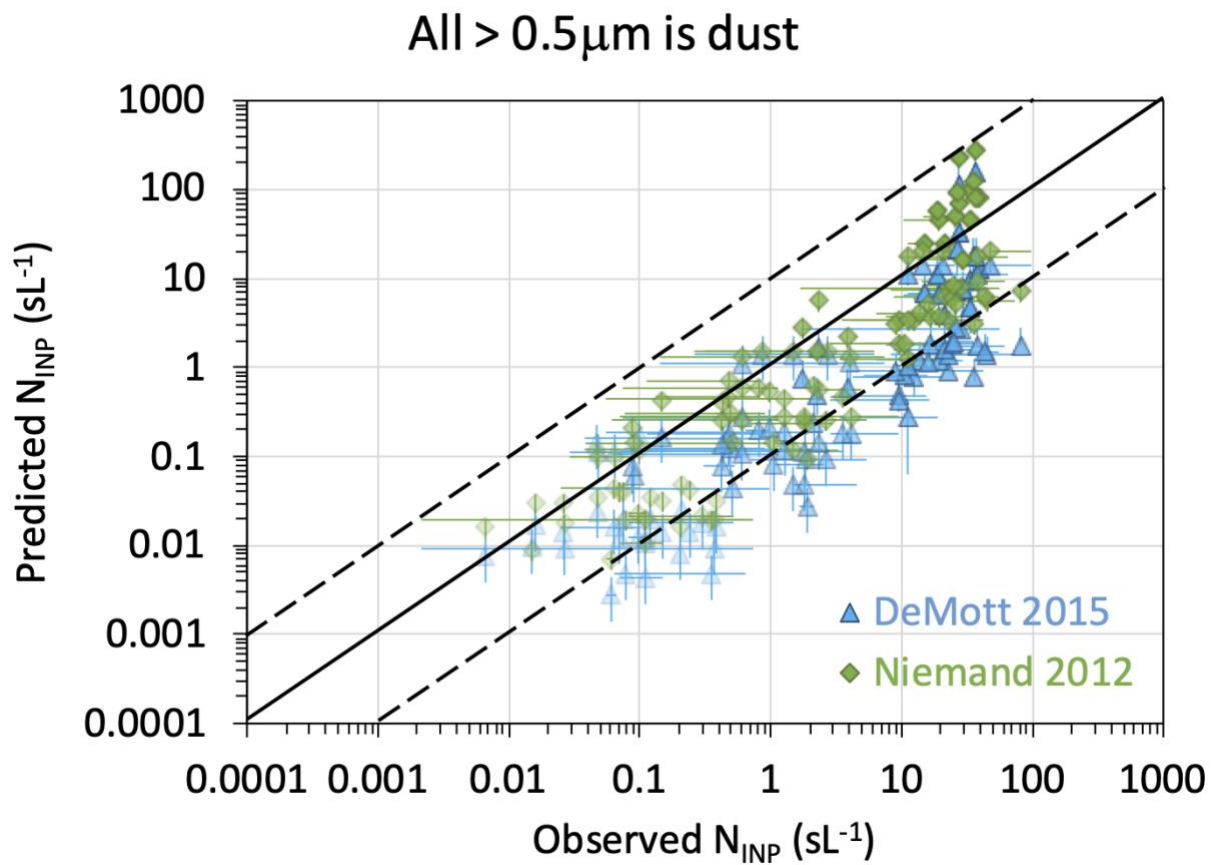


**Figure S5.** As in Figure 9 of the main manuscript, but for dust INP parameterizations on the assumption that all particles at sizes above  $0.5\mu\text{m}$  are dust particles.